OPTICAL BREAST IMAGING

Stephanie Maria Wilhelmina Yvonne van de Ven

Optical Breast Imaging

Thesis, Utrecht University

ISBN: 978-90-393-5509-1

Author: Stephanie MWY van de Ven
Cover design: California coastline by Michelle Mawer, edited by Roy Sanders
Lay-out: Roy Sanders
Printed by: Gildeprint drukkerijen, Enschede, The Netherlands

OPTICAL BREAST IMAGING

Optische Beeldvorming van de Borst

(met een samenvatting in het Nederlands)

Proefschrift

ter verkrijging van de graad van doctor aan de Universiteit Utrecht
op gezag van de rector magnificus, prof.dr. J.C. Stoof,
ingevolge het besluit van het college voor promoties
in het openbaar te verdedigen
op donderdag 3 maart 2011
des middags te 13.00 uur

door

Stephanie Maria Wilhelmina Yvonne van de Ven
geboren op 18 april 1980 te Eindhoven

Promotoren: Prof. Dr. W.P.Th.M. Mali
Prof. Dr. P. Luijten

Copromotores: Dr. S.G. Elias
Dr. A.J. Wiethoff

Publication of this thesis was financially supported by Philips Healthcare and Röntgen Stichting Utrecht.

In the right light,

at the right time,

everything is extraordinary

- Aaron Rose -

CONTENTS

Chapter 1	General introduction	9
Chapter 2	Optical imaging of the breast	17
Chapter 3	Diffuse optical tomography of the breast: preliminary findings of a new prototype and comparison with Magnetic Resonance Imaging	37
Chapter 4	Diffuse optical tomography of the breast: initial validation in benign cysts	51
Chapter 5	A novel fluorescent imaging agent for diffuse optical tomography of the breast: first clinical experience in patients	67
Chapter 6	Molecular imaging using light absorbing imaging agents and a clinical optical breast imaging system – a phantom study	83
Chapter 7	Optical imaging with HER2-targeted affibody molecules can monitor Hsp90 treatment response in a xenograft mouse model	103
Chapter 8	General discussion	127
Chapter 9	Summary	133
	Samenvatting	137
Chapter 10	Acknowledgements	141
	Curriculum vitae	147
	List of publications	151

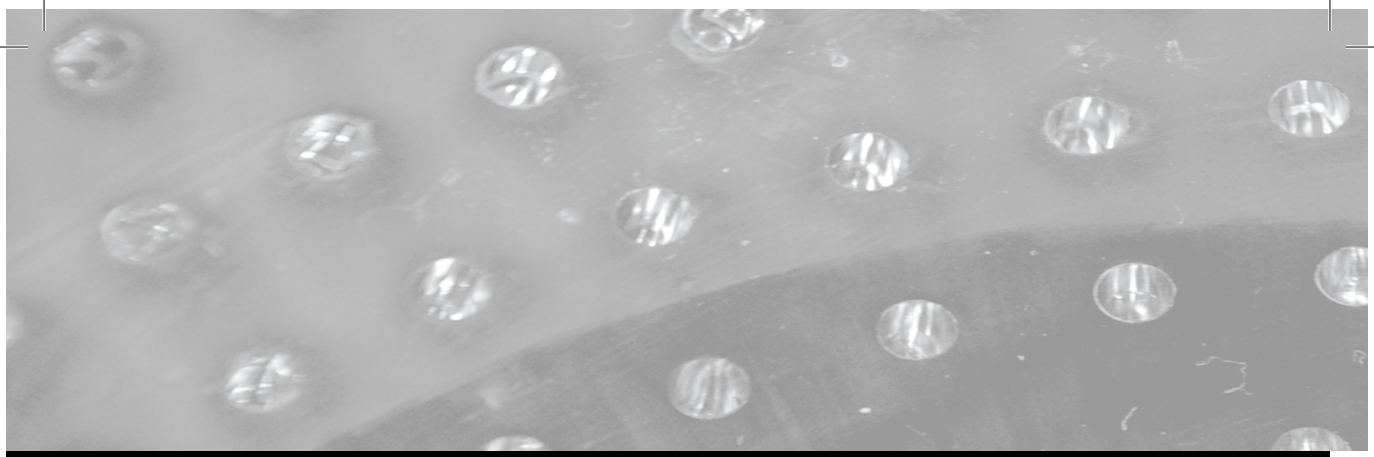

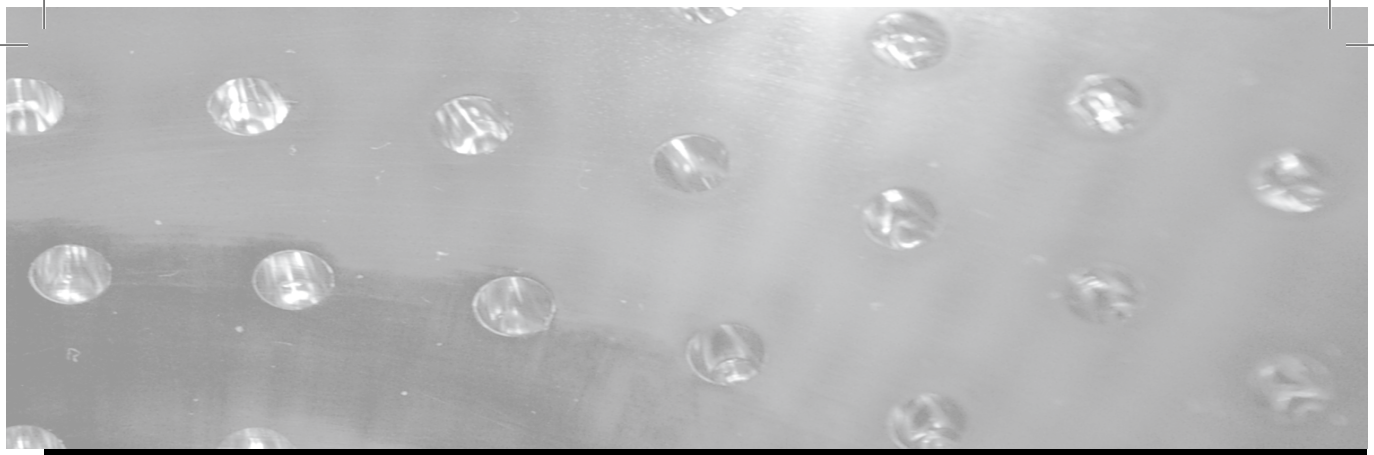

General introduction

Breast cancer is a major health problem worldwide. In the United States, the expected number of new invasive breast cancer cases in 2009 is 192,370 and about 40,170 women are expected to die from the disease this year [1]. In the Netherlands, the incidence of invasive breast cancer is more than 13,000 each year and 3,327 women died of breast cancer in 2008 [2]. While the incidence of breast cancer has increased over the past years, death rates remained constant. This is partly a result of better treatment strategies but also because of breast cancer screening. X-ray mammography is used in screening programs and reduces mortality significantly due to earlier detection of breast cancer [3,4]. For younger women, the benefit from screening with X-ray mammography is markedly smaller than for women over the age of fifty. This is probably caused by the lower incidence of breast cancer at younger age, the more rapidly growing tumors, and the higher radiographic breast density in young women [5]. The overall sensitivity of X-ray mammography for breast cancer detection is moderate (75%), and even more reduced in women with dense breasts, i.e. 62% [6]. This is an important problem, especially since these women are at a four to six times increased breast cancer risk [7]. In addition, positive predictive value of X-ray mammography is relatively low and discrimination between benign and malignant lesions with further diagnostic tests is difficult, leading to a high number of unnecessary biopsies [8]. Ultrasound is very useful to guide biopsies and to discriminate cystic from solid lesions. It could be used in combination with X-ray mammography to improve sensitivity in dense breasts, but positive predictive value remains low and ultrasound is user-dependent and time-consuming when used for screening [9]. Magnetic resonance imaging (MRI) has very high sensitivity (> 95%) and is clinically used as an adjunct to X-ray mammography in high risk patients [10, 11]. However, MRI generally only allows detection and classification of lesions ≥ 5 mm and has a high false-positive rate also [12]. As described above, currently used modalities have been proven very valuable in breast imaging, but unfortunately not without substantial limitations. New methods are being investigated to bridge the current gaps in clinical utility. Examples of such experimental techniques are elastography, tomosynthesis, dedicated computed tomography (CT) and positron emission tomography (PET), photoacoustic (or optoacoustic) imaging, and optical imaging. Elastography evaluates the elastic properties of tissue using compression of the area of interest, assuming these mechanic properties are important indicators for malignancy [13]. Combining elastography with ultrasound might improve specificity and potentially reduce unnecessary breast biopsies [14]. Tomosynthesis takes multiple digital X-ray views at different angles of a stationary compressed breast and three-dimensional images are then reconstructed. This evaluation

might decrease the number of false-positive and false-negative mammogram results from overlapping breast tissue [15]. Another way to eliminate superimposition of glandular tissues is by dedicated breast CT, which also offers the advantage of three-dimensional anatomic detail [16]. PET is most helpful in staging recurrent or metastatic breast cancer and in evaluating the response of locally advanced and metastatic breast cancer to treatment [17]. However, spatial resolution limits its use for the early detection of primary breast lesions. To improve sensitivity for small breast lesions, dedicated breast PET systems are being developed [18, 19]. The photoacoustic imaging technique fuses optical and acoustic imaging in one modality by utilizing optical illumination and ultrasonic detection of resulting signals [20]. Optical imaging uses light propagation through tissue to assess its optical properties. This thesis will focus on optical imaging of the breast.

Optical breast imaging can be performed (1) relying on intrinsic breast tissue contrast alone (mapping hemoglobin, water, and lipid content); or (2) with the use of exogenous imaging agents that accumulate at the tumor site, either by targeting cancer-specific molecules or by extravasation due to leaky tumor vasculature. The light used in optical imaging is commonly monochromic and in the near-infrared (NIR) range permitting imaging up to several centimetres deep in soft tissue. Different tissue components have unique scattering and absorption characteristics for each wavelength. The use of one wavelength gives some diagnostic information about the tissue of interest, e.g. if there is high total blood content, associated with angiogenesis. By combining data from multiple wavelengths, more precise information on relative concentrations of oxy- and deoxyhemoglobin, lipid, and water in the tissue can be extracted (spectroscopic imaging), which may allow for better discrimination between malignant and benign tissue. With the use of exogenous imaging agents, such discrimination may be improved even further, especially with imaging agents specifically targeted to cancer-associated molecular changes (molecular imaging).
Albeit in its infancy, optical breast imaging has some intrinsic advantages compared to other breast imaging modalities. It uses no ionizing radiation (versus X-ray mammography), the technology is relatively inexpensive (versus MRI), and is not user-dependent (versus ultrasound). Optical breast imaging may be able to play a role where currently used breast imaging modalities show limitations in clinical utility (in early detection, diagnosis, or treatment monitoring of breast cancer) [8, 21-23]. Optical imaging is being pursued as an adjunct to the current imaging modalities due to its potential to provide biophysical and molecular information on breast tissue. Optical imaging is already widely used in preclinical

studies and novel molecular imaging agents specifically targeting cancer-associated molecules are rapidly being developed [24].

This thesis starts with a literature overview on optical breast imaging (**Chapter 2**). Then, the first clinical experiences in the evaluation of a new Diffuse Optical Tomography (DOT) prototype dedicated for breast imaging are reported (**Chapters 3-5**). The potential of optical breast imaging to discriminate between benign and malignant tissue was evaluated first, using solely data on intrinsic tissue contrast at four different NIR wavelengths. Also, the inter- and intra-observer agreement of DOT image interpretation was assessed under ideal circumstances (**Chapter 3**). Second, we investigated the added value of spectroscopic analysis for imaging well-defined benign cysts, by combining all information from the four wavelengths (**Chapter 4**). Third, we evaluated optical breast imaging using escalating doses of a novel fluorescent non-targeted imaging agent in patients highly suspected of breast cancer (**Chapter 5**). Finally, preclinical experiments focusing on newly developed targeted imaging agents for molecular optical imaging are described (**Chapters 6-7**). Phantom studies based on modulating light transmission using a time-domain clinical optical breast scanner were conducted first (**Chapter 6**), followed by experiments in mice assessing the potential of treatment monitoring using a fluorescent targeted imaging agent and a time-domain preclinical optical imaging system (**Chapter 7**).

References

1. American Cancer Society. Breast Cancer Facts & Figures 2009-2010. Atlanta, GA, American Cancer Society Inc.
2. Vereniging Integrale Kankercentra. www.ikcnet.nl ; updated 22 June 2010. Utrecht, The Netherlands.
3. Fletcher SW, Elmore JG. Clinical practice. Mammographic screening for breast cancer. N.Engl.J.Med. 2003; 348: 1672-1680.
4. Humphrey LL, Helfand M, Chan BK, Woolf SH. Breast cancer screening: a summary of the evidence for the U.S. Preventive Services Task Force. Ann.Intern.Med. 2002; 137: 347-360.
5. Buist DS, Porter PL, Lehman C, Taplin SH, White E. Factors contributing to mammography failure in women aged 40-49 years. J.Natl.Cancer Inst. 2004; 96: 1432-1440.
6. Carney PA, Miglioretti DL, Yankaskas BC, Kerlikowske K, Rosenberg R, Rutter CM et al. Individual and combined effects of age, breast density, and hormone replacement therapy use on the accuracy of screening mammography. Ann.Intern.Med. 2003; 138: 168-175.
7. Boyd NF, Guo H, Martin LJ, Sun L, Stone J, Fishell E et al. Mammographic density and the risk and detection of breast cancer. N.Engl.J.Med. 2007; 356: 227-236.
8. Pisano, E.D., et al., Diagnostic performance of digital versus film mammography for breast-cancer screening. N.Engl.J.Med., 2005. 353(17): p. 1773-1783.
9. Berg WA, Blume JD, Cormack JB, et al. Combined screening with ultrasound and mammography vs mammography alone in women at elevated risk of breast cancer. JAMA 2008; 299:2151-2163.
10. Lehman, C.D., et al., MRI evaluation of the contralateral breast in women with recently diagnosed breast cancer. N Engl J Med, 2007. 356(13): p. 1295-303.
11. Lehman, C.D., et al., Cancer yield of mammography, MR, and US in high-risk women: prospective multi-institution breast cancer screening study. Radiology, 2007. 244(2): p. 381-388.
12. Liberman, L., et al., Does size matter? Positive predictive value of MRI-detected breast lesions as a function of lesion size. AJR Am.J.Roentgenol., 2006. 186(2): p. 426-430.
13. Ophir J, Cespedes I, Ponnekanti H, Yazdi Y, Li X. Elastography: a quantitative method for imaging the elasticity of biological tissues. Ultrason Imaging 1991; 13:111-134.
14. Leong LC, Sim LS, Lee YS, et al. A prospective study to compare the diagnostic performance of breast elastography versus conventional breast ultrasound. Clin Radiol; 65:887-894.

15. Andersson I, Ikeda DM, Zackrisson S, et al. Breast tomosynthesis and digital mammography: a comparison of breast cancer visibility and BIRADS classification in a population of cancers with subtle mammographic findings. Eur Radiol 2008; 18:2817-2825.
16. Lindfors KK, Boone JM, Nelson TR, Yang K, Kwan AL, Miller DF. Dedicated breast CT: initial clinical experience. Radiology 2008; 246:725-733.
17. Rosen EL, Eubank WB, Mankoff DA. FDG PET, PET/CT, and breast cancer imaging. Radiographics 2007; 27 Suppl 1:S215-229.
18. Bowen SL, Wu Y, Chaudhari AJ, et al. Initial characterization of a dedicated breast PET/CT scanner during human imaging. J Nucl Med 2009; 50:1401-1408.
19. Peng H, Levin CS. Design study of a high-resolution breast-dedicated PET system built from cadmium zinc telluride detectors. Phys Med Biol 2010; 55:2761-2788.
20. Ermilov SA, Khamapirad T, Conjusteau A, et al. Laser optoacoustic imaging system for detection of breast cancer. J Biomed Opt 2009; 14:024007.
21. Peters, N.H., et al., Meta-analysis of MR imaging in the diagnosis of breast lesions. Radiology, 2008. 246(1): p. 116-124.
22. Raza, S., et al., BI-RADS 3, 4, and 5 Lesions: Value of US in Management--Follow-up and Outcome. 2008. p. 773-781.
23. Yeh, E., et al., Prospective comparison of mammography, sonography, and MRI in patients undergoing neoadjuvant chemotherapy for palpable breast cancer. AJR Am.J.Roentgenol., 2005. 184(3): p. 868-877.
24. Pierce MC, Javier DJ, Richards-Kortum R. Optical contrast agents and imaging systems for detection and diagnosis of cancer. Int J Cancer 2008; 123:1979-1990.

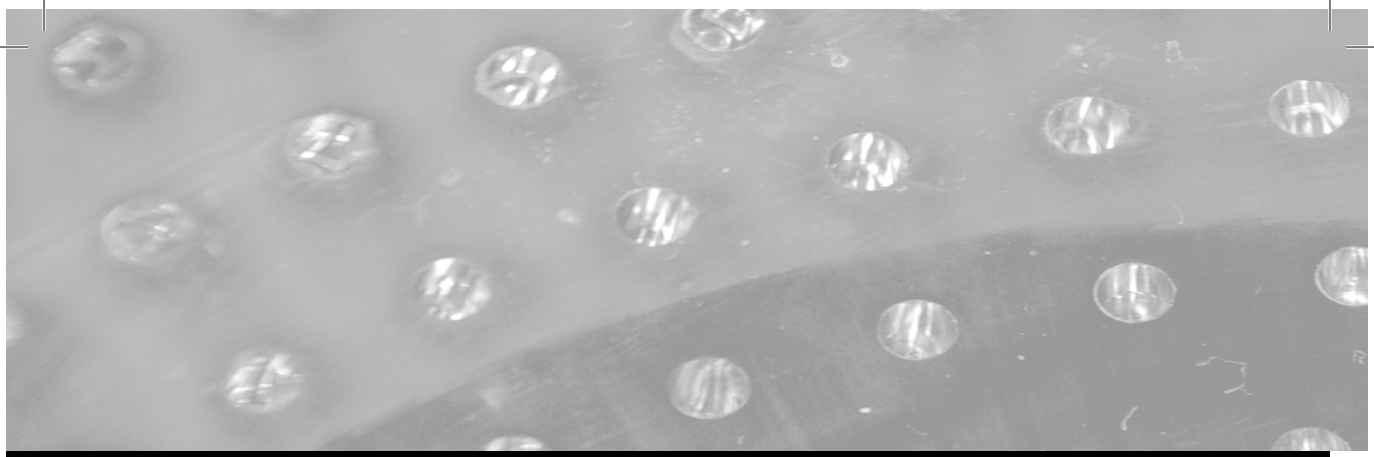

Authors

S.M.W.Y. van de Ven, S.G. Elias, M.A.A.J. van den Bosch, P. Luijten, W.P.Th.M. Mali.

Cancer Imaging 2008;8:206-215

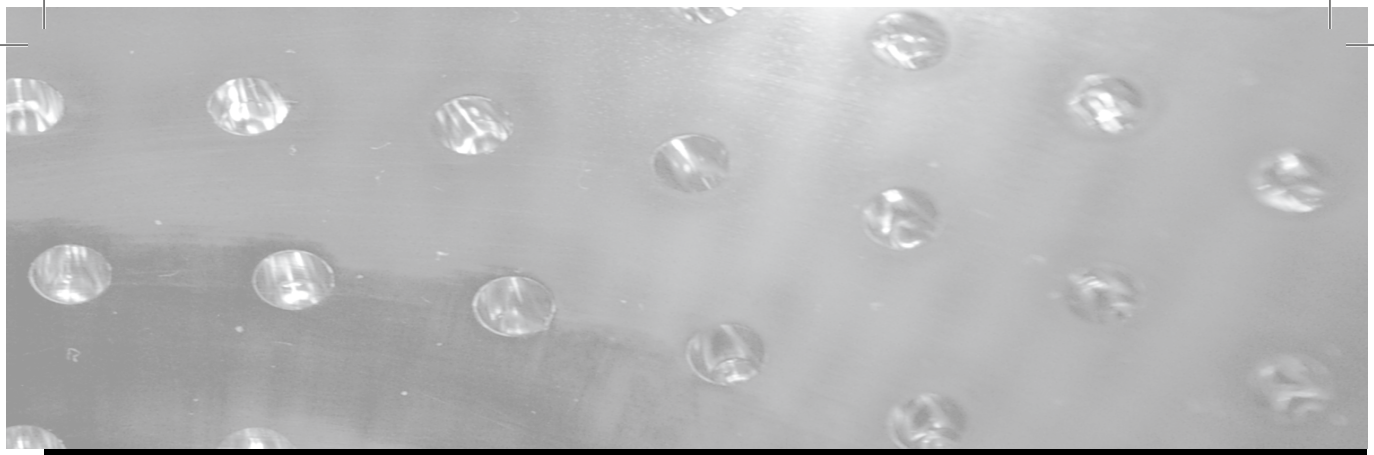

Optical imaging of the breast

Background

Breast cancer is a major global health problem. In 2007, an estimated 1.3 million new cases of invasive breast cancer will be diagnosed and about 465,000 women are expected to die from this disease worldwide [1]. X-ray mammography is used in screening programs and reduces mortality significantly due to earlier detection of breast cancer [2,3]. For younger women, the benefit from screening with X-ray mammography is markedly smaller than for women over the age of fifty. This is probably caused by the lower incidence of breast cancer at younger age, the more rapidly growing tumors, and the higher radiographic breast density in young women [4]. Sensitivity of X-ray mammography for breast cancer detection in women with fatty breasts is approximately 88%, but this sensitivity is strongly reduced in women with dense breasts, i.e. 62% [5]. This is an important problem, especially since these women have an increased breast cancer risk [6].

Optical breast imaging is a novel imaging technique that uses near-infrared (NIR) light to assess optical properties of tissue, and is expected to play an important role in breast cancer detection. It dates back to 1929 when Cutler investigated the shadows of light transmitted through the breast with a normal lamp (transillumination) [7]. Although large malignant lesions with high vascularization could be detected, the method did not achieve sufficient sensitivity and specificity to be used in clinical practice at the time. During the last decade, progress in source and detector technology, light propagation modeling, and potential fluorescent contrast agents, has resulted in a renewed interest in optical imaging [8]. Optical breast imaging uses near-infrared (NIR) light in the wavelength range of 600 to 1000 nm to assess optical properties of tissue. Functional information of tissue components, i.e. absorption characteristics of oxy- and deoxyhemoglobin, water, and lipid, can be obtained by combining images acquired at various wavelengths. When using only intrinsic breast tissue contrast in optical breast imaging, this is referred to as optical breast imaging without contrast agent. The other modality, i.e. optical breast imaging with a contrast agent, uses exogenous fluorescent probes that target molecules specific for breast cancer. The use of fluorescent probes has great potential in early breast cancer detection, since in vivo imaging of molecular changes associated with breast cancer formation is technically feasible. Additional advantages of optical breast imaging are that it uses no ionizing radiation and that it is relatively inexpensive, which can realize repeated use (also in young women) and easy access to the technique. Aim of this review is to provide a summary of the current state of optical breast imaging and to describe its potential future clinical applications in breast cancer imaging.

The basic concepts of optical breast imaging

In general, optical imaging devices transmit light through the breast, where it is both absorbed and scattered by the tissue components present. NIR in the wavelength range of 600-1000 nm is used to allow for sufficient tissue penetration. After passing through the breast, the remaining light is registered by detectors and advanced computer algorithms are used to reconstruct the images (**Figures 1 and 2**) [9-11]. Determining tissue properties and their spatial distribution is complex due to the irregular and long pathways over which light travels through the breast [12].

Figure 1. Prototype of the Diffuse Optical Tomography system used for clinical research (Philips Healthcare, Best, The Netherlands)

Different optical breast imaging systems have been investigated. In transillumination, sources and detectors are positioned at opposite sites of the breast. It generates two-dimensional projection views, comparable to X-ray mammography, and usually requires breast compression [13-17]. In tomography, sources and detectors are placed over the entire breast surface [18,19]. This enables the acquisition of three-dimensional optical breast images. Another approach is the use of handheld devices that are placed manually at the position of interest, comparable to imaging with ultrasound probes [20-22].

Although companies and academic institutions put vast effort in designing optical breast imaging systems, only three of them are commercially available at this moment. The ComfortScan® system, developed by DOBI Medical, is a transillumination system that requires breast compression to generate two-dimen-

sional optical images (http://www.dobimedical.com/dobisys1.html). SoftScan®, by Advanced Research Technologies Inc. (ART), is a system that uses slight breast compression, but is able to generate tomographic images of a chosen region of interest of the breast. This is the only commercial system that uses more than one laser, namely four, to be able to transmit light of different wavelengths through the breast. (http://www.art.ca/en/products/softscan.html) [23]. The Computed Tomography Laser Mammography system CTLM®, developed by Imaging Diagnostic Systems Inc. (IDSI), is a tomographic system that requires no breast compression to generate volumetric optical images of the breast (http://www.imds.com/products/ctlm/).

All optical imaging systems in general, use three different illumination methods: time domain, frequency domain, and continuous wave. The time domain technique uses short (50-400 picoseconds) light pulses to assess the temporal distribution of photons [15,16,24]. In this way, distinction between scattering and absorption can be made. This technology collects the most information on the optical properties of tissue and therefore has better contrast and spatial resolution compared to the other methods. However, time domain equipment is more expensive and acquisition times are longer. Frequency domain devices modulate the amplitude of the light that is continuously transmitted at high frequencies (50-500 megahertz) [25]. By measuring phase shifts of photons and their amplitude decay (compared to a reference signal), information on optical properties of tissue is acquired and scattering and absorption can be distinguished. Frequency domain devices could generate the same information as time domain systems if a large range of frequencies is used [25]. Continuous wave systems emit light at constant intensity or modulated at low frequencies (0.1-100 kilohertz) [26]. It is a straightforward technique, which basically measures the attenuation of light transmitted between two points on the breast surface. Because of its simplicity, continuous wave equipment is cheap and image acquisition fast. However, it is very difficult to discriminate scattering from absorption with this technique and data analysis requires complex reconstruction algorithms [27].

Optical breast imaging without contrast agent

Optical breast imaging uses NIR light to assess the optical properties of breast tissue. Light absorption at these wavelengths is minimal, allowing for sufficient tissue penetration (up to 15 cm). The main components of the breast all have specific absorption characteristics as a function of the wavelength. By combining images acquired at various wavelengths (spectroscopy) concentrations of oxy- and

deoxyhemoglobin, water and lipid can be determined. **Figure 3** demonstrates an example of a benign cyst imaged with both MRI and optical imaging; spectroscopic analysis of the optical data confirmed the high water and low blood concentration in this lesion [28].

In a malignant tumor, hemoglobin concentration is directly related to angiogenesis, the key factor required for tumor growth and metastases [29]. In addition, the proportions of oxy- and deoxyhemoglobin change in such a tumor due to its metabolism [30]. By measuring concentrations of the breast components, discrimination of benign and malignant tumors may be possible with diffuse optical imaging (**Figures 2A and 2B**).

Clinical studies thus far performed on optical breast imaging without contrast agent are shown in **Table 1** [13-24,31-34].

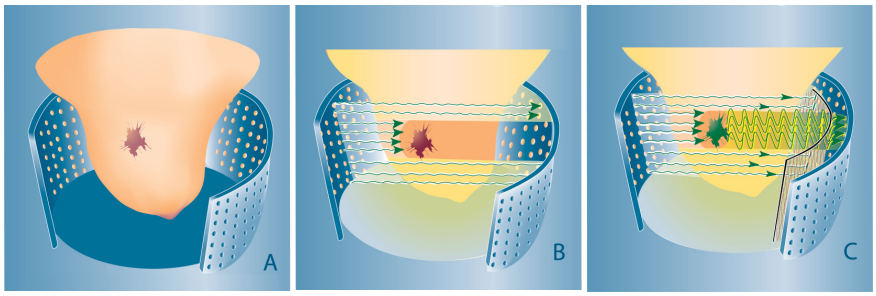

Figure 2. Concepts of optical breast imaging. A-C Optical breast imaging lay-out (A) with source and detector fibres covering the entire breast surface. In optical breast imaging without contrast agent (B) higher absorption by tumor components (predominantly hemoglobin) results in decreased light intensity registered by the detectors. In optical breast imaging with contrast agent (C) a fluorescent probe is administered that ideally accumulates at the tumor site. After excitation, light is emitted at a higher wavelength by this agent and the excitation wavelength is filtered to only detect the fluorescent signal.

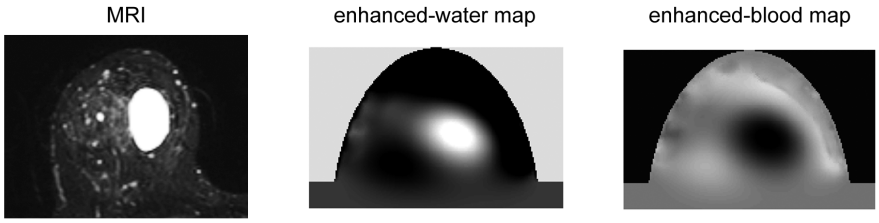

Figure 3. T2 weighted MRI with fat-suppression compared to the enhanced-water map and the enhanced-blood map of the optical data set. The cyst shows a high signal intensity on the MRI and the enhanced-water map (high water content), and a low signal intensity on the enhanced-blood map (low blood content) [28].

Table 1. Clinical studies on optical breast imaging without contrast agent

Author (year)	Number of patients	System			Pre-knowledge on localisation
		Technique	*Wavelengths (in nm)**	*Imaging approach*	
Rinneberg (2005)	159	Time domain	**670**, **785**, 843, 884	Transillumination	Yes X-ray and MRI
Floery (2005)	100	Continuous wave	808	Tomography	Yes X-ray
Taroni (2005)	194	Time domain	637, 656, 683, **785**, 913, 975	Transillumination	Yes X-ray
Yates (2005)	24	Time domain	**780, 815**	Tomography	Yes Different modalities (e.g. MRI, US)
Zhu (2005)	65	Frequency domain	**780, 830**	Handheld with US guidance	Yes US
Götz (1998)	119	Frequency domain	**690, 750, 790, 860**	Transillumination	Yes X-ray
Tomandl (1995)	102	Frequency domain	**794, 850**	Transillumination	No
Franceschini (1997)	15	Frequency domain	**690, 810**	Transillumination	Yes X-ray and US
Chance (2005)	116	Continuous wave	**760, 805, 850**	Handheld	Yes unspecified
Gu (2004)	6	Continuous wave	**785, 808, 830**	Tomography	Yes X-ray and US
Hsiang (2005)	6	Frequency domain	**658, 682, 785, 810, 830, 850**	Handheld	Yes MRI
Intes (2005)	49	Time domain	**760, 780, 830, 850**	Tomography with breast compression	Yes X-ray
Durduran (2005)	7	Continuous wave	**785**	Handheld	Yes Palpation
Cerussi (2006)	57	Frequency domain + Continuous wave	**650-1000**	Handheld	Yes X-ray
Cerussi (2007)	11	Frequency domain + Continuous wave	**650-1000**	Handheld	Yes X-ray, US, palpation
Ntziachristos (2002)	14	Time domain	**780, 830**	Transillumination Combined with MRI	Yes Concurrent MRI

*Wavelengths in bold were used in all measurements, others only in part of the measurements; † When there were less than 5% invasiveness available. US: ultrasound; MRI: magnetic resonance imaging

Detection cut-off	Detection rate		
	Invasive carcinomas†	*In situ carcinomas*†	*Benign lesions*
Weak contrast, tumor only detectable provided exact location of inhomogeneity is known	0.95 (80/84)	0.78 (7/9)	0.89 (39/44)
Increased absorption; an area clearly more luminous than the surrounding parenchyma	0.76 (32/42)	0.38 (3/5)	0.33 (18/55)
Weak contrast	0.89 (50/56)	-	0.60 (101/169)
Weak contrast	*0.50 (1/2)*		0.91 (10/11)
Maximum hemoglobin concentration > 95 μmol/L	1.00 (8/8)	-	0.04 (3/73)
Clearly visible contrast	*0.86 (51/59)*		0.58 (14/24)
Based on non-specified criteria developed by an experienced radiologist who compared optical images with X-ray and US findings	*0.58 (23/40)*		0.27 (6/22)
Visible optical inhomogeneity corrected for edge effects (so-called dimensionless N value)	*0.73 (11/15)*		-
Relatively high hemoglobin content and low oxygenation	*0.95 (42/44)*		0.94 (68/72)
Lower absorption and/or scattering coefficients than surrounding parenchyma	-	-	0.83 (5/6)
Optical index > 2.4	1.00 (6/6)	-	-
Malignant lesions show higher hemoglobin content and lower oxygenation than surrounding parenchyma			
Blood flow increases to 230% in malignant lesions and to 153% in benign lesions			
Malignant lesions show increase in deoxyhemoglobin, oxyhemoglobin, and water (>50%), and decrease in lipid (~20%) compared to normal tissue; tumor spectra appeared age-dependent			
Responders to chemotherapy showed significant decrease in deoxyhemoglobin (27%) and relative water content (20%) compared to non-responders; oxyhemoglobin decreased in both groups, but significantly more in responders (33%) compared to non-responders (18%)			
Malignant lesions show higher hemoglobin content and lower oxygenation than surrounding parenchyma			

5% in situ carcinomas, this group was combined with invasive carcinomas (italic), and also when there was no information on

Case reports are not presented in this overview. Most studies report the number of lesions detected on the optical images (detection rates), irrespective of their classification (benign/malignant). Sensitivity and specificity have not been determined yet. Detection rates for carcinomas range from 0.50 to 1.00 in these studies. Studies performed with handheld devices report high detection rates (0.95-1.00) [20-22]. Detection rates for the transillumination approach range from 0.58 to 0.94 [13-17]. With tomography, carcinomas were detected in 74% and 50% respectively [18,19]. Detection rates of benign lesions vary between 0.04 and 0.94 [14-21,31]. Benign cysts were detected with tomography in 83% [31]. Malignant lesions were detected by their higher optical attenuation compared to the surrounding tissue, mainly related to increased light absorption by their higher hemoglobin content [20-24,33,34]. Solid benign lesions were more difficult to detect, but sometimes showed increased attenuation, although to a lesser extent than malignant lesions [14-21,31]. As opposed to the other lesions, benign cysts showed lower optical attenuation, associated with lower light absorption or scattering by their high water content [16,24,31]. Some groups found lower oxygenation for carcinomas compared to the surrounding tissue [21,23,24,33]. In addition, Cerussi et al. described increased water content and decreased lipid content in malignant lesions, and age-dependency of the tumor spectra [33]. This group also investigated the response to chemotherapy in breast cancer patients and reported significant decrease in deoxyhemoglobin (27%) and relative water content (20%) in responders compared to non-responders; oxyhemoglobin decreased in both groups, but significantly more in responders (33%) compared to non-responders (18%) [32].

Optical breast imaging with contrast agent

In optical breast imaging with contrast agent, fluorescent probes are used that emit photons at predefined wavelengths after excitation by laser light. These photons are detected while the light of the excitation wavelength is filtered (**Figure 2C**).

Fluorescent probes that target molecules specific for breast cancer are currently being developed and validated in preclinical animal studies. An overview of these studies is provided in **Table 2** [35-43]. All animal studies were performed with breast cancer mouse models with NIR continuous wave optical imaging devices. In most studies, transillumination was used, whereas two research groups applied a tomographic approach [35,41]. A variety of optical probes for specific breast cancer cell targeting has been designed. The group of Bremer and Mahmood et al. developed so-called “smart” optical probes to target proteases [35-37]. These

probes are non-fluorescent in their native state, but convert to a highly fluorescent active state when their backbone is cleaved by cathepsins. In four animals with human breast cancer xenografts, tumors showed strong fluorescence signal in vivo after injection of the cathepsin-sensing probe. Signal-to-noise ratio (SNR) after 48 hours was 21 in tumors with mean diameters < 2 mm. The smallest detectable tumor was < 1 mm in diameter [37]. This technique using smart optical probes also showed good results in transgenic mice that spontaneously developed tumors. With transillumination, all 24 tumors in 10 animals could be clearly delineated after injection of the cathepsin-sensing probe. Tumor fluorescence in vivo was significantly higher compared to background fluorescence measured in the adjacent skin (380 $\pm$ 23 AU vs. 179 $\pm$ 8 AU; $p < 0.01$). Tomography was performed in four animals; coregistration with MRI revealed a strong fluorescence signal within the tumor tissue and virtually no background fluorescence in the corresponding slices [35]. Differences in tumor aggressiveness could be depicted by this technique when comparing eight well-differentiated, with eight highly invasive metastatic human breast cancer models. The highly aggressive cancers, which expressed higher levels of proteases, revealed significantly higher tumor fluorescence compared to well-differentiated tumors (861 $\pm$ 88 AU vs. 566 $\pm$ 36 AU; $p < 0.01$). Tumors in noninjected animals were not visible due to identical autofluorescence in tumor and adjacent skin [36].

Three research groups focused on targeting the human epidermal growth factor-2 (HER2) receptor with probes containing the humanized monoclonal anti-HER2 antibody trastuzumab, Herceptin, coupled to a NIR dye [39,41,42]. Hilger et al. compared such probes in three animals with HER2-overexpressing tumors and three animals with normal HER2-expression. Distinctly higher relative fluorescence signals were found in the tumors with HER2-overexpression compared to the tumors with normal HER2-expression (e.g. 16 hours after injection: 2.2 $\pm$ 0.1 vs. 1.3 $\pm$ 0.2) [39]. Sampath and colleagues designed a dual-labelled probe consisting of trastuzumab as targeting component, a ^{111}In complex as radiotracer, and a NIR dye as optical signal generator. Fluorescence signal intensities obtained after injection with this HER2-specific probe in three mice bearing HER2-overexpressing tumors, were significantly higher (tumor-to-muscle ratio (TMR) 2.25 $\pm$ 0.2) compared to fluorescence signal intensities after injection of two non-specific probes (TMR 1.35 $\pm$ 0.1 and 1.44 $\pm$ 0.18; $p \leq 0.001$), each administered in five mice. TMR in five mice pre-injected with trastuzumab before receiving the HER2-specific probe was significantly lower than in the mice not pre-injected ($p = 0.0048$). Single photon emission computed tomography (SPECT) fused with computed tomography (CT)

Table 2. Preclinical studies on optical breast imaging with contrast agent

Author (year)	Subjects (n)	System			Use of other modality
		Technique	Wavelengths (nm) Excitation/ Emission	Imaging approach	
Bremer (2005)	Transgenic mice, spontaneously developing breast cancer (10)	Continuous wave	610-650/680-720; Tomography: 670	Transillumination & Tomography (n=4)	MRI
Wang (2007)	Mice bearing human breast cancer xenograft in thigh	Continuous wave	785	Transillumination	SPECT/CT
Mahmood (1999)	Mice bearing human breast cancer xenograft in mammary fat pad or thigh (4)	Continuous wave	610-650/680-720	Transillumination	-
Bremer (2002)	Mice bearing aggressive (8) or non-aggressive (8) human breast cancer xenograft in mammary fat pad	Continuous wave	610-650/680-720	Transillumination	-
Sampath (2007)	Mice bearing HER2-overexpressing human breast cancer xenograft in thigh (18)	Continuous wave	785/830	Transillumination	SPECT/CT
Ke (2003)	Mice bearing EGF receptor-positive / negative human breast cancer xenograft in mammary fat pad	Continuous wave	660/710	Transillumination	-
Hilger (2004)	Mice bearing human breast cancer xenograft in thigh, with or without HER2-overexpression (6)	Continuous wave	675/708	Transillumination	-
Montet (2005)	Mice bearing HER2-overexpressing human breast cancer xenograft in mammary fat pad (5)	Continuous wave	672, 748	Tomography	MRI and SPECT/ CT
Yang (2007)	Mice bearing human breast cancer xenograft in forepaw	Continuous wave	730/790	Transillumination	X-ray

MPEG: methoxypolyethylene glycol; NIR: near-infrared; MRI: magnetic resonance imaging; SPECT: single photon emission factor; ICG: indocyanine green;

Target	Optical imaging probe	Injection	Results
Cathepsin-B (protease)	Cathepsin-sensing probe with Cy5.5 fluorochrome residues bound to a poly-lysine backbone sterically shielded through MPEG side chains, activated by enzymatic cleavage of the backbone	intravenous 2 nmol	Strong fluorescence signal within tumor tissue with virtually no background fluorescence in corresponding slices
Interleukin-11 receptor alpha-chain	Dual-labeled probe consisting of a cyclic nona-peptide as targeting component, a ^{111}In complex as radiotracer, and a NIR dye as optical signal generator	intravenous 2 nmol	Both optical imaging and SPECT/CT show high uptake of probe at the tumor site
Cathepsins B and H (pro-teases)	Ezyme-activatable probe with Cy5.5 fluorochrome residues bound to a poly-lysine backbone sterically shielded through MPEG side chains, activated by enzymatic cleavage of the backbone	intravenous 10 nmol	Strong fluorescence signal within tumor tissue, detection of tumor < 1mm
Cathepsin-B (protease)	Cathepsin-sensing probe with Cy5.5 fluorochrome residues bound to a poly-lysine backbone sterically shielded through MPEG side chains, activated by enzymatic cleavage of the backbone	intravenous 2 nmol	Clearly visible fluorescence signal in all tumors; aggressive tumors -with strong-er cathepsin-B expression- showed significantly higher fluorescence values than non-aggressive tumors
HER2	Dual-labeled probe consisting of trastuzumab (monoclonal antibody) as targeting component, a ^{111}In complex as radiotracer, and a NIR dye as opti-cal signal generator	intravenous 0.43 nmol	Strong fluorescence signal at tumor site, uptake significantly higher compared to non-specific probes and to mice pretreated with trastuzumab; SPECT/CT showed similar patterns in probe uptake
EGF receptor	EGF-Cy5.5 conjugate	intravenous 1 nmol	Clearly visible fluorescence signal in EGF receptor-positive tumors, no uptake in EGF receptor-negative tumors, antibody C225 specifically blocked uptake
HER2	Herceptin (monoclonal antibody) coupled to Cy5.5	intravenous	Distinct fluorescence signal in HER2-overexpressing tumors compared to normal expressing tumors
Angiogenesis and HER2	Angiosense-750 (a NIR fluorochrome labelled vascular marker), and Herceptin (monoclonal antibody) coupled to Cy5.5	intravenous co injection	Significant fluorescence signal at tumor site for both the HER2 and the angio-genesis targeting probe
Non-specific tumor accumu-lation	Core-cross-linked polymeric micelles (CCPMs) conjugated with Cy7-like NIR dye (intravenous injection 4.5 nmol)	intravenous	Strong fluorescence signal at tumor site

computed tomography; CT: computed tomography; HER: human epidermal growth factor receptor; EGF: epidermal growth

showed similar patterns in probe uptake [42]. Montet et al. co injected two optical probes, a NIR fluorochrome labelled vascular marker (Angiosense-750) and Herceptin coupled to a NIR dye, at the same time in a HER2-overexpressing breast cancer mouse model. This model showed significant tumoral uptake of both the vascular marker (3.1 ± 0.5%) and the HER2-specific probe (14.7 ± 1.3 pmol), indicating that studying two different physiologic variables simultaneously is feasible with this technique [41].

Ke et al. used human epidermal growth factor (EGF) coupled to a NIR dye to detect the EGF receptor in breast cancer cells. Fluorescence signal was clearly visualized in EGF receptor-positive tumors but not in EGF receptor-negative tumors. The uptake of the probe was blocked by the anti-EGF receptor antibody C225, indicating specificity of the probe for the EGF receptor [40]. Another target for breast cancer detection with fluorescent probes is the Interleukin-11 receptor alpha-chain, investigated by Wang et al. They designed a dual-labeled probe consisting of a cyclic nonapeptide as targeting component, a ^{111}In complex as radiotracer, and a NIR dye as optical signal generator. Both optical imaging and SPECT/CT showed high uptake of this probe at the tumor site in mice [44].

Non-specific tumor accumulation through polymeric micelles was studied by Yang et al. These micelles remained in the circulation for a prolonged time and effectively accumulated at the tumor site through microvascular hyperpermeability, displaying a strong fluorescence signal [45].

Aforementioned studies demonstrate proof of principle of optical breast imaging with fluorescent probes in an animal model. Thus far, only two clinical optical breast imaging studies with contrast agent have been described in literature, both using Indocyanine Green (ICG) in 3 patients [46,47]. ICG is a non-specific blood pool agent that is both absorbing and fluorescent in the NIR range. It is used clinically, mainly for retinal angiography and liver function tests. Both studies observed differences in ICG pharmacokinetics between malignant and benign lesions on the optical images. In the study by Intes et al. a maximal increase in absorption of 0.042 cm^{-1} was measured in an invasive ductal carcinoma. For an adenoma, an absorption increase of 0.025 cm^{-1} was found. The absorption increase observed in a fibroadenoma was ~0.03 cm^{-1} [46]. Ntziachristos et al. found in a patient with invasive ductal carcinoma an increase in absorption at the tumor position of ~0.05 cm^{-1}. The increase in absorption in a fibroadenoma was ~0.03 cm^{-1}. In healthy tissue some moderate enhancements were seen of ~0.025 cm^{-1} [47].

Discussion

Clinical studies performed on optical breast imaging without contrast agent showed cancer detection rates ranging from 0.50 to 1.00 for different optical imaging systems. Since knowledge on lesion localisation within the breast was available in almost all studies, true detection rates will probably be substantially lower. Information available from literature is too scarce to determine sensitivity and specificity of optical breast imaging without the use of contrast agent for breast cancer detection. Albeit the differences found in hemoglobin and oxygenation between carcinomas and benign lesions, the sensitivity and specificity achieved by optical breast imaging without contrast agent seem currently not sufficient to use this modality in clinical practice. In a study setting, optical breast imaging without contrast agent is presently explored to evaluate the response to neoadjuvant chemotherapy in patients with a known breast cancer. These patients have large tumors of which the position is known a priori. Biochemical changes in tumor tissue often precede anatomical alterations (e.g. tumor shrinkage) after chemotherapy. Optical breast imaging can thus potentially be applied to predict the response to neoadjuvant chemotherapy earlier in the treatment cycle.

Preclinical studies showed that probes designed to target specific proteins characteristic for breast cancer can successfully detect breast tumors using optical imaging in animal models. Optical imaging probes have been developed to target the following proteins: Cathepsin B and H, HER2, EGF receptor, and Interleukin-11 receptor alpha-chain. Blood pool agents without a specific target, such as Angiosense-750, ICG, and polymeric micelles, have also been assessed to visualize tumors and their associated angiogenesis. With the exception of ICG, the optical probes have not yet been tested in humans. In breast cancer mouse models, optical imaging with contrast agent showed very promising results. Strong fluorescence signal was obtained from tumor tissue in comparison to tissue that did not overexpress the target of interest. Most studies confirmed their results with histology and/or SPECT/CT imaging of probe uptake.

As mentioned before, currently used breast imaging modalities have some limitations. Sensitivity of X-ray mammography for breast cancer detection is reduced in women with dense breasts (62%) [5]. This issue is especially important since these women have an increased breast cancer risk [6]. Breast MRI has high sensitivity (> 95%) and is currently used in clinical practice as adjunct to X-ray mammography for screening of high risk patients [48,49]. Despite substantial improvements in imaging technology, MRI in general only allows lesion detection and classification when tumor size is 5 mm or more [50]. As lesion size upon discovery decreases

with more efficient screening programs, the need for a non-invasive tool that provides more specific information on small breast lesions becomes obvious.
Optical breast imaging could be the modality with this potential, because of its molecular imaging capability. Molecular imaging is defined as the visualization, characterization, and measurement of biological processes at the molecular and cellular levels in humans and other living systems [51]. Major advantage is that molecular changes associated with cancer formation may possibly be detected in a very early stage, even before anatomical changes occur. With the use of target-specific probes, optical imaging could be a valid candidate for the early detection of breast cancer, e.g. in young women with dense breasts. Other potential applications of this technique may be the selection of appropriate treatment and evaluation of response to treatment in breast cancer patients. If molecular characteristics of breast tumors can be identified in vivo using optical breast imaging with contrast agents, this molecular tumor profile can be used to select appropriate therapies for individual patients (personalized medicine). Moreover, response to therapy can be evaluated using the same imaging technique.
Important advantages of optical imaging with contrast agent are that it does not use any radioactive components (as in PET and SPECT), and that its sensitivity for probe detection is very high (possibly in the nanomolar to the 100 picomolar concentration range) as compared to MRI (micromolar to millimolar range). Moreover, optical imaging uses no ionizing radiation and can thus be used repeatedly, also in younger women. Non-toxic fluorescent probes that can be applicable in clinical practice are currently being developed. At present, a single molecular marker that is expressed by all different types of breast cancers is not available. Likely, a combination of fluorescent probes would have to be administered to be able to detect all breast cancer types with this technique. The use of a single probe targeting one of the breast cancer types could nevertheless be valuable to select patients for, and monitor certain cancer treatments. The need to inject one or more contrast agent(s) intravenously prior to the optical imaging studies may comprise some practical limitations. For instance, interactions between the probes need to be thoroughly investigated, as well as the optimal imaging time points after their injection. Another limitation of optical breast imaging is its low spatial resolution. Spatial resolution in optical imaging is dependent on the length of the light pathways, resulting in lower spatial resolution when tissue penetration is deeper. If detailed anatomical information is needed also, a second imaging technique or a multi-modality imaging approach in which the optical scanner is combined with another modality (e.g. MRI, ultrasound) could offer a solution.

In conclusion, diagnostic performance of optical breast imaging without contrast agent is likely inadequate for clinical application. Development of contrast agents that target specific molecular changes associated with breast cancer formation is the opportunity for clinical success of optical breast imaging.

References

1. Garcia M, Jemal A, Ward EM, Center MM, Hao Y, Siegel RL, Thun MJ. Global Cancer Facts & Figures 2007. Atlanta, GA, American Cancer Society, 2007.
2. Fletcher SW, Elmore JG. Clinical practice. Mammographic screening for breast cancer. N.Engl.J.Med. 2003; 348: 1672-1680.
3. Humphrey LL, Helfand M, Chan BK, Woolf SH. Breast cancer screening: a summary of the evidence for the U.S. Preventive Services Task Force. Ann.Intern.Med. 2002; 137: 347-360.
4. Buist DS, Porter PL, Lehman C, Taplin SH, White E. Factors contributing to mammography failure in women aged 40-49 years. J.Natl.Cancer Inst. 2004; 96: 1432-1440.
5. Carney PA, Miglioretti DL, Yankaskas BC, Kerlikowske K, Rosenberg R, Rutter CM et al. Individual and combined effects of age, breast density, and hormone replacement therapy use on the accuracy of screening mammography. Ann.Intern.Med. 2003; 138: 168-175.
6. Boyd NF, Guo H, Martin LJ, Sun L, Stone J, Fishell E et al. Mammographic density and the risk and detection of breast cancer. N.Engl.J.Med. 2007; 356: 227-236.
7. Cutler M. Transillumination as an aid in the diagnosis of breast lesions. Surgery, gynecology & obstetrics 1929; 48: 721-728.
8. Gibson AP, Hebden JC, Arridge SR. Recent advances in diffuse optical imaging. Phys.Med. Biol. 2005; 50: R1-43.
9. Arridge SR, Schweiger M. Image reconstruction in optical tomography. Philos.Trans.R.Soc. Lond B Biol.Sci. 1997; 352: 717-726.
10. Schweiger M, Arridge SR, Nissila I. Gauss-Newton method for image reconstruction in diffuse optical tomography. Phys.Med.Biol. 2005; 50: 2365-2386.
11. Schweiger M, Nissila I, Boas DA, Arridge SR. Image reconstruction in optical tomography in the presence of coupling errors. Appl.Opt. 2007; 46: 2743-2756.
12. Arridge SR, Hiraoka M, Schweiger M. Statistical basis for the determination of optical pathlength in tissue. Phys.Med.Biol. 1995; 40: 1539-1558.
13. Franceschini MA, Moesta KT, Fantini S, Gaida G, Gratton E, Jess H et al. Frequency-domain techniques enhance optical mammography: initial clinical results. Proc.Natl.Acad.Sci.U.S.A 1997; 94: 6468-6473.
14. Gotz L, Heywang-Kobrunner SH, Schutz O, Siebold H. [Optical mammography in preoperative patients]. Aktuelle Radiol. 1998; 8: 31-33.
15. Rinneberg H, Grosenick D, Moesta KT, Mucke J, Gebauer B, Stroszczynski C et al. Scanning time-domain optical mammography: detection and characterization of breast tumors in vivo. Technol.Cancer Res.Treat. 2005; 4: 483-496.

16. Taroni P, Torricelli A, Spinelli L, Pifferi A, Arpaia F, Danesini G et al. Time-resolved optical mammography between 637 and 985 nm: clinical study on the detection and identification of breast lesions. Phys.Med.Biol. 2005; 50: 2469-2488.

17. Tomandl B, Doinghaus K, Schulz-Wendtland R. [Laser mammography with near-infrared light]. Rontgenpraxis 1995; 48: 197-201.

18. Floery D, Helbich TH, Riedl CC, Jaromi S, Weber M, Leodolter S et al. Characterization of benign and malignant breast lesions with computed tomography laser mammography (CTLM): initial experience. Invest Radiol. 2005; 40: 328-335.

19. Yates T, Hebden JC, Gibson A, Everdell N, Arridge SR, Douek M. Optical tomography of the breast using a multi-channel time-resolved imager. Phys.Med.Biol. 2005; 50: 2503-2517.

20. Zhu Q, Cronin EB, Currier AA, Vine HS, Huang M, Chen N et al. Benign versus malignant breast masses: optical differentiation with US-guided optical imaging reconstruction. Radiology 2005; 237: 57-66.

21. Chance B, Nioka S, Zhang J, Conant EF, Hwang E, Briest S et al. Breast cancer detection based on incremental biochemical and physiological properties of breast cancers: a six-year, two-site study. Acad.Radiol. 2005; 12: 925-933.

22. Hsiang D, Shah N, Yu H, Su MY, Cerussi A, Butler J et al. Coregistration of dynamic contrast enhanced MRI and broadband diffuse optical spectroscopy for characterizing breast cancer. Technol.Cancer Res.Treat. 2005; 4: 549-558.

23. Intes X. Time-domain optical mammography SoftScan: initial results. Acad.Radiol. 2005; 12: 934-947.

24. Ntziachristos V, Yodh AG, Schnall MD, Chance B. MRI-guided diffuse optical spectroscopy of malignant and benign breast lesions. Neoplasia. 2002; 4: 347-354.

25. Nissila I, Hebden JC, Jennions D, Heino J, Schweiger M, Kotilahti K et al. Comparison between a time-domain and a frequency-domain system for optical tomography. J.Biomed. Opt. 2006; 11: 064015.

26. Siegel A, Marota JJ, Boas D. Design and evaluation of a continuous-wave diffuse optical tomography system. Optics Express 1999; 4: 287-298.

27. Arridge SR, Lionheart WR. Nonuniqueness in diffusion-based optical tomography. Opt. Lett. 1998; 23: 882-884.

28. van de Ven SM, Wiethoff AJ, van der Voort M, Nielsen T, Brendel B, Bakker L et al. Spectroscopic Diffuse Optical Imaging of the Breast: first clinical experiences in the characterization of cysts. Joint Molecular Imaging Conference 2007. Providence, RI. Academy of Molecular Imaging & Society for Molecular Imaging.

29. Rice A, Quinn CM. Angiogenesis, thrombospondin, and ductal carcinoma in situ of the breast. J.Clin.Pathol. 2002; 55: 569-574.

30. Vaupel P, Harrison L. Tumor hypoxia: causative factors, compensatory mechanisms, and cellular response. Oncologist. 2004; 9: 4-9.

31. Gu X, Zhang Q, Bartlett M, Schutz L, Fajardo LL, Jiang H. Differentiation of cysts from solid tumors in the breast with diffuse optical tomography. Acad.Radiol. 2004; 11: 53-60.

32. Cerussi A, Hsiang D, Shah N, Mehta R, Durkin A, Butler J et al. Predicting response to breast cancer neoadjuvant chemotherapy using diffuse optical spectroscopy. Proc.Natl.Acad. Sci.U.S.A 2007; 104: 4014-4019.

33. Cerussi A, Shah N, Hsiang D, Durkin A, Butler J, Tromberg BJ. In vivo absorption, scattering, and physiologic properties of 58 malignant breast tumors determined by broadband diffuse optical spectroscopy. J.Biomed.Opt. 2006; 11: 044005.

34. Durduran T, Choe R, Yu G, Zhou C, Tchou JC, Czerniecki BJ et al. Diffuse optical measurement of blood flow in breast tumors. Opt.Lett. 2005; 30: 2915-2917.

35. Bremer C, Ntziachristos V, Weitkamp B, Theilmeier G, Heindel W, Weissleder R. Optical imaging of spontaneous breast tumors using protease sensing 'smart' optical probes. Invest Radiol. 2005; 40: 321-327.

36. Bremer C, Tung CH, Bogdanov A, Jr., Weissleder R. Imaging of differential protease expression in breast cancers for detection of aggressive tumor phenotypes. Radiology 2002; 222: 814-818.

37. Mahmood U, Tung CH, Bogdanov A, Jr., Weissleder R. Near-infrared optical imaging of protease activity for tumor detection. Radiology 1999; 213: 866-870.

38. Wang LV. Optical tomography for biomedical applications. IEEE Eng Med.Biol.Mag. 1998; 17: 45-46.

39. Hilger I, Leistner Y, Berndt A, Fritsche C, Haas KM, Kosmehl H et al. Near-infrared fluorescence imaging of HER-2 protein over-expression in tumour cells. Eur.Radiol. 2004; 14: 1124-1129.

40. Ke S, Wen X, Gurfinkel M, Charnsangavej C, Wallace S, Sevick-Muraca EM et al. Near-infrared optical imaging of epidermal growth factor receptor in breast cancer xenografts. Cancer Res. 2003; 63: 7870-7875.

41. Montet X, Ntziachristos V, Grimm J, Weissleder R. Tomographic fluorescence mapping of tumor targets. Cancer Res. 2005; 65: 6330-6336.

42. Sampath L, Kwon S, Ke S, Wang W, Schiff R, Mawad ME et al. Dual-labeled trastuzumab-based imaging agent for the detection of human epidermal growth factor receptor 2 overexpression in breast cancer. J.Nucl.Med. 2007; 48: 1501-1510.

43. Yang M, Baranov E, Li XM, Wang JW, Jiang P, Li L et al. Whole-body and intravital optical imaging of angiogenesis in orthotopically implanted tumors. Proc.Natl.Acad.Sci.U.S.A 2001; 98: 2616-2621.

44. Wang W, Ke S, Kwon S, Yallampalli S, Cameron AG, Adams KE et al. A new optical and nuclear dual-labeled imaging agent targeting interleukin 11 receptor alpha-chain. Bioconjug.Chem. 2007; 18: 397-402.

45. Yang Z, Zheng S, Harrison WJ, Harder J, Wen X, Gelovani JG et al. Long-circulating near-infrared fluorescence core-cross-linked polymeric micelles: synthesis, characterization, and dual nuclear/optical imaging. Biomacromolecules. 2007; 8: 3422-3428.

46. Intes X, Ripoll J, Chen Y, Nioka S, Yodh AG, Chance B. In vivo continuous-wave optical breast imaging enhanced with Indocyanine Green. Med.Phys. 2003; 30: 1039-1047.

47. Ntziachristos V, Yodh AG, Schnall M, Chance B. Concurrent MRI and diffuse optical tomography of breast after indocyanine green enhancement. Proc.Natl.Acad.Sci.U.S.A 2000; 97: 2767-2772.

48. Lehman CD, Isaacs C, Schnall MD, Pisano ED, Ascher SM, Weatherall PT et al. Cancer yield of mammography, MR, and US in high-risk women: prospective multi-institution breast cancer screening study. Radiology 2007; 244: 381-388.

49. Lehman CD, Gatsonis C, Kuhl CK, Hendrick RE, Pisano ED, Hanna L et al. MRI evaluation of the contralateral breast in women with recently diagnosed breast cancer. N.Engl.J.Med. 2007; 356: 1295-1303.

50. Liberman L, Mason G, Morris EA, Dershaw DD. Does size matter? Positive predictive value of MRI-detected breast lesions as a function of lesion size. AJR Am.J.Roentgenol. 2006; 186: 426-430.

51. Mankoff DA. A definition of molecular imaging. J.Nucl.Med. 2007; 48: 18N, 21N.

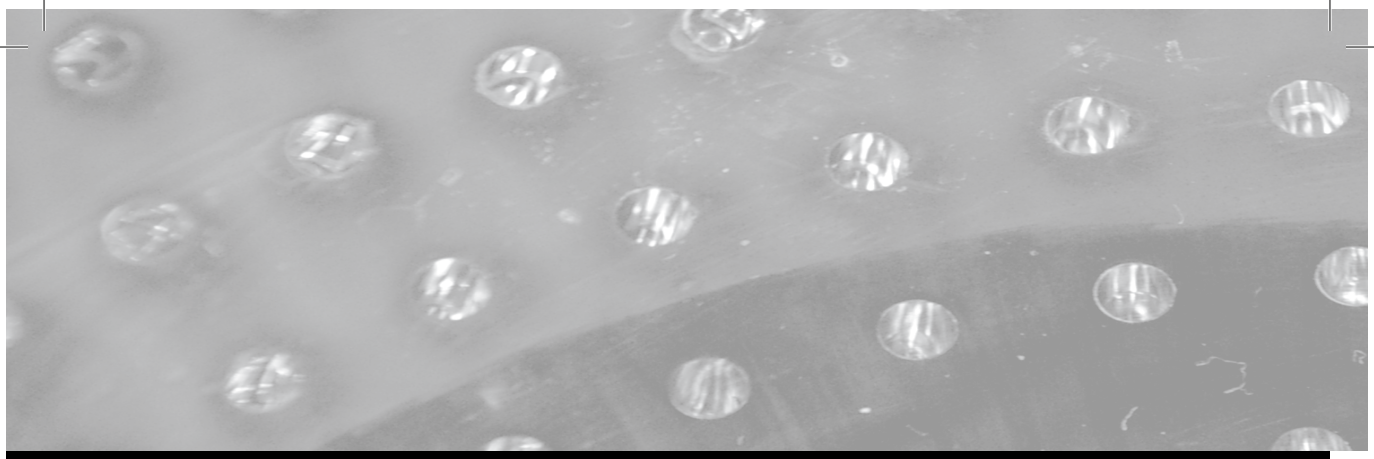

Authors

S.M.W.Y. van de Ven, S.G. Elias, A.J. Wiethoff, M. Van der Voort, T. Nielsen, B. Brendel, C. Bontus, R. Nachabe, R. Harbers, M. Van Beek, L.. Bakker, M.B. Van der Mark, W.P.Th.M. Mali, P. Luijten.

European Radiology 2009;19:1108-1113

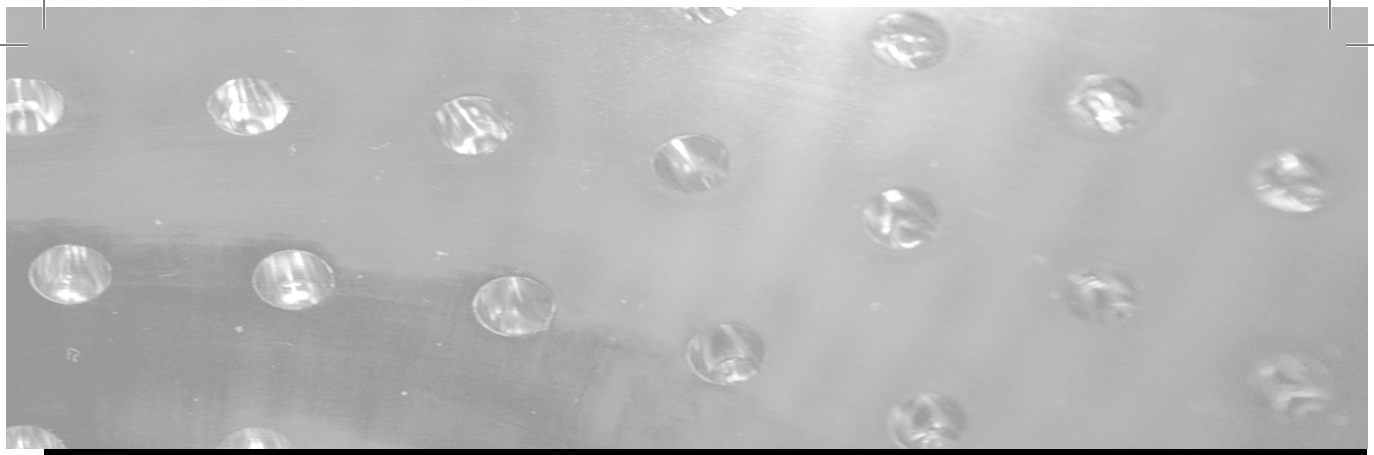

Diffuse optical tomography of the breast:

preliminary findings of a new prototype and comparison with Magnetic Resonance Imaging

Abstract

Purpose

Evaluation of a prototype Diffuse Optical Tomography (DOT) system.

Methods

Seventeen women with eighteen breast lesions (10 invasive carcinomas, 2 fibroadenomas, and 6 benign cysts; diameters 13-54 mm) were evaluated with DOT and Magnetic Resonance Imaging (MRI). A substantial fraction of the original 36 recruited patients could not be examined by this prototype due to technical problems. A region of interest (ROI) was drawn at the lesion position as derived from MRI and at the mirror image site in the contralateral healthy breast. ROIs were assessed quantitatively and also qualitatively, by two observers independently in two separate readings. Intra- and interobserver agreements were calculated using kappa statistics (κ) and intraclass correlation coefficients (ICC). Discriminatory values for presence of malignancy were determined by Receiver Operating Characteristic (ROC) analyses.

Results

Intra-observer agreements were excellent (κ 0.88 and 0.88; ICC 0.978 and 0.987), interobserver agreements were good-excellent (κ 0.77-0.95; ICC 0.96-0.98). Discriminatory values for presence of malignancy were 0.92-0.93 and 0.97-0.99 for quantitative and qualitative ROC analysis, respectively.

Conclusion

This DOT system has the potential to discriminate malignant from benign breast tissue in a reproducible qualitative and quantitative manner. Important technical improvements are required before this technique is ready for clinical application.

Introduction

Diffuse Optical Tomography (DOT) employs light in the near-infrared (NIR) spectrum where light absorption is minimal (650-1000 nm), to assess the optical properties of tissue [1]. Information on the composition of the breast tissue, i.e. relative concentrations of oxy- and deoxyhemoglobin, water and lipid can be obtained by combining images acquired at different wavelengths (spectroscopic imaging). Hemoglobin concentration in a malignant tumor is directly related to angiogenesis [2], and proportions of oxy- and deoxyhemoglobin change due to its metabolism [3]. By using multiple wavelengths to measure concentrations of the main chromophores in the breast, discrimination between benign and malignant tissue may be possible with DOT. This technique could potentially have added value to currently used breast imaging modalities: mammography, ultrasound, and dynamic contrast enhanced magnetic resonance imaging (DCE-MRI), which all have drawbacks regarding sensitivity and specificity in the diagnosis, early detection, and treatment monitoring of breast cancer [4-7].
Since optical breast imaging is still in its infancy with several techniques being explored [8], thorough system evaluation and validation is essential. We used MRI as a benchmark for the first diagnostic evaluation of our new prototype since it provides three-dimensional data and excellent soft tissue contrast. We initiated the evaluation under optimal settings in a small patient group by (1) investigating optical properties of different types of breast lesions; (2) assessing the potential to discriminate between benign and malignant tissue with a known lesion position; and (3) assessing the effect of intra- and interobserver variability on the obtained results.

Methods

Patients

Seventeen women (mean age 54, range 22 to 85) diagnosed with one or more breast lesion(s) 13 to 54 mm in diameter were prospectively included between August 2006 and September 2007 from the University Medical Center Utrecht and the Diakonessenhuis Utrecht, The Netherlands. Patients were referred either by their family doctor or breast surgeon for diagnostic purposes, or via the screening program for further work-up. They were asked to participate in our study if a BI-RADS (Breast Imaging Reporting and Data System) 2-5 lesion was diagnosed on mammography/ultrasound, and if needle aspiration was not performed before the other study procedures could be executed, since this could influence the

optical images. All patients underwent optical imaging and DCE-MRI. In total, 36 patients were recruited consecutively, however, 19 of these were excluded due to (a) technical limitations of our DOT system, i.e. leakage of matching fluid from the system (6 patients) and the inability to measure lesions located close to the patient's chest wall due to the geometry of the cup (8 patients); and (b) the inability to undergo DCE-MRI for reason of claustrophobia (3 patients) and physical limitations (2 patients did not fit in the MRI bore). The protocol was approved by the ethics committee of the University Medical Center Utrecht, and written informed consent was obtained from all patients.

Optical Imaging

DOT was performed on a Philips Diffuse Optical Tomography system (Philips Healthcare, Best, The Netherlands). A patient was placed in the prone position on the system bed with her breast suspended in a cup on which 507 optical fibers are mounted (**Figure 1**). The 253 source fibers are connected to four continuous wave solid-state lasers (wavelengths: 690, 730, 780, and 850 nm) and interleaved with 254 detector fibers. The cup was filled with a matching fluid, which has optical properties similar to an average breast, to enable a stable optical coupling between fibers and breast, and to eliminate optical short cuts around the breast. During imaging, the breast was sequentially illuminated from all source positions and light emanating from the breast was detected in parallel for each source position. Acquisition duration was ~1 minute per wavelength per breast, leading to a total examination time of ~10 minutes per patient. After optical data acquisition, three-dimensional absorption images were reconstructed for each wavelength by a linear reconstruction algorithm based on the Rytov-approximation [9].

Figure 1. Diffuse Optical Tomography prototype (Philips Healthcare, Best, The Netherlands)

MRI

Dynamic contrast enhanced breast MRI was performed on a 3.0T clinical MR system (3.0T Achieva, Philips Healthcare, Best, The Netherlands). Patients were placed in prone position on a dedicated four-element SENSE compatible phased-array bilateral breast coil (MRI devices, Würzburg, Germany) utilized for simultaneous imaging of both breasts. The MR protocol included an axial high-resolution T1-weighted fast gradient echo (HR-T1FFE) fat suppressed series (TE / TR 1.7 / 4.5 msec; inversion delay SPAIR 130 msec; flip angle 10º; FOV 340 × 340 mm^2, acquired voxel size 0.66 x 0.66 x 1.6 mm^3, reconstructed voxel size 0.66 x 0.66 x 0.80 mm^3), followed by an axial T2-weighted fat suppressed series (TE / TR 120 / 9022 msec; inversion delay SPAIR 125 msec; flip angle 90º; FOV 340 × 340 mm^2, acquired voxel size 1.01 x 1.31 x 2.0 mm^3, reconstructed voxel size 0.66 x 0.66 x 2.00 mm^3). Finally, dynamic contrast-enhanced fat-suppressed T1-weighted images were acquired (TE / TR 1.3 / 3.4 ms; flip angle 10°; FOV 320 mm × 320 mm, acquired voxel size 0.91 mm × 0.91 mm × 2.00 mm, reconstructed voxel size 0.83 mm × 0.83 mm × 1.00 mm, temporal resolution 50 s per dynamic acquisition) with a total of six dynamic acquisitions, one obtained before, and five obtained 0, 60, 120, 180, and 240 seconds after administration of a bolus injection of 0.1 mmol/kg Gadolinium (Magnevist, Schering, Berlin, Germany) followed by a 20-ml saline flush at an injection rate of 3 ml/s with an automatic injector.

Image interpretation

MR images were interpreted by two breast radiologists with >10 years of experience and were used to derive the location of the lesions. A region of interest (ROI) was drawn at the lesion site location for all four optical absorption images (Example in **Figure 2**).

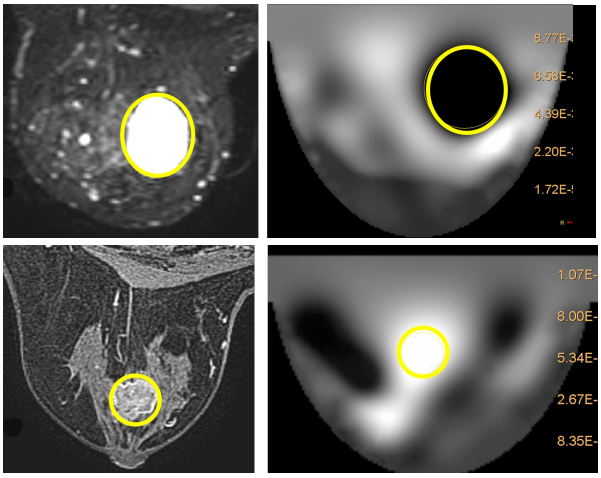

Figure 2. Examples of ROIs on DOT images compared to MRI. *Upper row:* 60 year old woman with lesion in the right breast; BIRADS category 2 on MRI (left image: T2 weighted MRI with fat suppression); visibility score -4 on DOT (right image); final diagnosis: benign cyst. *Lower row:* 56 year old woman with lesion in the right breast; BI-RADS category 5 on MRI (left image: DCE-MRI); visibility score +4 on DOT (right image); final diagnosis: invasive ductal carcinoma.

For comparison, a similar ROI was drawn at the mirror image lesion site location of the contralateral breast, where no lesion was found. The visibility of the lesions on DOT was assessed both quantitatively and qualitatively. Quantitative values were computed from the volume images of the optical absorption coefficient obtained from the DOT system. The mean absorption coefficient of the ROI was divided by the mean absorption of the background, which included the rest of the breast on that slice except for the lesion (the quantitative score). Qualitative scores for contrast relative to background were given independently by two readers for every ROI, on a scale from –4 to 4, where: 0 = no visibility; 1 = slight heterogeneity seen at the site of the known lesion; 2 = moderate contrast, but less/more than other structures, seen at the site of the known lesion; 3 = contrast at the known lesion site comparable to that of other structures; 4 = major contrast at the known lesion site; a minus sign was used if the signal at the ROI is lower than the background, and a plus sign when it was higher. To learn how to score the images, readers were shown an example set of classified images (not from the study population) before they started the scoring process. All images were made anonymously, placed in random order, and scored by two readers separately, without knowledge from other examinations. Images were scored again after three months in a second independent reading by the two investigators.

The reference standard for final diagnosis of the solid lesions was histopathology; while for the benign cysts and the healthy contralateral breast (mirror image) reference standard was MRI. The patients diagnosed with benign cysts received a follow up mammography and ultrasound after 6 months.

Statistics

Intra- and interobserver agreements between the two readers were calculated using kappa statistics and intraclass correlation coefficients [10]. Discriminatory values for presence of malignancy were determined by Receiver Operating Characteristic (ROC) analyses. Cancer detection rates were calculated using a qualitative score of ≥ 2 as a cut-off. The package SPSS 15.0 (SPSS Inc., Chicago, IL, USA) was used for all statistical computations.

Results

Seventeen patients (mean age 54, range 22 to 85) with 18 breast lesions underwent optical imaging and DCE-MRI. Of the 18 lesions, 10 lesions were diagnosed as malignant by histopathology after surgery (9 invasive ductal carcinomas and

1 invasive lobular carcinoma; final BI-RADS score was BI-RADS 5 in 7 lesions and BI-RADS 4 in 3 lesions) with a median diameter of 23.5 mm (range 13 – 54 mm); 2 lesions were confirmed to be benign fibroadenomas (final BI-RADS score 3) by large core needle biopsy, with diameters of 13 and 24 mm; and 6 lesions were diagnosed as benign cysts (final BI-RADS score 2) by ultrasound and MRI, with a median diameter of 28.5 mm (range 20 – 40 mm); the 23 mirror image regions of the contralateral breasts appeared as normal breast tissue without lesions on DCE-MRI.

Quantitative scores (ROI-to-background ratios) are shown in **Table 1**. Scores for malignant lesions were higher (2.15 - 3.03) than those for fibroadenomas (1.30 - 1.75), cysts (0.13 - 0.23), and the contralateral normal breast (1.16 - 1.39). Discriminatory values of quantitative scores for presence of malignancy are shown in **Table 2**, with areas under the ROC curves from 0.92 - 0.93.

Table 1. Median (range) of quantitative score according to lesion presence and lesion type

Wavelength	Lesion type			No lesion (n=18)
	Malignant (n=10)	*Fibroadenoma (n=2)*	*Cyst (n=6)*	
690	3.03 (1.91 to 3.40)	1.75 (1.36 to 2.14)	0.23 (0.10 to 0.73)	1.39 (0.32 to 3.21)
730	2.94 (1.74 to 6.31)	1.50 (1.01 to 1.98)	0.17 (0.07 to 0.75)	1.34 (0.29 to 3.18)
780	2.57 (1.54 to 3.22)	1.36 (1.13 to 1.58)	0.13 (0.08 to 0.82)	1.29 (0.72 to 2.58)
850	2.15 (1.27 to 2.55)	1.30 (1.24 to 1.35)	0.13 (0.08 to 0.89)	1.16 (0.71 to 2.34)

Table 2. Discriminatory value of quantitative score for presence of malignancy (n=10; total of 36 breasts)

Wavelength	Area under ROC curve (95% Confidence Interval)
690	0.93 (0.86 to 1.00)
730	0.92 (0.85 to 1.00)
780	0.95 (0.88 to 1.00)
850	0.93 (0.86 to 1.00)

For intra-observer agreements, intraclass correlation coefficients and kappa statistics were excellent (**Table 3**). Intraclass correlation coefficients were excellent and kappa statistics good-excellent for the interobserver agreement (**Table 4**).

Table 3. Intra-observer agreement for visibility scores (total of 36 breasts, 4 wavelengths per breast)

Wavelength	Intraclass correlation coefficient[a] (95% Confidence Interval)		Kappa statistic[b] (95% Confidence Interval)	
	Observer 1	Observer 2	Observer 1	Observer 2
all	0.978 (0.970 to 0.983)	0.987 (0.982 to 0.990)	0.88 (0.82 to 0.94)	0.88 (0.82 to 0.94)

[a]Original visibility scores; one-way random effects model where people effects are random (single measures); [b]Recoded visibility scores into categories (<-1, -1 to 1, >1).

Table 4. Interobserver agreement for visibility scores (total of 36 breasts, 4 wavelengths per breast)

Wavelength	Intraclass correlation coefficient[a] (95% Confidence Interval)	Kappa statistic[b] (95% Confidence Interval)
690	0.96 (0.92 to 0.98)	0.77 (0.58 to 0.96)
730	0.98 (0.95 to 0.99)	0.95 (0.85 to 1.00)
780	0.96 (0.92 to 0.98)	0.80 (0.61 to 0.99)
850	0.97 (0.95 to 0.99)	0.89 (0.74 to 1.00)

[a]Original visibility scores; one-way random effects model where people effects are random (single measures); [b]Recoded visibility scores into categories (<-1, -1 to 1, >1).

Qualitative visibility scores are shown in **Table 5**. Scores for malignant lesions were higher (2 – 4) than for fibroadenomas (0 – 2), cysts (-4), and the contralateral normal breast (0). **Table 6** shows the discriminatory values of qualitative scores for presence of malignancy for both observers (equal results), with areas under the ROC curves from 0.97 - 0.99. Cancer detection rates for the 4 wavelengths (690, 730, 780, and 850 nm, respectively) were 70%, 80%, 80%, and 70% for observer 1; and 60%, 70%, 70%, and 60% for observer 2. Between 0% and 22% false positive results were found per wavelength for both observers.

Table 5. Median (range) visibility score according to lesion presence and lesion type

Wavelength	Lesion type						No lesion (n=18)	
	Malignant (n=10)		Fibroadenoma (n=2)		Cyst (n=6)			
	Observer 1	*Observer 2*	*Observer 1*	*Observer 2*	*Observer 1*	*Observer 2*	*Observer 1*	*Observer 2*
690	2 (0 to 4)	2 (0 to 4)	1 (0 to 2)	2 (0 to 4)	-4 (-4 to -1)	-4 (-4 to -1)	0 (-2 to 2)	0 (0 to 3)
730	2 (0 to 4)	2 (0 to 4)	1 (1 to 1)	0 (0 to 0)	-4 (-4 to 0)	-4 (-4 to 0)	0 (0 to 2)	0 (0 to 3)
780	2 (0 to 4)	4 (0 to 4)	0 (0 to 0)	0 (0 to 0)	-4 (-4 to -1)	-4 (-4 to 0)	0 (-1 to 1)	0 (-2 to 2)
850	2 (0 to 4)	2 (0 to 4)	0 (0 to 0)	0 (0 to 0)	-4 (-4 to 0)	-4 (-4 to 0)	0 (-1 to 1)	0 (0 to 2)

Table 6. Discriminatory value of visibility score for presence of malignancy (n=10; total of 36 breasts)

Wavelength	Area under ROC curve (95% Confidence Interval)
	Observer 1 and 2
690	0.97 (0.89 to 1.00)
730	0.99 (0.95 to 1.00)
780	0.97 (0.89 to 1.00)
850	0.99 (0.95 to 1.00)

Discussion

This study describes the first diagnostic evaluation under optimal settings of a new prototype DOT system with MRI as a benchmark in patients with breast lesions. Using a known lesion position, malignant lesions could be discriminated from benign tissue both quantitatively and qualitatively, mainly due to higher hemoglobin contents causing more light absorption. Intra- and interobserver agreement were good-excellent, indicating a reproducible method.

Our results are in agreement with previously published studies using different techniques [11-26]. Detection rates ranging from 0.04 to 1.00 were reported, irrespective of lesion classification (benign/malignant). Cancer detection rates in our study were between 60% and 80% for each wavelength separately, using a cut-off value of 2; detection rates and false positive results can likely be improved when combining information of four different wavelengths in one model (spectroscopic imaging). Similar to other research groups, we used knowledge on lesion locali-

zation from a reference standard (MRI in this instance) for the evaluation of the optical data. This approach in image interpretation may have resulted in limited false-positive findings with as a consequence overestimation of the ROC analyses. However, the areas under the ROC curves justify further evaluation and development of the technique.

As this study represents a first evaluation of a new prototype for malignant lesion detection conclusions should be drawn with care due to important limitations of the system. In addition, because the sample size of the study was small and the study group was selective, obtained results cannot be extrapolated directly to a clinical diagnostic or screening setting. Technical limitations of the DOT system resulted in the exclusion of 14 of the 36 patients for image analysis. These major limitations comprised the leakage of matching fluid from the system resulting in large artifacts, and the limitation in the current geometry of the system to measure lesions located close to the patient's chest wall. Most likely during optical imaging, these lesions were physically located too far above the upper optical fibers in the cup to influence the light pathways. Improvement in cup shape is feasible and should be realized to visualize these lesions. A limitation of DOT in general is the poor spatial resolution [1, 16]. This results in a lower signal-to-noise ratio and limited detection of very small lesions. Median diameters of the included lesions in our study were relatively long, the smallest detected lesion by DOT in our study sample was 13 mm, and may therefore not be representative for the routine clinical and screening situation. Further studies including more patients with smaller lesions will be performed to get a more realistic estimate of the system's diagnostic value. A molecular imaging approach using certain fluorescent probes may vastly improve signal-to-noise ratios by signal amplification [27]. Target-specific fluorescent probes for optical imaging have already been used successfully in animal experiments [28-30].

In conclusion, this novel DOT system has the potential to discriminate malignant from benign breast tissue by assessing optical properties of the tissue in a reproducible quantitative and qualitative way. Important technical improvements are required before this technique will be ready for use in clinical practice.

References

1. Gibson AP, Hebden JC, Arridge SR (2005) Recent advances in diffuse optical imaging. Phys Med Biol 50:R1-43.
2. Rice A, Quinn CM (2002) Angiogenesis, thrombospondin, and ductal carcinoma in situ of the breast. J Clin Pathol 55:569-574.
3. Vaupel P, Harrison L (2004) Tumor hypoxia: causative factors, compensatory mechanisms, and cellular response. Oncologist 9 Suppl 5:4-9.
4. Peters NH, Borel RI, Zuithoff NP, et al. (2008) Meta-analysis of MR imaging in the diagnosis of breast lesions. Radiology 246:116-124.
5. Raza S, Chikarmane SA, Neilsen SS, et al. (2008) BI-RADS 3, 4, and 5 Lesions: Value of US in Management-Follow-up and Outcome. Radiology 248:773-781.
6. Pisano ED, Gatsonis C, Hendrick E, et al. (2005) Diagnostic performance of digital versus film mammography for breast-cancer screening. N Engl J Med 353:1773-1783.
7. Yeh E, Slanetz P, Kopans DB, et al. (2005) Prospective comparison of mammography, sonography, and MRI in patients undergoing neoadjuvant chemotherapy for palpable breast cancer. Am J Roentgenol 184:868-877.
8. Leff DR, Warren OJ, Enfield LC, et al. (2008) Diffuse optical imaging of the healthy and diseased breast: A systematic review. Breast Cancer Research and Treatment 108:9-22.
9. Nielsen T, Brendel B, Ziegler R, et al. (2008) Linear Image Reconstruction for a Diffuse Optical Mammography System in a Non-Compressed Geometry Using Scattering Fluid. Biomedical Optics. Optical Society of America, BMD23. URL: http://www.opticsinfobase.org/abstract.cfm?URI=BIOMED-2008-BMD23; date of access March 16, 2008.
10. Brennan P, Silman A (1992) Statistical methods for assessing observer variability in clinical measures. BMJ Clinical research ed 304:1491-1494.
11. Chance B, Nioka S, Zhang J, et al. (2005) Breast cancer detection based on incremental biochemical and physiological properties of breast cancers: a six-year, two-site study. Acad Radiol 12:925-933.
12. Floery D, Helbich TH, Riedl CC, et al. (2005) Characterization of benign and malignant breast lesions with computed tomography laser mammography (CTLM): initial experience. Invest Radiol 40:328-335.
13. Franceschini MA, Moesta KT, Fantini S, et al. (1997) Frequency-domain techniques enhance optical mammography: initial clinical results. Proc Natl Acad Sci USA 94:6468-6473.
14. Gotz L, Heywang-Kobrunner SH, Schutz O, et al. (1998) Optical mammography in preoperative patients. Aktuelle Radiol 8:31-33.
15. Gu X, Zhang Q, Bartlett M, et al. (2004) Differentiation of cysts from solid tumors in the breast with diffuse optical tomography. Acad Radiol 11:53-60.

16. Hsiang D, Shah N, Yu H, et al. (2005) Coregistration of dynamic contrast enhanced MRI and broadband diffuse optical spectroscopy for characterizing breast cancer. Technol Cancer Res Treat 4:549-558.
17. Intes X (2005) Time-domain optical mammography SoftScan: initial results. Acad Radiol 12:934-947.
18. Ntziachristos V, Yodh AG, Schnall MD, et al. (2002) MRI-guided diffuse optical spectroscopy of malignant and benign breast lesions. Neoplasia 4:347-354.
19. Rinneberg H, Grosenick D, Moesta KT, et al. (2005) Scanning time-domain optical mammography: detection and characterization of breast tumors in vivo. Technol Cancer Res Treat 4:483-496.
20. Taroni P, Torricelli A, Spinelli L, et al. (2005) Time-resolved optical mammography between 637 and 985 nm: clinical study on the detection and identification of breast lesions. Phys Med Biol 50:2469-2488.
21. Tomandl B, Doinghaus K, Schulz-Wendtland R (1995) Laser mammography with near-infrared light. Rontgenpraxis 48:197-201.
22. Yates T, Hebden JC, Gibson A, et al. (2005) Optical tomography of the breast using a multi-channel time-resolved imager. Phys Med Biol 50:2503-2517.
23. Zhu Q, Cronin EB, Currier AA, et al. (2005) Benign versus malignant breast masses: optical differentiation with US-guided optical imaging reconstruction. Radiology 237:57-66.
24. Cerussi A, Hsiang D, Shah N, et al. (2007) Predicting response to breast cancer neoadjuvant chemotherapy using diffuse optical spectroscopy. Proc Natl Acad Sci USA 104:4014-4019.
25. Cerussi A, Shah N, Hsiang D, et al. (2006) In vivo absorption, scattering, and physiologic properties of 58 malignant breast tumors determined by broadband diffuse optical spectroscopy. Journal of Biomedical Optics 11:044005.
26. Durduran T, Choe R, Yu G, et al. (2005) Diffuse optical measurement of blood flow in breast tumors. Opt Lett 30:2915-2917.
27. Mahmood U, Weissleder R (2003) Near-Infrared Optical Imaging of Proteases in Cancer. Molecular Cancer Therapeutics 2:489-496.
28. Bremer C, Ntziachristos V, Weitkamp B, et al. (2005) Optical imaging of spontaneous breast tumors using protease sensing 'smart' optical probes. Invest Radiol 40:321-327.
29. Hilger I, Leistner Y, Berndt A, et al. (2004) Near-infrared fluorescence imaging of HER-2 protein over-expression in tumour cells. Eur Radiol 14:1124-1129.
30. Kumar SR, Quinn TP, Deutscher SL (2007) Evaluation of an 111In-radiolabeled peptide as a targeting and imaging agent for ErbB-2 receptor expressing breast carcinomas. Clin Cancer Res 13:6070-6079.

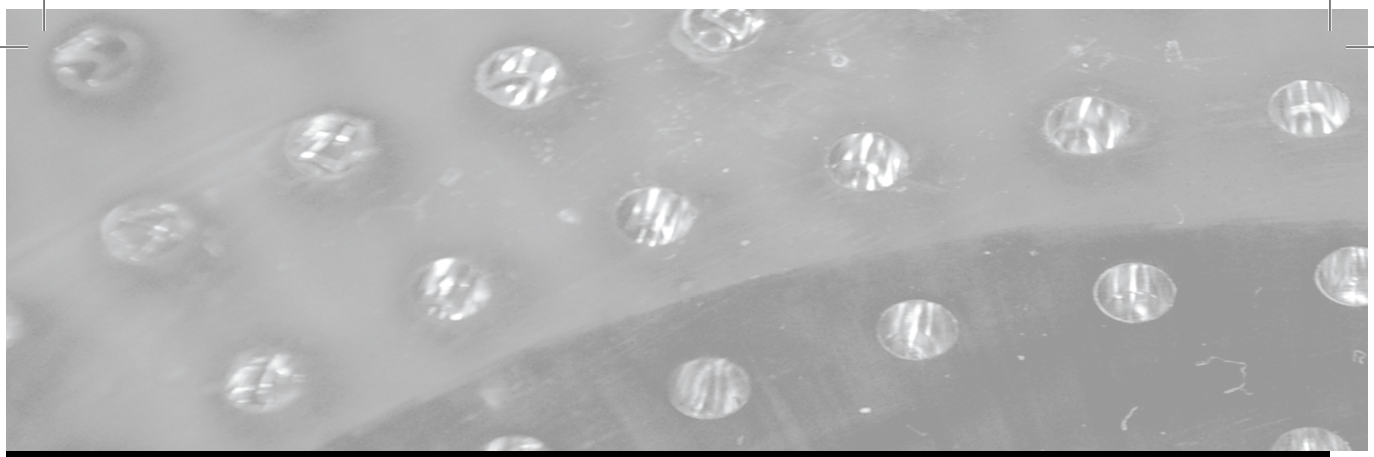

Authors

S.M.W.Y. van de Ven, S.G. Elias, A.J. Wiethoff, M. Van der Voort, T. Nielsen, B. Brendel, L.. Bakker, M.B. Van der Mark, W.P.Th.M. Mali, P. Luijten.

Molecular Imaging and Biology 2009;11:64-70

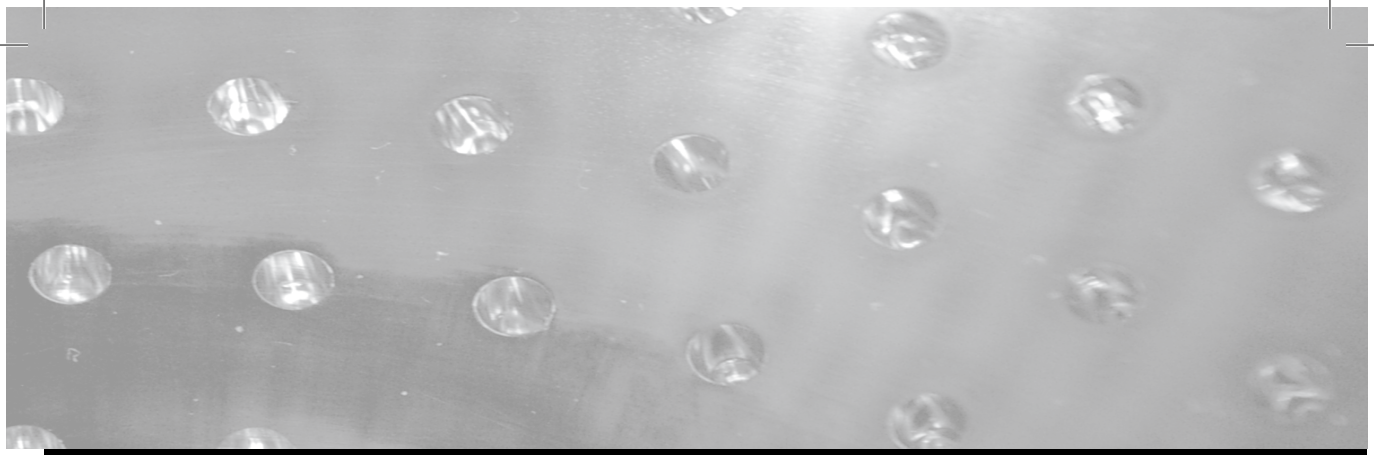

Diffuse optical tomography of the breast:

initial validation in benign cysts

Abstract

Purpose

To validate a newly developed Diffuse Optical Tomography (DOT) system on benign cysts in the breast.

Procedures

Eight patients with 20 benign cysts were included. Study procedures consisted of optical breast imaging and breast magnetic resonance imaging (MRI) for comparison. A reconstruction algorithm computed three-dimensional images for each of the four near-infrared wavelengths used by our DOT system (Philips Healthcare, Best, The Netherlands). These images were combined using a spectroscopic model to assess tissue composition and lesion size.

Results

20 cysts were analyzed in 8 patients. By using the spectroscopic information, 13 of 20 cysts (65%) were visualized with DOT, confirming their high water and low total hemoglobin content. Lesion size and location showed good agreement with MRI, Pearson correlation coefficient was 0.7 ($p < 0.01$).

Conclusions

DOT can visualize benign cysts in the breast and elucidate their high water and low total hemoglobin content by spectroscopic analysis.

Introduction

Diffuse Optical Tomography (DOT) is a novel imaging technique that uses near-infrared (NIR) light in the wavelength range of 690 to 1000 nm to assess optical properties of tissue [1]. Light absorption at these wavelengths is minimal, allowing for sufficient tissue penetration (up to 15 cm) in breast imaging. Information on tissue composition, i.e. concentrations of oxy- and deoxyhemoglobin, water and lipid, can be obtained by combining images acquired at various wavelengths. In a malignant tumor, hemoglobin concentration is directly related to angiogenesis, a key factor required for tumor growth and metastases [2]. In addition, the proportions of oxy- and deoxyhemoglobin change in such a tumor due to its metabolism [3]. By measuring concentrations of the main chromophores in the breast, discrimination of benign and malignant tumors may be possible with DOT. This technique could complement currently used breast imaging modalities, ultrasound, X-ray mammography and magnetic resonance imaging (MRI), in the diagnosis and early detection of breast cancer,. Ultrasound can easily distinguish cysts from solid lesions, but is less specific than X-ray mammography in differentiating benign from malignant masses [4]. It is used as an adjunct to X-ray mammography, not as stand-alone screening tool, and is limited by its operator-dependence as well as the lack of standardized examination criteria [5]. The overall sensitivity of X-ray mammography for breast cancer detection is moderate (75%), though in (young) women with dense breasts, the sensitivity drops to near 62% [6]. Since these women are at a four to six times increased breast cancer risk, this is a major disadvantage of X-ray mammography [7]. MRI has high sensitivity (> 90%), also in dense breasts, but is very costly [8, 9]. Positive predictive value of MRI is decreased in lesions < 5 mm [10]. As lesion size upon diagnosis decreases with more efficient screening programs, the need for a non-invasive tool that provides more specific information on lesions becomes relevant. DOT has great potential in the early detection of breast cancer if target-specific fluorescent probes allow for in vivo imaging of molecular changes associated with cancer formation [11]. Moreover, DOT uses no ionizing radiation and can thus be used repeatedly, also in younger women. The technique is relatively inexpensive leading to relatively easy access which is an important advantage in regions where no MRI scanner is available.

Optical imaging systems are still in their infancy and several research groups are investigating different techniques [12]. Three distinct illumination methods are being employed: time-domain [13-15], frequency domain [16, 17], and continuous wave [18-20]. Some groups combine their optical system with another modality, such as ultrasound or MRI [17, 21]. Furthermore, compression of the breast [13-15], optical fluid [13], and various wavelengths in the NIR range are being investigated.

To create a robust platform for optical breast imaging, it is important to validate systems in an adequate manner. We started our validation process in a simple breast model, benign cysts with the aim to determine the optical characteristics of these lesions. MRI was the benchmark for DOT because it also provides three-dimensional data and has excellent soft tissue contrast.
The purpose of this study was to validate a newly developed DOT system on benign cysts in the breast.

Methods

Patients

Eight women (mean age 48, range 38 - 60) diagnosed with a total of 20 cystic breast lesions were prospectively included between October 2006 and September 2007 at the University Medical Center Utrecht, The Netherlands. Patients were asked to participate in the study if a benign cyst larger than 10 mm was found by ultrasound and needle aspiration had not yet been performed, since this would influence the optical images. Additional to the normal clinical diagnostic procedure of mammography and ultrasound, patients underwent optical imaging and non-contrast enhanced MRI as part of the study protocol. Patients with contra-indications for MRI were excluded. The protocol was approved by the ethics committee of the University Medical Center Utrecht, and written informed consent was obtained from all patients.

Optical Imaging

a) Data acquisition
Diffuse optical tomography (DOT) scans were performed on a Philips Diffuse Optical Tomography system (Philips Healthcare, Best, The Netherlands). A patient was placed in the prone position on the system bed with one breast suspended in the cup (**Figure 1**). The scanning module of the DOT system consists of a cup with a total of 507 optical fibers mounted on the surface. The 253 source fibers on all sides of the cup are connected to a fiber switch, to direct the light of four continuous wave solid-state lasers into the cup. These fibers are interleaved with 254 detector fibers connected to 254 detectors. For each scan, the cup was filled with a matching fluid that has optical properties approximately equal to those of the average breast. This matching fluid enables a stable optical coupling between the fibers and the breast, and, it eliminates optical short cuts of the diffuse light around the breast. During imaging, the breast was sequentially illuminated with continuous wave near-infrared light from all source positions. Light emanating from the breast was detected for each source position by the detector fibers on

all sides of the cup. Images were obtained at four discrete wavelengths (690, 730, 780, and 850 nanometers). Each breast is scanned separately. The duration of the examination was approximately 1 minute per wavelength, in total about 10 minutes per patient.

Figure 1. The Philips Diffuse Optical Tomography system.

b) Image reconstruction

After optical data acquisition, three-dimensional absorption images were reconstructed by a linear reconstruction algorithm based on the Rytov-approximation [22-24]. One image was calculated for each wavelength. Since the reconstruction algorithm assumes constant scattering throughout the measurement cup, there is an influence of scattering variations on the reconstructed absorption images. If the average scattering of the breast is different from the scattering of the fluid, there will be an offset on the reconstructed breast absorption. If there is a variation of the scattering within the breast the reconstructed image also shows features due to these variations.

c) Spectral post-processing

In addition, optical images of the four wavelengths were combined to convert the absorption coefficients into hemoglobin, oxy-hemoglobin, water, and lipid concentrations. We assumed that these were the only chromophores present in the breast. To determine the concentrations, we used the relation $c = [\varepsilon]^{-1}\mu_{\alpha}$, where c refers to the concentrations of the four chromophores, $[\varepsilon]$ is a 4 x 4 matrix of molar absorption values of the four chromophores for the four wavelengths used by the DOT machine, and μ_{α} is the vector of reconstructed absorption coefficients at

each wavelength. The spectra that were used to fill [ε] are shown in **Figure 2** (data taken from [25], [26], and [27], for water, lipid, hemoglobin and oxy-hemoglobin, respectively). Finally, the Hb and HbO_2 concentrations were added to obtain a measure of the total hemoglobin concentration. However, as a consequence of using continuous wave light, our reconstruction algorithm could not account for scattering variations in the breast, in contrast with other research groups using time-domain or frequency domain techniques [13-17]. In addition, since the breast contains more than the four chromophores mentioned, this model only approximates the breast composition. We therefore choose to discuss "enhancement" by chromophores rather than their absolute concentration. Three-dimensional enhanced-water maps, with high signal intensity for high water concentration, and three-dimensional enhanced-blood maps, with high signal intensity for high blood concentration (and low signal intensity in case of blood-depletion), were generated.

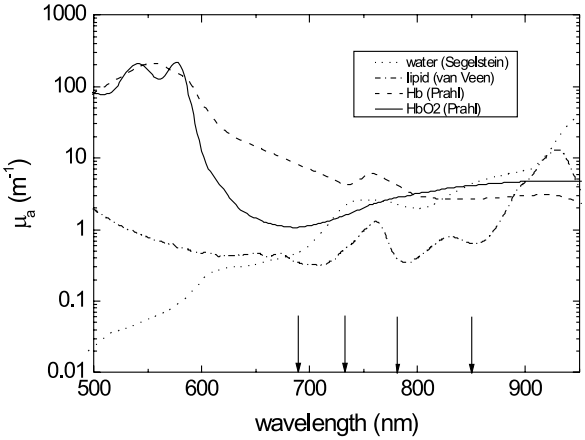

Figure 2. Absorption spectra of the main constituents of breast tissue, represented in terms of absorption coefficients for water and lipid, and molar absorption coefficients for hemoglobin (Hb) and oxy-hemoglobin (HbO_2). Data were taken from [25], [26], and [27], for water, lipid, Hb and HbO_2, respectively. The wavelengths of the lasers used for the DOT measurements are indicated by the vertical black arrows.

MRI

Non-contrast enhanced breast MRI was performed on a 3.0T clinical MR system (3.0T Achieva, Philips Healthcare, Best, The Netherlands). Patients were placed in prone position on a dedicated four-element SENSE compatible phased-array bilateral breast coil (MRI devices, Würzburg, Germany) utilized for simultaneous imaging of both breasts. The scan protocol included an axial high-resolution T1-weighted fast gradient echo (HR-T1FFE) fat suppressed series (TE / TR 1.7 / 4.5 msec; inversion delay SPAIR 130 msec; flip angle 10º; FOV 340 × 340 mm^2, acquired voxel size 0.66 x 0.66 x 1.6 mm^3, reconstructed voxel size 0.66 x 0.66 x 0.80 mm^3) and an axial T2-weighted fat suppressed series (TE / TR 120 / 9022 msec;

inversion delay SPAIR 125 msec; flip angle 90°; FOV 340 × 340 mm^2, acquired voxel size 1.01 x 1.31 x 2.0 mm^3, reconstructed voxel size 0.66 x 0.66 x 2.00 mm^3).

Image interpretation and statistics

MRI data was used to derive the location of the cysts. Size measurements were performed on the axial MR slices showing the largest diameters of the cysts. This information was used as a reference standard for the optical measurements.
All four absorption images were viewed on the console of the DOT system. The visibility of the lesions on DOT was assessed in a qualitative manner. When the reconstructed values at the lesion site (derived from MRI) were clearly lower or higher than those of the surrounding tissue (background), the cyst was considered visible. Lower values can be expected when absorption and/or scattering properties of the lesion are lower than those of the background.
The physiological maps of water and total hemoglobin were evaluated and compared to the MRI data. Maximum diameters of the lesions were measured on the axial view of the physiological maps from the full width at half maximum of the signal intensity through the center of the cyst region, and compared to the maximum diameters measured on the axial MR images. The Bland Altman method was used to measure the agreement of lesion size between the MRI and DOT measurements [28]. The Pearson correlation coefficient was calculated to estimate the correlation between the two methods.

Results

Eight women with 20 benign cysts underwent optical breast imaging with the new DOT system and breast MRI for comparison. All cysts were clearly visible on MRI showing high signal intensity on the T2 weighted images. Maximum lesion sizes measured on the MR images ranged from 8 to 40 mm (median size 21 mm). Cysts smaller than 5 mm detected on MRI were not taken into account in this study. Based on the absorption images only, 6 of the 20 benign cysts (30%) were clearly distinguishable with DOT. These lesions had lower absorption compared to the surrounding tissue for all of the four wavelengths (**Figure 3**). By using the information from the physiological maps, 13 of 20 benign cysts (65%) were evident on DOT. The enhanced-water and -blood maps showed high water content and low total hemoglobin content at the position of these cysts (**Figure 4**).
Detected lesions had maximum diameters of 15 mm and larger. Two cysts with diameters of 10 and 8 mm on MRI were not visible with DOT. Five cysts that were located close to the chest wall were not detected because they were outside the field of view of the current DOT system.

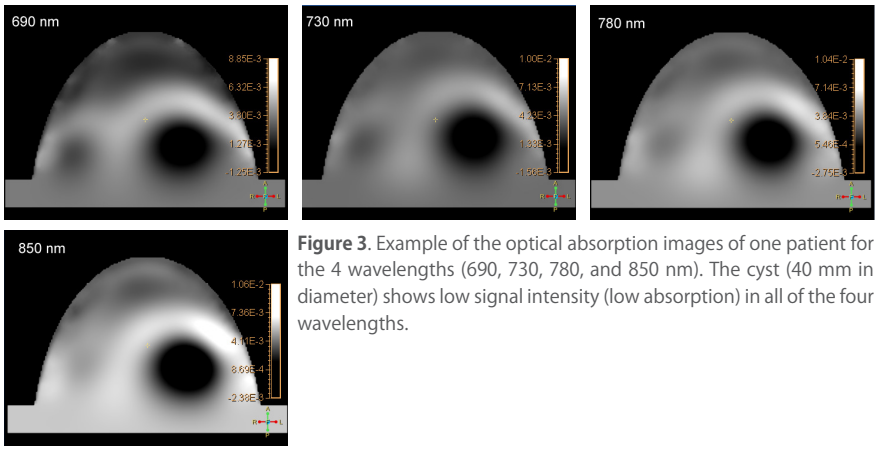

Figure 3. Example of the optical absorption images of one patient for the 4 wavelengths (690, 730, 780, and 850 nm). The cyst (40 mm in diameter) shows low signal intensity (low absorption) in all of the four wavelengths.

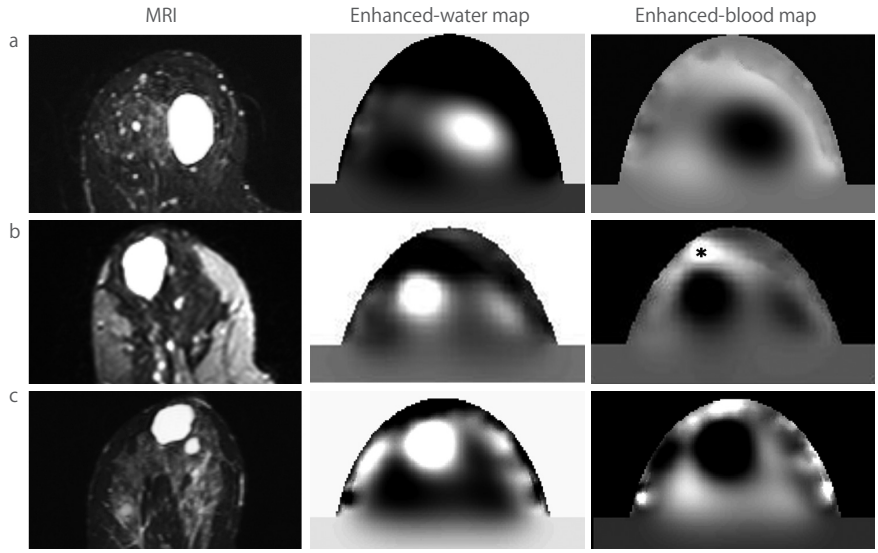

Figure 4. Examples of images of 3 patients (a,b,c): T2 weighted MRI with fat-suppression compared to the enhanced-water maps and the enhanced-blood maps of the optical data sets. The cysts show a high signal intensity on the MRI and the enhanced-water maps (high water content), and a low signal intensity on the enhanced-blood maps (low blood content). * nipple.

The maximum diameters of the detected lesions are plotted in **Figure 5**. There was a good agreement between the optical measurements and MRI, with a Pearson correlation coefficient of 0.7 ($p < 0.01$). **Figure 6** displays the Bland Altman plot in which the absolute differences between MRI and DOT are plotted against the mean of the two methods.

The three horizontal lines represent the mean difference (middle line) and the limits of agreement (outer lines: mean difference ± 2SD) [28]. DOT overestimated the lesion size on average by 2.5 mm (mean difference MRI-DOT: -2.5 mm; 95% confidence interval: -6.4 to 1.3).

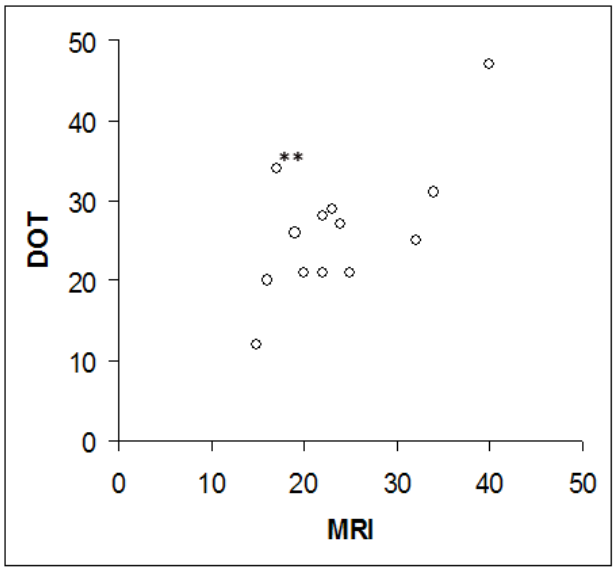

Figure 5. Scatter plot of diameters in mm measured with MRI (x-axis) and DOT (y-axis). Pearson correlation coefficient: 0.7 ($p < 0.01$). If merged lesions** were excluded from analysis, Pearson correlation coefficient increased to 0.8 ($p < 0.01$).

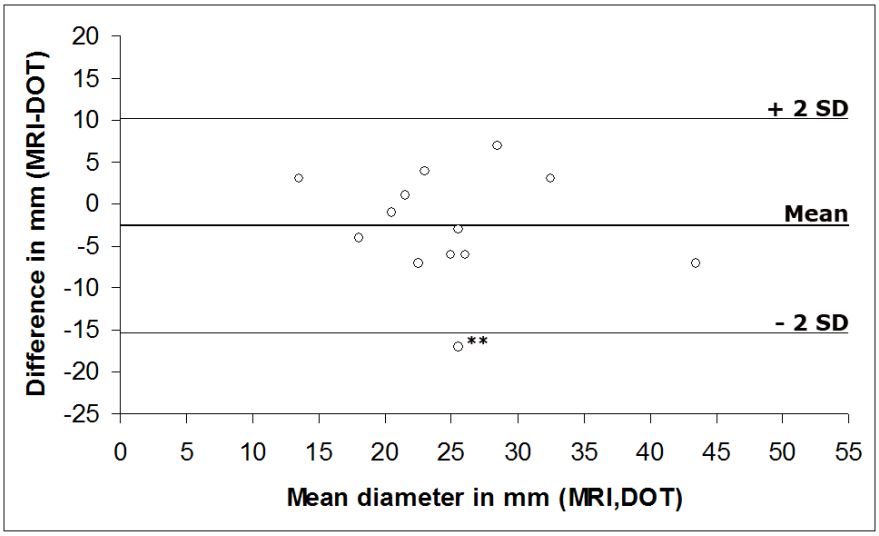

Figure 6. Bland Altman plot of lesion sizes in mm. Absolute differences between MRI and DOT (y-axis) are plotted against the mean of the two methods (x-axis). The horizontal lines represent the mean difference (middle line) and limits of agreement (mean difference ± 2SD). ** merged lesions.

Discussion

In this study we validated a new DOT system for breast imaging on benign cysts with MRI as a benchmark. Cysts were visible with DOT and spectroscopic analysis showed high water and low total hemoglobin content. Lesion sizes on DOT correlated well with MRI measurements.

As described previously, most recent optical imaging studies focused on solid tumors. They showed higher absorption for carcinomas than for the surrounding normal parenchyma due to increased hemoglobin content [13-19, 21]. Few studies reported on the characterization of cysts with optical imaging devices. Ntziachristos et al. reported on low absorption for cysts [21], and Taroni et al. described low scattering in cysts [15]. In Gu et al. it was shown that cysts had a lower optical attenuation than the background [20]. They described both low absorption and low scattering in four of the cysts, and only low scattering in one case.

In our study, the cysts visible on optical absorption images appeared as regions darker than the surrounding tissue (**Figure 3**). This could be caused by either lower absorption properties, lower scattering properties, or the combination of both. The use of continuous wave light transmission hampers the distinction between scattering and absorption [29]. With other illumination techniques, time domain (e.g. used by the groups of Intes, Rinneberg, and Taroni [13-15]) and frequency domain (e.g. used by the groups of Tromberg and Zhu [16, 17]), it is more straightforward to make this distinction. These methods have the disadvantage of being more expensive and requiring longer acquisition times than the continuous wave technique.

In one of the patients in our study, an opposite effect was seen: the cyst had a higher signal intensity (higher absorption/scattering) compared to the surrounding tissue, with lower water and higher total hemoglobin content on the physiological maps. On MRI and ultrasound this cyst had similar characteristics as the other cysts in our study. Such an opposite effect was also reported by Gu et al. who described a cyst with both higher absorption and higher scattering compared to the surrounding tissue [20]. As suggested by Gu et al., an explanation for this opposite effect could be a different content of the cyst. To verify this hypothesis, future aspiration and evaluation of cyst contents could be considered.

Spectroscopic analysis of the cysts in our study elucidated their high water content and low hemoglobin content (**Figure 4**). Combining the four wavelengths improved lesion detection: without spectral information only six cysts were visible, while with spectroscopic analysis 13 of the 20 lesions could be detected.

Seven of the twenty cysts were not detected by our DOT system. We believe there are two reasons for this. First, five cysts were located too close to the chest wall

for the current dimensions of the optical scanner to image. These lesions were most likely physically located too far above the upper optical fibers in the cup to influence the light pathways. Advances in cup geometry are feasible and would result in improved visualization of lesions near the chest wall. Second, spatial resolution of DOT is poor [1, 30], resulting in a lower signal-to-noise ratio and limited detectability for small lesions: two lesions of 10 and 8 mm were too small to be visualized by our DOT system. One of these cysts was probably merged with the nearby larger lesion in the optical image, leading to a significant overestimation of that cyst (**Figure 5**). All detected lesions had diameters of at least 15 mm. For lesions visible on DOT images, a good agreement in lesion size with MRI was found (**Figures 5 and 6**). Pearson correlation coefficient was 0.7 ($p < 0.01$). If the lesion that we believed to be merged with the nearby lesion was excluded from the analysis, Pearson correlation coefficient increased to 0.8 ($p < 0.01$). On average, lesion size was overestimated by 2.5 mm with DOT, and most optical size measurements did not differ more than 6 mm from MRI measurements. By exclusion of the supposedly merged lesion, overestimation was reduced to 1.3 mm (mean difference MRI-DOT: -1.3 mm; 95% confidence interval: -4.4 to 1.7). Lesions overestimated by more than 6 mm with DOT were located in a central position in the cup where the spatial resolution of the system is the lowest leading to partial volume effects. Lesion detection is more difficult and size measurement less precise in the center of the cup compared to the edge of the cup, because longer light pathways decrease spatial resolution. This may be a limitation in large breasts with centrally located lesions. Optical data acquisition using slab geometry with slight breast compression could offer a solution to this problem. We did not encounter variations in lesion visibility for different breast densities in this data set.

Typically, close to the boundary of the cup, structures were noted with very high signal intensities (e.g. **Figure 4**, patient c). These are reconstruction artifacts caused by inconsistencies in the data. They show up strongest at the source and detector positions and can be identified as artifacts due to their position at the cup wall. Also, in most patients, the nipples were visible as regions of high signal intensity on the enhanced-blood maps (**Figure 4**, patient b), and low signal intensity on the enhanced-water maps.

For evaluation of the optical data we used the knowledge of lesion location from the MRI data. This approach in image interpretation possibly resulted in the exclusion of false-positive findings, such as the high signal intensities caused by artifacts. Blinded reading of images should be performed to give a better estimate of the diagnostic value.

This study was the first step in the validation of a new DOT system. Further steps will involve validation on malignant breast lesions (including discrimination of

malignant from benign lesions, such as cysts) and feasibility studies with fluorescent optical probes to increase specificity. Such fluorescent probes emit photons at predefined wavelengths after excitation by laser light and have already been used successfully in animal experiments [31, 32].

In conclusion, we initiated the validation of a new DOT system on benign cysts in the breast. DOT was able to visualize cysts and elucidate their high water and low total hemoglobin content by spectroscopic analysis.

References

1. Gibson AP, Hebden JC, Arridge SR . Recent advances in diffuse optical imaging. Phys.Med. Biol. 2005;50:R1-43.
2. Rice A, Quinn CM . Angiogenesis, thrombospondin, and ductal carcinoma in situ of the breast. J.Clin.Pathol. 2002;55:569-574.
3. Vaupel P, Harrison L . Tumor hypoxia: causative factors, compensatory mechanisms, and cellular response. Oncologist. 2004;9, Suppl 5:4-9.
4. Irwig L, Houssami N, van VC . New technologies in screening for breast cancer: a systematic review of their accuracy. Br.J.Cancer 2004;90:2118-2122.
5. Elmore JG, Armstrong K, Lehman CD, Fletcher SW . Screening for breast cancer. JAMA 2005;293:1245-1256.
6. Carney PA, Miglioretti DL, Yankaskas BC et al. Individual and combined effects of age, breast density, and hormone replacement therapy use on the accuracy of screening mammography. Ann.Intern.Med. 2003;138:168-175.
7. Boyd NF, Guo H, Martin LJ et al. Mammographic density and the risk and detection of breast cancer. N.Engl.J.Med. 2007;356:227-236.
8. Peters NH, Borel R, I, Zuithoff NP, Mali WP, Moons KG, Peeters PH . Meta-analysis of MR imaging in the diagnosis of breast lesions. Radiology 2008;246:116-124.
9. Kuhl CK . Current status of breast MR imaging. Part 2. Clinical applications. Radiology 2007;244:672-691.
10. Liberman L, Mason G, Morris EA, Dershaw DD . Does size matter? Positive predictive value of MRI-detected breast lesions as a function of lesion size. AJR Am.J.Roentgenol. 2006;186: 426-430.
11. Hoffman JM, Gambhir SS . Molecular imaging: the vision and opportunity for radiology in the future. Radiology 2007;244:39-47.
12. Leff DR, Warren OJ, Enfield LC et al. Diffuse optical imaging of the healthy and diseased breast: A systematic review. Breast Cancer Res.Treat. 2007.
13. Intes X . Time-domain optical mammography SoftScan: initial results. Acad.Radiol. 2005;12:934-947.
14. Rinneberg H, Grosenick D, Moesta KT et al. Scanning time-domain optical mammography: detection and characterization of breast tumors in vivo. Technol.Cancer Res.Treat. 2005;4:483-496.
15. Taroni P, Torricelli A, Spinelli L et al. Time-resolved optical mammography between 637 and 985 nm: clinical study on the detection and identification of breast lesions. Phys.Med. Biol. 2005;50:2469-2488.

16. Tromberg BJ, Cerussi A, Shah N et al. Imaging in breast cancer: diffuse optics in breast cancer: detecting tumors in pre-menopausal women and monitoring neoadjuvant chemotherapy. Breast Cancer Res. 2005;7:279-285.

17. Zhu Q, Cronin EB, Currier AA et al. Benign versus malignant breast masses: optical differentiation with US-guided optical imaging reconstruction. Radiology 2005;237:57-66.

18. Chance B, Nioka S, Zhang J et al. Breast cancer detection based on incremental biochemical and physiological properties of breast cancers: a six-year, two-site study. Acad.Radiol. 2005;12:925-933.

19. Floery D, Helbich TH, Riedl CC et al. Characterization of benign and malignant breast lesions with computed tomography laser mammography (CTLM): initial experience. Invest Radiol. 2005;40:328-335.

20. Gu X, Zhang Q, Bartlett M, Schutz L, Fajardo LL, Jiang H . Differentiation of cysts from solid tumors in the breast with diffuse optical tomography. Acad.Radiol. 2004;11:53-60.

21. Ntziachristos V, Yodh AG, Schnall MD, Chance B . MRI-guided diffuse optical spectroscopy of malignant and benign breast lesions. Neoplasia. 2002;4:347-354.

22. Bakker L, van der Mark MB, van Beek M et al. Optical Imaging of Breast Cancer. Biomedical Optics 2006 Technical Digest SH 56. Washington, DC., Optical Society of America.

23. Bakker L, van der Mark MB, van Beek M et al. Optical Fluorescence Imaging of Breast Cancer. International Symposium on Biophotonics, Nanophotonics and Metamaterials 2006. IEEE conference proceedings 06EX1462, 23-25.

24. Colak SB, van der Mark MB, 't Hooft GW, Hoogenraad JH, van der Linden ES, Kuijpers FA . Clinical Optical Tomography and NIR Spectroscopy for Breast Cancer Detection. IEEE J.Sel.Topics Quantum Electron 1999;5:1143-1158.

25. Segelstein DJ The complex refractive index of water. University of Missouri-Kansas City: 1981.

26. van Veen RL, Sterenborg HJ, Pifferi A, Torricelli A, Cubeddu R . Determination of VIS-NIR absorption coefficients of mammalian fat, with time- and spatially resolved diffuse reflectance and transmission spectroscopy. 2004. OSA Annual BIOMED Topical Meeting.

27. Prahl S . Optical Absorption of Hemoglobin. Available at: http://omlc.ogi.edu/spectra/hemoglobin.

28. Bland JM, Altman DG . Statistical methods for assessing agreement between two methods of clinical measurement. Lancet 1986;1:307-310.

29. Arridge SR, Lionheart WR . Nonuniqueness in diffusion-based optical tomography. Opt. Lett. 1998;23:882-884.

30. Boas DA, Brooks DH, Miller EL, DiMarzio CA, Kilmer ME . Imaging the Body with Diffuse Optical Tomography. IEEE Signal Processing Magazine 2001;18:57-75.

31. Hilger I, Leistner Y, Berndt A et al. Near-infrared fluorescence imaging of HER-2 protein over-expression in tumour cells. Eur.Radiol. 2004;14:1124-1129.

32. Montet X, Ntziachristos V, Grimm J, Weissleder R . Tomographic fluorescence mapping of tumor targets. Cancer Res. 2005;65:6330-6336.

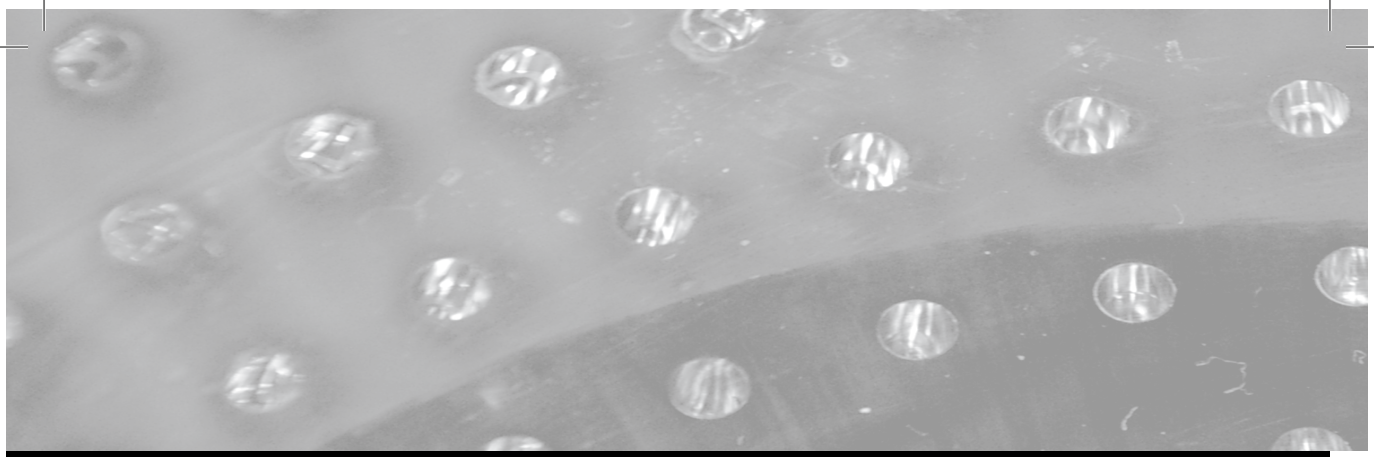

Authors

S.M.W.Y. van de Ven, A.J. Wiethoff, T. Nielsen, B. Brendel, C. Bontus, M. Van der Voort, R. Nachabi, M.B. Van der Mark, M. Van Beek, L. Bakker, L. Fels, S.G. Elias, P. Luijten, W.P.Th.M. Mali.

Molecular Imaging and Biology 2010;12:343-8.

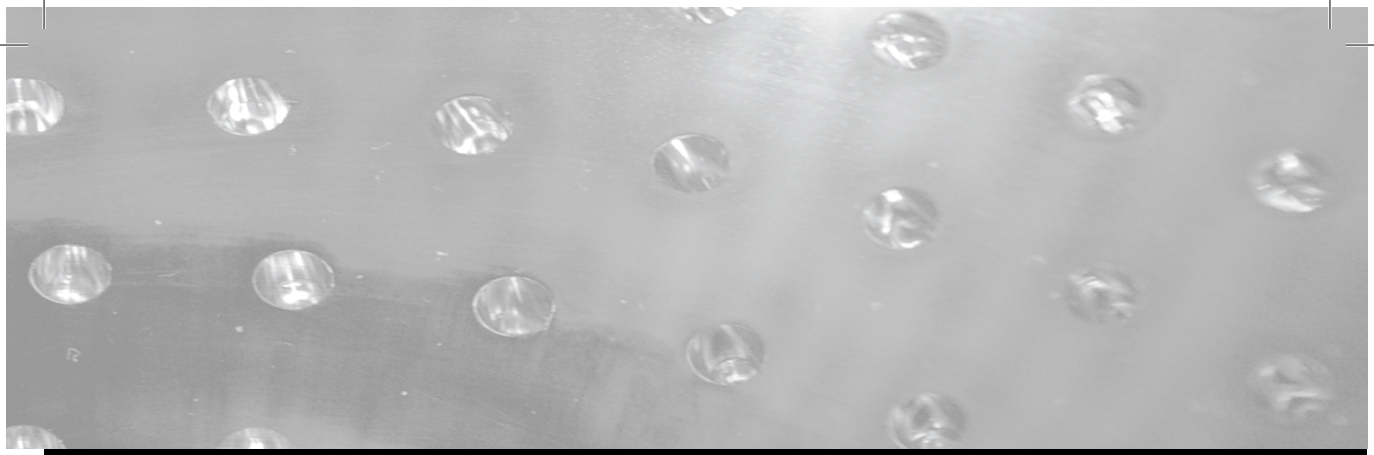

A novel fluorescent imaging agent for diffuse optical tomography of the breast:

first clinical experience in patients

Abstract

Purpose

First clinical evaluation of a novel fluorescent imaging agent (Omocianine) for breast cancer detection with Diffuse Optical Tomography (DOT).

Procedures

Eleven women suspected of breast cancer were imaged with DOT at multiple time points (up to 24 hours) after receiving an intravenous injection of Omocianine (doses 0.01 to 0.1 mg/kg bodyweight). Breast MRI was obtained for comparison.

Results

Histopathology showed invasive cancer in ten patients and fibroadenoma in one patient. With the lowest dose of Omocianine, 2/3 lesions were detected; with the second dose, 3/3 lesions were detected; with the two highest doses, 0/5 lesions were detected. Lesion location on DOT showed excellent agreement with MRI. Optimal lesion-to-background signals were obtained after 8 hours. No adverse events occurred.

Conclusions

Lowest doses of Omocianine performed best in lesion detection; DOT using a low dose fluorescent agent is feasible and safe for breast cancer visualization in patients.

Introduction

Optical breast imaging is a novel imaging technique that uses near-infrared (NIR) light to assess optical properties of tissue, and is expected to play an important role in breast cancer detection. It dates back to 1929 when Cutler investigated the shadows of light transmitted through the breast [1]. Although large, highly vascular, malignant lesions could be detected, the method did not achieve sufficient sensitivity and specificity to be used in clinical practice at the time. During the last decade, progress in source and detector technology, light propagation modeling, and potential fluorescent contrast agents, has resulted in a renewed interest in optical imaging [2]. Optical breast imaging uses near-infrared (NIR) light in the wavelength range of 650 to 1000 nm to assess optical properties of tissue. Functional information of tissue components, i.e. absorption characteristics of oxy- and deoxyhemoglobin, water, and lipid, can be obtained by combining images acquired at various wavelengths. Until now, studies have focused on using the intrinsic optical properties of the breast to visualize lesions without the use of fluorescent contrast agents. These studies described higher absorption for carcinomas than for the surrounding parenchyma due to increased blood content associated with angiogenesis [3-11]. However, intrinsic contrast alone is probably not sensitive enough for (early) lesion detection [12]. Optical breast imaging using a fluorescent contrast agent may improve lesion contrast and can potentially detect changes in breast tissue earlier. When fluorescent probes are excited by NIR light, they emit photons at predefined wavelength ranges, detectable by an optical imaging system. The fluorescent probes can either bind specifically to certain targets associated with cancer or can non-specifically accumulate at the tumor site, mostly by extravasation through leaky vessels. Several of these probes have already been tested successfully in animal experiments [13-15]. Major advantages of optical imaging with fluorescent probes are that it does not use any radioactive components (as in PET and SPECT), and that its sensitivity is very high (nanomolar to picomolar concentration range) compared to MRI. This technique has great potential in early breast cancer detection, since in vivo imaging of molecular changes associated with breast cancer formation is technically feasible. Optical breast imaging provides us with functional information of the tissue, in contrast to X-ray mammography which merely relies on structural information. Additional advantages are that it uses no ionizing radiation, it is relatively inexpensive, which can result in repeated use even in young women, and is easily accessible. However, this technique is still in a very early phase of development. Systems need to be thoroughly evaluated first, before the diagnostic value of the technique in a

clinical setting can be determined. Few studies reported on optical breast imaging with the use of a fluorescent contrast agent. Two case reports described their experiences using the non-specific agent Indocyanine Green (ICG), the only fluorescent agent approved for use in humans today [16,17]. Both groups observed a marked absorption increase in the malignant tumors due to accumulation of ICG, which besides its fluorescent characteristics also acts as a light absorber. In addition, differences in pharmacokinetics between malignant and benign lesions were found. However, ICG characteristics are suboptimal for fluorescence optical breast imaging, in particular the low fluorescence quantum yield is a problem [18]. Nevertheless, in the study by Corlu et al. it was shown that the use of ICG is feasible for fluorescence Diffuse Optical Tomography (DOT). This was the first and thus far the only study to demonstrate fluorescence DOT in vivo in three women with breast cancer [19].

In our study we investigated a non-specific cyanine-based fluorescent dye (Omocyanine) in patients using a Diffuse Optical Tomography (DOT) system dedicated for breast imaging. Aim of this study was to evaluate if our DOT system could detect malignant breast lesions using this new dye, and to assess diagnostic efficacy, target dose, imaging window, and safety of the fluorescent contrast agent.

Methods

Patients

A total of twelve women (mean age 54, range 23 to 81) diagnosed with a 1 – 5 cm BI-RADS 4/5 breast lesion on X-ray mammography were prospectively included at the University Medical Center Utrecht, The Netherlands, between January and July 2007. Additional to the normal clinical diagnostic procedure of mammography and ultrasound, patients underwent optical imaging at different time points and received a single intravenous administration of the fluorescent contrast agent. MRI was obtained in all patients for comparison. For every patient the study consisted of a screening period to verify inclusion criteria; an imaging period, during which optical images were acquired and the study drug was administered; and a follow up period of one week to monitor adverse events. Patients were excluded from the study if they were clinically unstable, had severe renal or hepatic problems, had a history of anaphylactic reactions, were pregnant or lactating, had more than two lesions in the ipsilateral breast, or if they underwent a breast biopsy less than 6 months before the study. The study protocol was approved by the ethics committee of the University Medical Center Utrecht, The Netherlands, and written informed consent was obtained from all patients.

Contrast material and administration

As study drug, a single intravenous injection of Omocyanine (Bayer Schering Pharma, Berlin, Germany) suspended in saline (1 mg/ml) was used. Doses of 0.01, 0.02, 0.05, and 0.1 mg/kg bodyweight were administered in a dose escalating scheme with three patients per dose level, starting at the lowest dose. All doses were administered intravenously at a rate of 1 ml/sec by manual injection, followed by a saline flush of 10-20 ml.

Before the injection of the study drug, baseline optical images were acquired for both breasts. After injection, optical images were acquired up to 24 hours, with respectively 8 and 5 imaging time points for the ipsilateral, and contralateral breast (see flow chart in **Figure 1**).

Figure 1. Flow chart of the study's imaging period.

X: Ipsilateral breast XX: Both breasts SE: Blood sample, urine sample, ECG, vital signs, physical examination (safety examination)
CI: Contrast Injection VS: Vital Signs

Safety evaluations

Standard safety procedures (physical examinations, ECG recordings, laboratory tests), were carried out up to 24 hours after study drug administration. Adverse events were recorded starting at the moment of study drug administration and throughout the one week follow up period. Adverse events were defined as untoward medical occurrences which are not necessarily causally related to the drug administration. Signs and symptoms present before the study drug administration were recorded as baseline findings.

Optical Imaging

a) Data acquisition

Diffuse optical tomography (DOT) scans were performed on a Philips Diffuse Optical Tomography system (Philips Healthcare, Best, The Netherlands). A patient was placed in the prone position on the system bed with one breast suspended in the cup [20]. The scanning module of the DOT system consists of a cup with a total of 507 optical fibers mounted on the surface. The 253 source fibers on all sides of the cup are connected to a fiber switch, to direct the light of four continuous wave solid-state lasers into the cup. These fibers are interleaved with 254 detector fibers connected to 254 detectors. For each scan, the cup was filled with a matching fluid that has optical properties approximately equal to those of the

average breast. This matching fluid enables a stable optical coupling between the fibers and the breast, as well as eliminating optical short cuts of the diffuse light around the breast. During imaging, the breast was sequentially illuminated with continuous wave near-infrared light from all source positions. Light emanating from the breast was detected for each source position by the detector fibers on all sides of the cup. Images were obtained at four discrete wavelengths (690, 730, 780, and 850 nanometers). Each breast is scanned separately. During one scan the system was operated in two modes: transmission and fluorescence mode. The transmission measurements aimed at getting information on the optical absorption and scattering properties of the breast at four wavelengths. The fluorescent measurements were performed at one wavelength (730 nm) and the fluorescent signal was detected at a different wavelength (>750 nm), while the laser light was blocked by filters in the detection path. These measurements aimed at getting information on the concentration and distribution of the fluorescent dye in the breast.
The duration of the examination was approximately 1 minute per wavelength and 5 minutes for the fluorescence, for a total of 9 minutes per breast.

b) Image reconstruction

After optical data acquisition, three-dimensional absorption images were reconstructed by a linear reconstruction algorithm based on the Rytov-approximation [21]. For reconstruction of three-dimensional fluorescence images an algorithm based on the Born-approximation was used [22]. One absorption image was calculated for each wavelength (4 per scan). Since the reconstruction algorithm assumes constant scattering throughout the measurement cup, there is an influence of scattering variations on the reconstructed absorption images. If the average scattering of the breast is different from the scattering of the fluid, there will be an offset on the reconstructed breast absorption. If there is a variation of the scattering within the breast the reconstructed image also shows features due to these variations. The fluorescence images (1 per scan) only show fluorescence signal coming from the injected contrast agent; no absorption information is displayed in these images.

MRI

Contrast enhanced breast MRI was performed on a 3.0T clinical MR system (3.0T Achieva, Philips Healthcare, Best, The Netherlands). Patients were placed in prone position on a dedicated four-element SENSE compatible phased-array bilateral breast coil (MRI devices, Würzburg, Germany) that was utilized for si-

multaneous imaging of both breasts. The scan protocol included an axial high-resolution T1-weighted fast gradient echo (HR-T1FFE) fat suppressed series (TE / TR 1.7 / 4.5 msec; inversion delay SPAIR 130 msec; flip angle 10°; FOV 340 × 340 mm^2, acquired voxel size 0.66 x 0.66 x 1.6 mm^3, reconstructed voxel size 0.66 x 0.66 x 0.80 mm^3), followed by an axial T2-weighted fat suppressed series (TE / TR 120 / 9022 msec; inversion delay SPAIR 125 msec; flip angle 90°; FOV 340 × 340 mm^2, acquired voxel size 1.01 x 1.31 x 2.0 mm^3, reconstructed voxel size 0.66 x 0.66 x 2.00 mm^3). Finally, dynamic contrast-enhanced fat-suppressed T1-weighted images (TE / TR 1.3 / 3.4 ms; flip angle 10°; FOV 320 mm × 320 mm, acquired voxel size 0.91 mm × 0.91 mm × 2.00 mm, reconstructed voxel size 0.83 mm × 0.83 mm × 1.00 mm; dynamic scan duration 60 s) were acquired, starting after intravenous bolus injection of 0.1 mmol/kg Gadolinium (Magnevist, Bayer Schering Pharma, Berlin, Germany).

Image interpretation

MRI data was used as a benchmark for the optical image interpretation, because it provides three-dimensional anatomical information.

When an enhanced fluorescent signal was visible on the optical images, its location was always compared to the position on MRI, to see if the optical signal matched with the lesion location as seen on MRI.

A region of interest (ROI) was drawn at a single slice of the lesion site location for all fluorescent images over time. Separate ROIs were drawn for each imaging time point, each time matching the location of the lesion with the MRI data. For comparison, a similar ROI was drawn for each time point at the mirror image lesion site location of the contralateral breast, where no lesion was found. The visibility of the lesions on DOT was assessed quantitatively by the DOT system. For all the ROI's that were drawn, quantitative values were computed from the images of the optical absorption coefficient obtained from the DOT system. The mean fluorescence intensity of the ROIs was determined. To calculate the lesion-to-background ratio, this value was divided by the mean fluorescence of the background, which included the rest of the breast on that slice except for the lesion and the nipple (very high intensity). The same was done for the mirror image ROI to compare the values in the ipsilateral and contralateral breast. Absorption images obtained before contrast administration were also assessed for lesion visibility; lesion-to-background ratios were calculated in the same way as for the fluorescence images, in the cases that an enhanced fluorescent signal was observed.

To assess the pharmacokinetics of the new contrast agent in the breast, the uptake over time was compared quantitatively on the fluorescence images for the

different ROIs in the ipsi- and contralateral breast and the optimal imaging time point was estimated.
The reference standard for final diagnosis of the lesions was histopathology after surgery or large core needle biopsy.

Statistics

To assess whether lesion size and administered dose were different between the lesions detected with DOT and the lesions not detected with DOT, a Mann-Whitney test was performed. The software package SPSS version 15.0 (SPSS Inc., Chicago, IL, USA) was used for all statistical computations.

Results

Twelve women suspected of breast cancer were included in this study. One patient was excluded after screening measurements due to severe renal failure and therefore did not receive the contrast agent or the optical measurements. Eleven patients (mean age 54, range 23 to 81) underwent the total study procedures. Of these patients histopathology results of the breast lesions showed invasive ductal carcinoma in 8 patients (median lesion diameter 21 mm), invasive lobular carcinoma in two patients (median lesion diameter 40 mm), and a benign fibroadenoma (lesion diameter 15 mm) in one patient (**Table 1**).

Table 1. Overview of study results per patient

Patient	Age	Contrast Agent Dose (mg/kg)	Lesion Type	Lesion Diameter on MRI (mm)	Detected by DOT
1	48	0.01	IDC	25	No *
2	81	0.01	ILC	29	Yes
3	59	0.01	IDC	18	Yes
4	74	0.02	IDC	24	Yes
5	40	0.02	IDC	74	Yes
6	55	0.02	IDC	34	Yes
7	47	0.05	IDC	14	No
8	23	0.05	FA	15	No
9	62	0.05	IDC	14	No
10	51	0.1	ILC	51	No *
11	55	0.1	IDC	13	No

IDC – Invasive Ductal Carcinoma; ILC – Invasive Lobular Carcinoma; FA – Fibroadenoma; * in these cases the lesion was located close to the patient's chest wall and physically too far above the upper optical fibers in the cup to be measured by the current DOT system.

In the lowest dose group, lesions were detected in two patients on the fluorescence DOT images. In the second dose group, all three lesions were detected by DOT. No lesions were detected in the two highest dose groups. In total, five of the ten malignant lesions (50%) were visualized by DOT using the fluorescent contrast agent. The locations of lesions detected with DOT showed excellent agreement with MRI. Lesion location on the optical images was reproducible over time (**Figure 2**). Optimal lesion-to-background signals were obtained after 8 hours, ranging from 1.8 to 2.8 for the detected lesions. Non-specific fluorescent enhancement of glandular tissue was clearly visible on all optical fluorescence images, starting after 30 minutes and still evident 24 hours later (**Figure 2**). Contrast agent signal evidently increased with dose. Higher concentrations were problematic for the reconstruction algorithm, due to the absorption of the agent being no longer negligible compared to the tissue absorption, an important assumption of the algorithm. A trend in the direction of a lower administered contrast agent dose was found for the detected lesions (exact p-value 0.052). Median diameter was larger for the detected lesions (29 mm) than for the non-detected lesions (14.5 mm), but this difference was not significant (exact p-value 0.13).

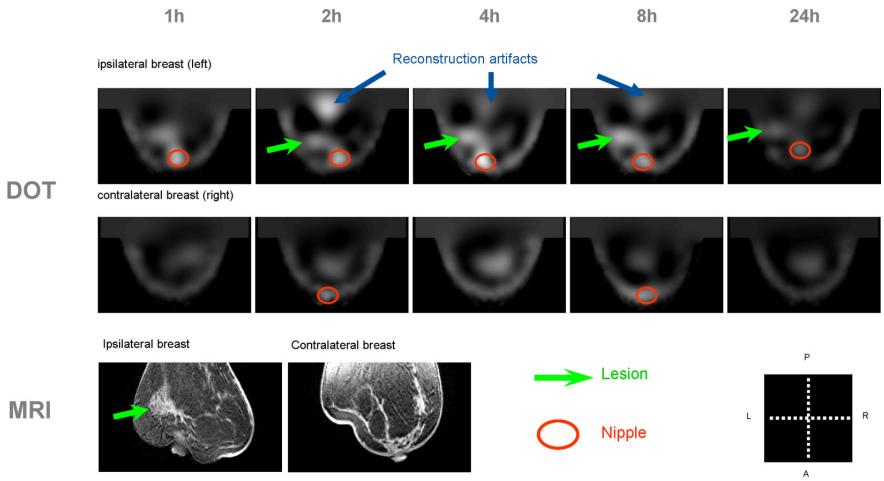

Figure 2. Example of the fluorescent images in a patient with invasive lobular carcinoma in the left breast (diameter 2.5 cm), optical images obtained 1, 2, 4, 8, and 24 hours after fluorescent contrast agent injection. Contralateral and ipsilateral breast are shown, the lesion is indicated by the arrows, nipple is encircled, some reconstruction artifacts are visible in the top middle of the images. MRI is shown for comparison. The gray scale of the optical images is adjusted individually for each image to range from 0 to 5 times the average background value. In this way the varying contrast between lesion and background in the ipsilateral breast is visible.

The absorption images obtained with DOT before the contrast administration showed higher attenuation in the lesions than in the surrounding normal parenchyma. Mean lesion-to-background ratios were 1.8, 2.6, 1.6, and 1.4, for the wavelengths 690, 730, 780, and 850 nm, respectively.

Safety

No adverse events related to the study drug were observed during this study.

Discussion

The current study shows that DOT using a low dose of the fluorescent agent Omocyanine is feasible and safe for breast cancer visualization in patients. To our knowledge, this is the first report of the use of a novel fluorescent contrast agent for optical imaging of the breast in women suspected of breast cancer.

The fluorescent signal emitted by the contrast agent after excitation by NIR light could be detected with our DOT system in all patients. Since four different dose levels of the fluorescent agent were administered (ranging from 0.01 to 0.1 mg/kg bodyweight), the absolute increase of fluorescence signal with higher doses of the contrast agent could be clearly observed. Corlu and co-workers were the first to demonstrate fluorescence DOT in patients using ICG [19]. Other investigators did not use the fluorescence, but the absorbance characteristics of ICG for their optical imaging technique [16,17]. In contrast to Corlu et al. we did not only investigate the breast with the lesion, but also the contralateral healthy breast, to obtain more information on the specificity of the technique.

In the present study, five of ten malignant lesions could be detected by fluorescence DOT. Best lesion-to-background ratios (range 1.8 - 2.8) were obtained after 8 hours. Limitations in lesion detection primarily resulted from the reconstruction algorithm and the cup geometry of the current DOT system. Lowest doses of Omocyanine performed best in lesion detection, while higher concentrations were problematic for the reconstruction algorithm. The reason was that at a higher dose level, the contrast agent absorption was no longer negligible compared to the tissue absorption, which is an important assumption of the algorithm. Even at later imaging time points (up to 24 hours) this reconstruction problem persisted due to the slow wash-out of the contrast agent. In two patients the lesions were located close to their chest walls and could not be measured by the DOT system. Most probably, during the optical scans, these lesions were physically located too far above the upper optical fibers in the cup to influence the light pathways. Advances in cup geometry are feasible and should be realized to improve visualization of these lesions.

The other important limitation in this study was that Omocyanine is a non-specific contrast agent. Ideally, this fluorescent probe would accumulate at the tumor site, by extravasation through leaky vessels. However, since it does not specifically bind to a cancer-associated target, enhancement of other normal tissues is also possible. This non-specific enhancement pattern was observed when comparing the uptake of the contrast agent over time for the lesion and mirror images in different patients. Differences were noted between patients whose breasts contained mostly fatty tissue and patients whose breasts contained mostly glandular (heterogeneously dense) tissue. To illustrate this observation, two examples are shown in **Figure 3**. As shown in the graphs, uptake of the contrast agent was much lower in fatty tissue (patient 2) than in glandular tissue (patient 5) if the lesion is compared to the mirror image location. In the patients with a high content of glandular tissue in their breasts, the uptake at the mirror image site vs. the background was quite similar to the uptake at the lesion site vs. the background. Although the sample size is small and we should be cautious in generalizing these observations, it indicates that the distinction between glandular and malignant tissue could be problematic with this non-specific fluorescent contrast agent. Clearly, there is a need for target-specific fluorescent agents to be tested in patient studies using an optical imaging device.

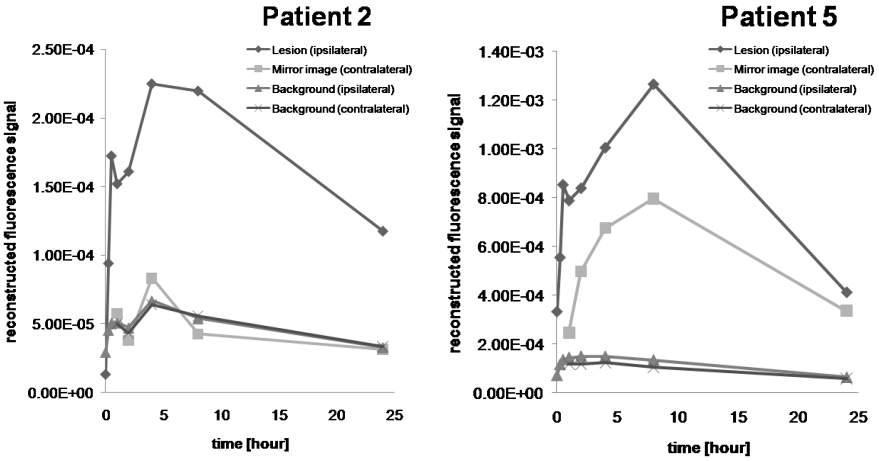

Figure 3. Dye uptake over time for patient 2 and patient 5. The dye kinetics for patient 2 with mainly fatty breast tissue (BI-RADS density category 1) show lower uptake (reconstructed fluorescence signal) of the mirror image vs. the lesion, while for patient 5 with more glandular breast tissue (BI-RADS density category 3) the dye kinetics show similar uptake of the mirror image vs. the lesion.

In the absorption mode, DOT showed around 2-fold higher absorption at the site of the malignant lesions using wavelengths 690 and 730 nm, which is in agreement with previous studies and probably related to increased light absorption by the tumors' higher hemoglobin content due to angiogenesis [7-9,11,19,23].
To gain more insight in the composition of the breast, i.e. determine relative concentrations of (de)oxyhemoglobin, fat, and water, a spectral analysis which combines data of the different wavelengths in one model could be performed. Potentially, this spectral absorption information could improve the identification of malignant lesions and the specificity of DOT.

In conclusion, in this first feasibility study we have shown that Diffuse Optical Tomography with the use of the fluorescent contrast agent Omocyanine has the potential to safely visualize malignant breast tumors in patients. Development and especially the clinical translation of fluorescent probes with specific binding affinity for relevant molecular targets will be crucial to translate molecular breast imaging to clinical applications.

References

1. Cutler M. Transillumination as an aid in the diagnosis of breast lesions. Surgery, gynecology & obstetrics 1929;48:721-728.
2. Gibson AP, Hebden JC, Arridge SR. Recent advances in diffuse optical imaging. Phys Med Biol 2005;50[4]:R1-43.
3. Chance B, Nioka S, Zhang J, et al. Breast cancer detection based on incremental biochemical and physiological properties of breast cancers: a six-year, two-site study. Acad Radiol 2005;12[8]:925-933.
4. Floery D, Helbich TH, Riedl CC, et al. Characterization of benign and malignant breast lesions with computed tomography laser mammography (CTLM): initial experience. Invest Radiol 2005;40[6]:328-335.
5. Ntziachristos V, Yodh AG, Schnall MD, Chance B. MRI-guided diffuse optical spectroscopy of malignant and benign breast lesions. Neoplasia 2002;4[4]:347-354.
6. Rinneberg H, Grosenick D, Moesta KT, et al. Scanning time-domain optical mammography: detection and characterization of breast tumors in vivo. Technol Cancer Res Treat 2005;4[5]:483-496.
7. Tromberg BJ, Cerussi A, Shah N, et al. Imaging in breast cancer: diffuse optics in breast cancer: detecting tumors in pre-menopausal women and monitoring neoadjuvant chemotherapy. Breast Cancer Res 2005;7[6]:279-285.
8. Zhu Q, Cronin EB, Currier AA, et al. Benign versus malignant breast masses: optical differentiation with US-guided optical imaging reconstruction. Radiology 2005;237[1]:57-66.
9. Intes X. Time-domain optical mammography SoftScan: initial results. Acad Radiol 2005;12[8]:934-947.
10. Taroni P, Torricelli A, Spinelli L, et al. Time-resolved optical mammography between 637 and 985 nm: clinical study on the detection and identification of breast lesions. Phys Med Biol 2005;50[11]:2469-2488.
11. Cerussi A, Shah N, Hsiang D, Durkin A, Butler J, Tromberg BJ. In vivo absorption, scattering, and physiologic properties of 58 malignant breast tumors determined by broadband diffuse optical spectroscopy. J Biomed Opt 2006;11[4]:044005.
12. Leff DR, Warren OJ, Enfield LC, et al. Diffuse optical imaging of the healthy and diseased breast: A systematic review. Breast Cancer Res Treat 2007;108[1]:9-22.
13. Hilger I, Leistner Y, Berndt A, et al. Near-infrared fluorescence imaging of HER-2 protein over-expression in tumour cells. Eur Radiol 2004;14[6]:1124-1129.

14. Montet X, Ntziachristos V, Grimm J, Weissleder R. Tomographic fluorescence mapping of tumor targets. Cancer Res 2005;65[14]:6330-6336.

15. Bremer C, Ntziachristos V, Weitkamp B, Theilmeier G, Heindel W, Weissleder R. Optical imaging of spontaneous breast tumors using protease sensing 'smart' optical probes. Invest Radiol 2005;40[6]:321-327.

16. Intes X, Ripoll J, Chen Y, Nioka S, Yodh AG, Chance B. In vivo continuous-wave optical breast imaging enhanced with Indocyanine Green. Med Phys 2003;30[6]:1039-1047.

17. Ntziachristos V, Yodh AG, Schnall M, Chance B. Concurrent MRI and diffuse optical tomography of breast after indocyanine green enhancement. Proc Natl Acad Sci USA 2000;97[6]:2767-2772.

18. Licha K, Riefke B, Ntziachristos V, Becker A, Chance B, Semmler W. Hydrophilic Cyanine Dyes as Contrast Agents for Near-infrared Tumor Imaging: Synthesis, Photophysical Properties and Spectroscopic In vivo Characterization P. Photochemistry and Photobiology 2000;72:392-398.

19. Corlu A, Choe R, Durduran T, et al. Three-dimensional in vivo fluorescence diffuse optical tomography of breast cancer in humans. Optics Express 2007;15[11]:6696-6716.

20. Van de Ven SMWY, Elias SG, Wiethoff AJ, et al. Diffuse Optical Tomography of the Breast: Initial Validation in Benign Cysts. Molecular Imaging and Biology 2008. DOI 10.1007/s11307-008-0176-x.

21. Nielsen T, Brendel B, Ziegler R, Uhlemann F, Bontus C, Koehler T. Linear Image Reconstruction for a Diffuse Optical Mammography System in a Non-Compressed Geometry Using Scattering Fluid. Biomedical Optics 2008; OSA Technical Digest: BMD23.

22. Scherleiter E, Zagar BG. Optical tomography imaging based on higher order born approximation of diffuse photon densitiy waves. IEEE Transactions on Instrumentation and Measurement 2005;54[4]:1607-1611.

23. Rice A, Quinn CM. Angiogenesis, thrombospondin, and ductal carcinoma in situ of the breast. J Clin Pathol 2002;55[8]:569-574.

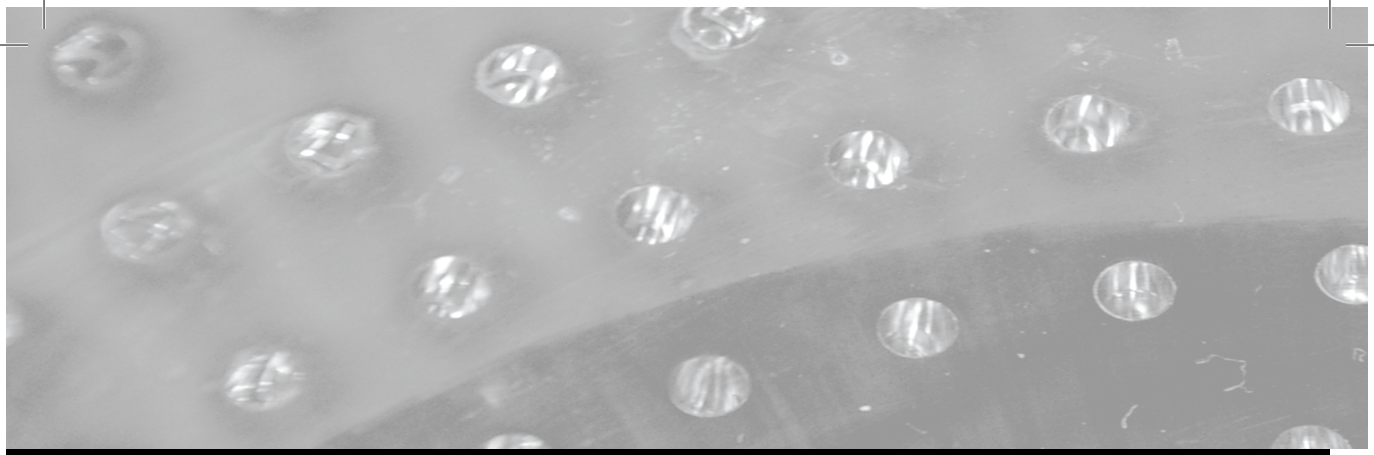

Authors

S.M.W.Y. van de Ven, N. Mincu, J. Brunette, G. Ma, M. Khayat, D.M. Ikeda, S.S. Gambhir.

Molecular Imaging and Biology. Epub 2010 Jun 8

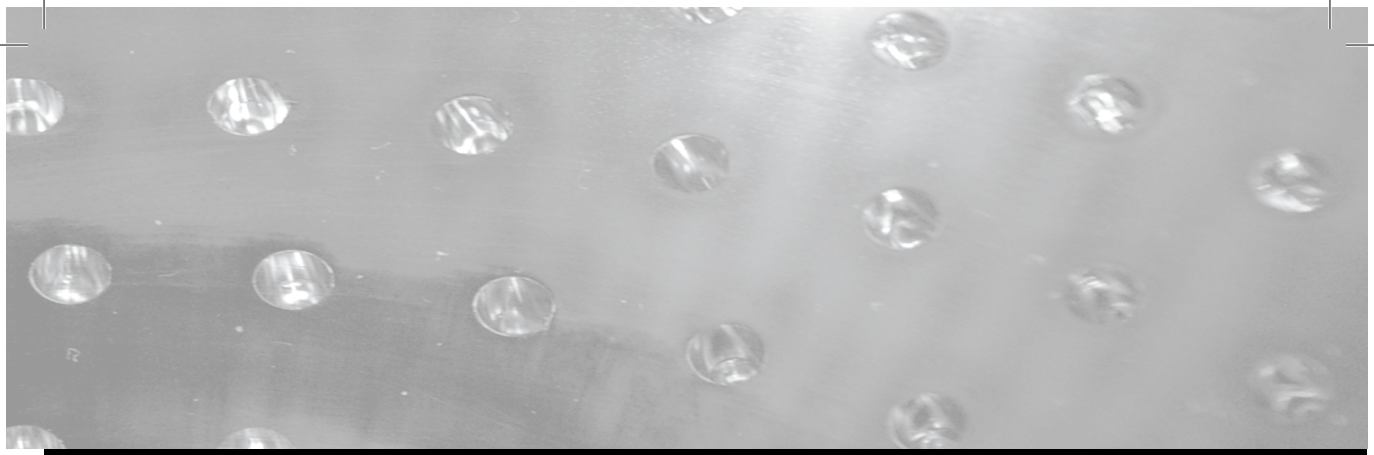

Molecular imaging using light-absorbing imaging agents and a clinical optical breast imaging system:

a phantom study

Abstract

Purpose

Determining the feasibility of using a clinical optical breast scanner with molecular imaging strategies based on modulating light transmission.

Procedures

Different concentrations of single-walled carbon nanotubes (SWNT; 0.8-20.0nM) and black hole quencher-3 (BHQ-3; 2.0-32.0μM) were studied in specifically designed phantoms (200-1570mm^3) with a clinical optical breast scanner using 4 wavelengths. Each phantom was placed in the scanner tank filled with optical matching medium (OMM). Background scans were compared to absorption scans and reproducibility was assessed.

Results

All SWNT phantoms were detected at 4 wavelengths, with best results at 684nm. Higher concentrations (≥8.0μM) were needed for BHQ-3 detection, with largest contrast at 684nm. Optical absorption signal was dependent on phantom size and concentration. Reproducibility was excellent (Intraclass Correlation 0.93-0.98).

Conclusion

Nanomolar concentrations SWNT and micromolar concentrations BHQ-3 in phantoms were reproducibly detected, showing the potential of light-absorbers, with appropriate targeting ligands, as molecular imaging agents for clinical optical breast imaging.

Introduction

Optical breast imaging uses near-infrared (NIR) light in the wavelength range of 600 to 1000 nm to assess optical properties of tissue [1]. It can provide spectroscopic information about physiological and functional tissue parameters such as angiogenesis and tissue oxygenation by using intrinsic optical contrast [2, 3]. This technique could potentially have added value to currently used breast imaging modalities: mammography, ultrasound, and dynamic contrast enhanced magnetic resonance imaging (DCE-MRI), which all have drawbacks regarding sensitivity and specificity in the diagnosis, early detection, and treatment monitoring of breast cancer [4-7]. However, several optical imaging studies have shown that differences in intrinsic optical absorption are not always pronounced enough to detect breast masses against normal tissue background [8].

A possible solution is to enhance neoplastic lesion detection with imaging agents that change light transmission. In optical imaging, different strategies for contrast enhancement are possible, such as influencing the absorption, scattering, or fluorescence properties of tissue using specific imaging agents. Fluorescent breast imaging has already been demonstrated by several research groups [9-11]. Light scattering properties could potentially be influenced by administering particles such as used in Raman spectroscopy [12]. The focus of this study is using highly light-absorbing imaging agents that absorb sufficient amounts of light to be detected by the optical imaging system. Examples of such agents are small molecules like Indocyanine Green (ICG), methylene blue (MB), or larger agents such as nanotubes or nanocages. The use of ICG in humans was reported by Ntziachristos et al. and Intes et al. [13, 14]. ICG and MB were previously used as non-targeted optical contrast agents in a rat model by Cuccia et al. [15]. Carbon nanotubes were demonstrated as photoacoustic molecular imaging agents by our laboratory (photoacoustic imaging also being based on the absorption of the molecules) [16]. If one could specifically target cancer-associated molecules with the light-absorbing imaging agents and deliver sufficient amounts to the tumor site, molecular imaging of the breast could be achieved with optical transmission imaging.

In this study we focused on light-absorbers (not fluorescent agents) to change light transmission. Our aim was to determine the feasibility of using a clinical optical breast scanner with molecular imaging strategies based on modulating light transmission. Physical phantoms based on single-walled carbon nanotubes (SWNT) and black hole quencher-3 (BHQ-3) were studied. To our knowledge this is the first report to test this new approach to molecular imaging.

Methods

Clinical Optical Breast Imaging System

A commercially available clinical optical breast imager, the SoftScan system (ART Advanced Research Technologies Inc.) was used for this study (**Figure 1**). An earlier version of this system has been previously described [17].

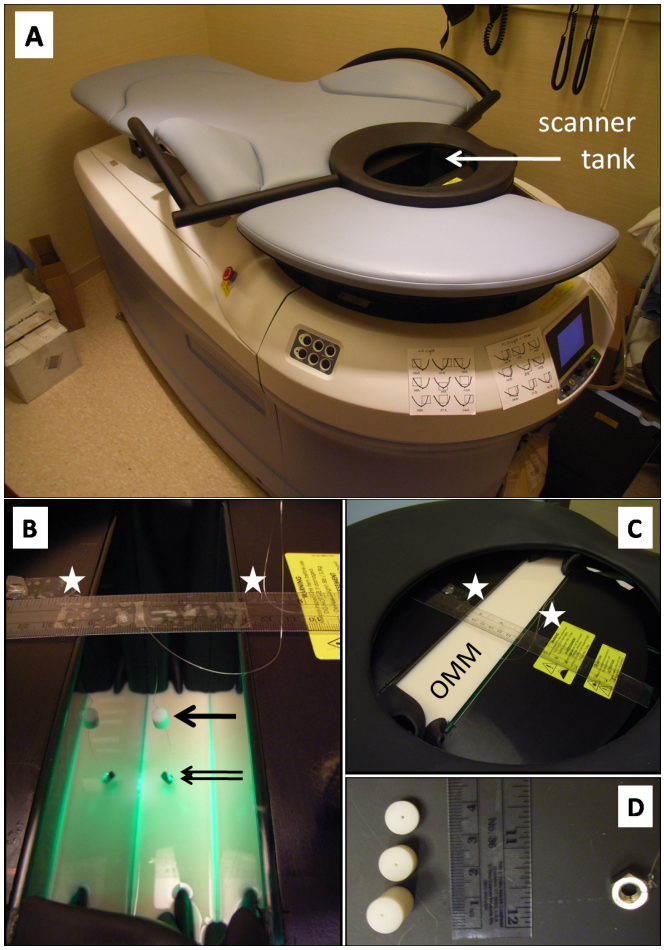

Figure 1. (A) The Clinical Optical Breast Imaging System (SoftScan, ART Advanced Research Technologies Inc.). (B) Positioning of the SWNT phantom (arrow) in the scanner tank hanging on a thin wire between the two stabilization plates (stars) with a weight at the bottom (double arrow) to keep the phantom in place; and (C) filling the tank completely with optical matching medium (OMM). (D) Examples of phantoms of three different sizes (200 mm^3, 780 mm^3, and 1570 mm^3).

This new version also uses a time resolved technique developed on a time correlated single photon counting (TCSPC) technology. It uses pulsed laser diodes (PicoQuant GmbH, Berlin- Germany) each driven at 20MHz and time multiplexed for simultaneous acquisition of all the wavelengths. The light is detected by a 5 detection channels array using optical systems comprised of lens-coupled multimode fibers that form an "M" shape constellation for collecting the photons. The detection array is placed opposite the emission fiber (transmission configuration), central detection fiber coaxial with the emission fiber.

The fibers transfer the photons to fast photomultiplier (PMT) detectors (H7422-50 from Hamamatsu Corporation, Bridgewater, NJ). The outputs of the PMTs are connected to time correlated single photon modules (SPC-130 from Becker & Hickl GmbH, Berlin-Germany) that generates the temporal histogram of the photons. The emission and detection fibers are raster scanned simultaneously over the region of examination. The patient lies in a prone position and her breast is pending in a tank with two mobile glass walls that are used for stabilizing the breast during the scan. The tank is filled up with Optical Matching Medium (OMM), containing 10% Liposyn II (Abbott Laboratories, Montreal, Canada), de-mineralized water, and India ink (Idee Cadres, Laval, Quebec, Canada) in a previously described dilution that mimics the average absorption and scattering properties of a normal breast. Data are collected at four discreet wavelengths: 684, 732, 781, and 827 nm, and consist of temporal point spread functions (TPSF) acquired with a 10 picosecond resolution within a 12.5 nanosecond time window. Among the critical aspects of the time resolved systems are the drift (<5 ps/hour) and the jitter (2 ps) [18].

Phantoms and contrast agents

Solid inclusions were made from polyurethane resin (Axson, Eaton Rapids, MI). Titanium dioxide (TiO2; Alfa Aesar, Ward Hill, MA) was added as scattering agent and ProJet 900NP (Avecia, Billingham, UK) as absorbing agent to mimic the optical properties of normal breast tissue: average scattering coefficient 1 mm^{-1} at 780 nm and minimum absorption coefficient 0.002 mm^{-1} at 780 nm. The details regarding the design and validation of phantoms are described in previous published papers [19, 20]. The imaging agents to be tested, the SWNT and BHQ-3, were added at various concentrations. They were dissolved in dimethyl sulfoxide (DMSO) before mixing with polyurethane resin and ultrasonication was used to ensure homogeneous phantoms. AP grade SWNTs were obtained from CarboLex Inc. (Lexington, KY) with typical sizes of approximately 1 nm in diameter and 1 μm in length. BHQ-3 was obtained from Biosearch Technologies Inc. (Novato, CA). Phantoms with no addition of imaging agent were fabricated as control phantoms.

Measurement procedures

For the measurements, the solid inclusions were positioned in the system scanner tank, hanging on a thin fish wire between the glass stabilization plates, where normally a patient's breast would be positioned (**Figure 1**).
The stabilization plates were positioned 60 mm apart, corresponding to the typical thickness expected for a breast. The volume of the tank was filled up with OMM. The solid inclusions were positioned in a central position within the scanner tank. Six concentrations of SWNTs (0.8, 1.6, 2.4, 4.0, 6.4, 20.0 nM) were measured in specifically designed solid phantoms of 3 sizes (200 mm^3, 780 mm^3, 1570 mm^3) on the clinical optical breast scanner using all 4 wavelengths. We first performed scans using only OMM to acquire the background signal. Then, SWNT absorption scans were done and compared to background absorption. Measurements were also repeated on 2 days at 4 weeks apart, to assess reproducibility. Five concentrations of BHQ-3 (2.0, 4.0, 8.0, 16.0, 32.0 μM) were tested in an equivalent experimental setup using phantoms of two different sizes (200 and 780 mm^3). These measurements were also repeated 4 weeks later.
Data for the tomographic view is acquired in transmission mode using 5 detection points for each illumination point positioned at angles optimized for maximizing the accuracy and sensitivity of the tomographic reconstruction. This 1x5 source-detectors configuration is moved inside the field of view using a raster scan in step-and-shoot mode. The step size is adjustable in the range 0.5mm to 10mm with 0.1mm accuracy. In the standard study workflow, data acquisition is performed in two steps: 1) a fast low precision scan is performed. The results of this scan are used for power optimization of the lasers during the high precision scan to maximize signal to noise ratio (SNR); and 2) a high precision scan with optimized SNR is performed, using the step size and field of view selected by the user. For this study a scan resolution of 3 x 3 mm (i.e. scan step size of 3 mm in both x and y directions) and a field of view of 54 x 54 mm were used for the high precision scan. For these settings the scan duration was ~6 min for the high precision and less than 2 min for the low precision scan.

Image analysis

The tomographic reconstruction and analysis of the images were performed using the SoftScan Review Workstation Software, (ART Advanced Research Technologies Inc.). The software includes a diffuse optical tomography (DOT) algorithm based on the diffusion equation [21], using the linearization of the heterogeneous time-domain diffusion equation within the first order of Rytov approximation [22].

Using the 0th and 1st moments of the temporal distributions of photons and the Levenberg-Marquard minimization algorithm the local differential scattering and absorption coefficients are evaluated for each of the four wavelengths. The thickness of the slice used for 3D reconstruction was 3 mm.

In this study, images of the absorption coefficient were used for the analysis of the contrast of the SWNT inclusions. Circular regions of interest (ROIs) of a constant size (10 mm diameter) were defined on the image of the slice that displays maximum absorption contrast for the inclusions. For the background scan, with OMM only, identical ROIs were placed at the same positions as for the inclusions. Average absorption was calculated by the software. Regression lines were fitted through the data sets using Microsoft Office Excel 2007.

Reproducibility of measurements was determined using intra-class correlation coefficients. The software package SPSS 15.0 (SPSS Inc., Chicago, IL, USA) was used for the statistical computations.

Results

All phantoms of different sizes and SWNT concentrations were detected by the system at all four wavelengths, with the best results obtained at 684 nm (**Figures 2 and 4**). SWNT absorption was between 10% and 80% higher than background absorption, which was statistically significant ($p < 0.05$; **Figure 4**).

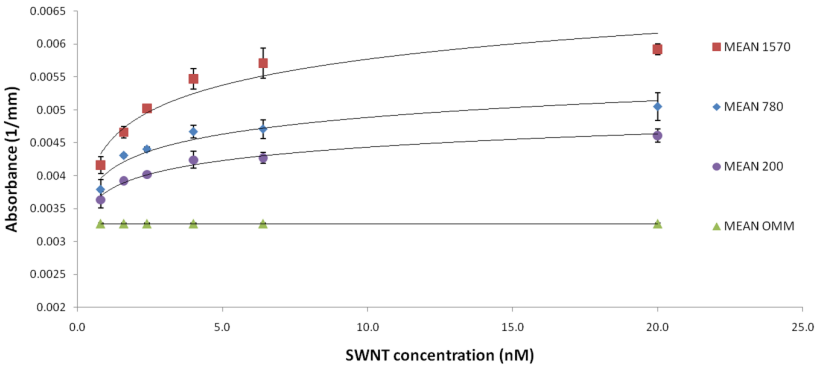

Figure 2. Average absorption measurements at 684 nm of phantoms of three sizes (200, 780, and 1570 mm^3) containing six concentrations of SWNTs (0.8, 1.6, 2.4, 4, 6.4, 20 nM). Error bars represent the standard deviation of duplicate measurements.

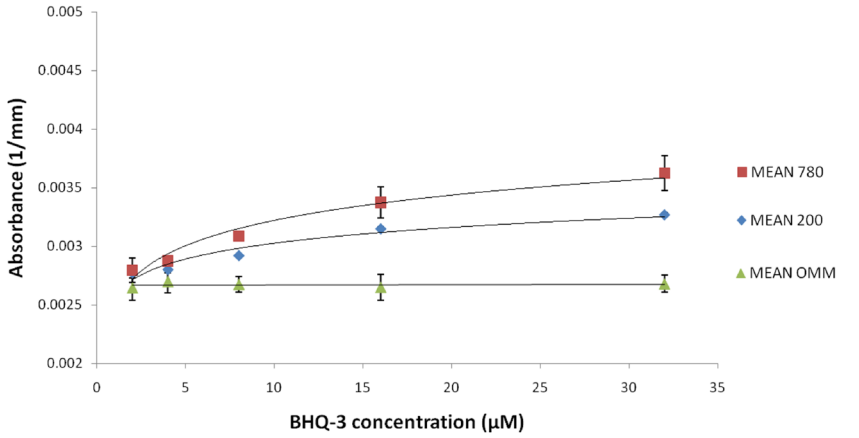

Figure 3. Average absorption measurements at 684 nm of phantoms of two sizes (200 and 780 mm^3) containing five concentrations of BHQ-3 (2.0, 4.0, 8.0, 16, 32 µM). Error bars represent the standard deviation of duplicate measurements.

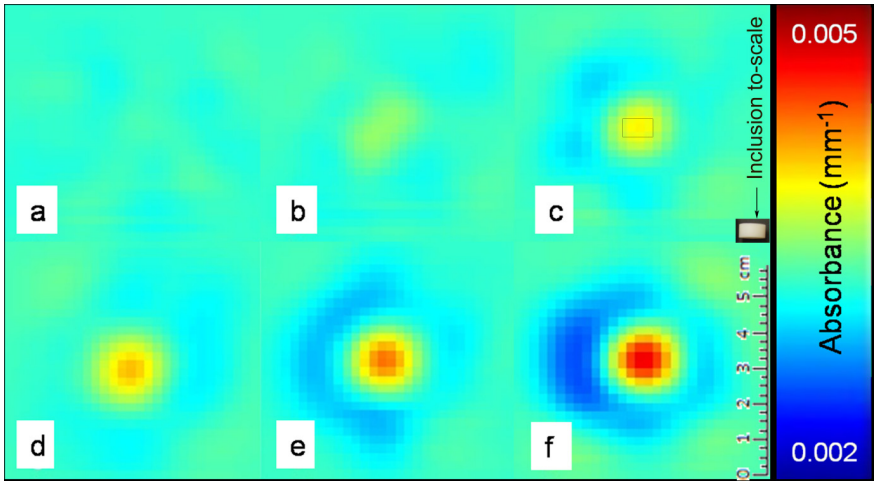

Figure 4. Optical absorption measurements at 684 nm: (a) optical matching medium only; (b-f) 200 mm^3 phantom with different SWNT concentrations, i.e. 0.8 (b), 1.6 (c), 2.4 (d), 6.4 (e), and 20 nM (f).

For the BHQ-3 phantoms 684 nm was also the most sensitive wavelength (**Figure 3**). Higher probe concentrations were needed in order to detect the BHQ-3 phantoms. Concentrations > 8.0 µM gave an increase in absorption between 15-30% compared to background absorption; phantoms containing BHQ-3 in concentrations < 8.0 µM were not visible on the optical images. To detect BHQ-3 at wave-

lengths other than 684 nm higher concentrations of the imaging agent would be required, as can be expected from the absorbance spectrum of BHQ-3 [23].
Optical absorption signal (y) was dependent on phantom size and SWNT concentration (x), e.g. for 200 mm^3 at 684 nm: $y = 0.0003 \ln(x) + 0.0038$, $R^2 = 0.98$. Similar size and concentration dependency was seen for the BHQ-3 phantoms, e.g. for 200 mm^3 at 684 nm: $y = 0.0002\ln(x) + 0.0026$, $R^2 = 0.94$. See Supplementary Information for all results. Absorption of the control phantoms that did not contain SWNT or BHQ-3 was approximately equal to the background (OMM) absorption (no statistically significant difference; $p > 0.65$). Reproducibility of measurements was excellent for both SWNT and BHQ-3 phantoms at all wavelengths with Intraclass Correlation Coefficients ranging from 0.93 to 0.98 (**Table 1**).

Table 1. Reproducibility of measurements for SWNT and BHQ-3 phantoms per wavelength.

Wavelength	Intraclass correlation coefficient for SWNT[a] (95% Confidence Interval)	Intraclass correlation coefficient for BHQ-3[a] (95% Confidence Interval)
684	0.97 (0.91 to 0.99)	0.93 (0.87 to 0.96)
732	0.97 (0.91 to 0.99)	0.93 (0.87 to 0.96)
781	0.98 (0.94 to 0.99)	0.94 (0.88 to 0.97)
827	0.96 (0.89 to 0.98)	0.94 (0.88 to 0.97)

[a]One-way random effects model where people effects are random (single measures).

Discussion

Detection of SWNT and BHQ-3 in phantoms in a clinical optical breast scanner is possible at nanomolar and micromolar concentrations, respectively, showing the potential of using highly light-absorbing molecular imaging agents as optical imaging agents for breast disease. We found a positive relationship between the optical absorption signal and the concentration of the imaging agent. The reproducibility of the results was excellent.
The use of multiple wavelengths showed differences in absorption changes for the tested phantoms. For both SWNT and BHQ-3, 684 nm showed the most optimal changes in absorption; for SWNT there were only small differences with the results at other wavelengths, but for BHQ-3 the same phantoms could not be detected at the higher wavelengths (**see Supplementary Figures 1-6**). These results can be predicted from the absorbance spectra of the imaging agents: for BHQ-3 optical absorbance decreases rapidly at wavelengths higher than 700 nm [23],

while for SWNT absorbance spectra are more constant, displaying only a slow and small decrease for wavelengths longer than 680 nm [16, 24].

In this initial study we tested a new approach to molecular imaging using a clinical optical breast scanner to detect changes in light transmission. We limited ourselves to one particular study set up, using phantoms that were positioned in the same way within the scanner tank each time, surrounded by optical matching media. This approach uses a relatively simple and homogeneous approximation of a patient's breast and may be one of the limitations of our study. Results should therefore be validated in future studies in heterogeneous breast tissue, preferably in vivo. However, in our strategy we regard the exogenous optical absorption as a relative change added on top of the existing endogenous optical absorption (determined in the first scan, before imaging agent administration). In this way, the tomographic reconstruction algorithm will take care of the heterogeneity of a breast, detecting the optical absorption changes after molecular imaging agent administration and thereby significantly reducing the impact of some well known limitations of diffuse optical tomography. Other limitations include the relatively poor spatial resolution of optical imaging and the complexities of its tomographic image reconstruction. The reconstruction models used by our system derive optical properties from the temporal histogram of the photons after propagation through diffuse media, the TPSF. When a TPSF is measured nearby a small inclusion with very high absorption contrast compared with the surrounding background, the inclusion will contribute to the TPSF in a way that can generate a transitory effect: the "ring-artifacts" around the inclusions as seen in **Figure 4** (in particular 4e-f). The spatial resolution of the images is determined by the optical properties of the tissue, the breast thickness, and step size for each scan. The step size and acquisition time were optimized for a breast thickness ranging from 40 mm to 80 mm (between the stabilization plates) and the expected contrast between the optical properties of breast tumors in early stages and the normal surrounding tissue (a tumor volume of ~ 1cm^3 shows an absorption increase of approximately 2 times due to angiogenesis). The addition of the molecular imaging agent will allow detection of tumors with smaller volumes at even earlier stages of development (<1 cm^3). Decreasing the step size would probably not influence the spatial resolution significantly due to the level of diffusion in the breast tissue. Due to this strong diffusion the photons arriving at the detection point propagate through large volumes, much wider than the size of inclusions used in the study. This is equivalent to using a beam larger than the sample in classic spectroscopy in non-scattering media: a very large percentage of the photons could arrive to the detec-

tion point without sensing the absorption effects of the inclusions by travelling around it. The result is the so called partial volume effect: a smaller contribution of the volume of interest to the overall absorption and by consequence a smaller contrast. When the absorption of the inclusions is close to that typical for breast tissue those values are small enough and all of the absorber's molecules (SWNT, BHQ, etc.) are still contributing to the overall absorption. In this case the contrast obtained is linear with their concentration, as one could observe in **Figure 2** for the first 2-3 concentration values, before the partial volume effect and/or the higher concentrations are shifting it towards more logarithmic dependence. For higher concentrations the absorption is dominated by the absorbers distributed near the surface, reducing the contribution of the inclusion's core drastically. This shelf-shielding process reduces the effective absorption of the inclusion. Due to the diffusion its higher absorption is sensed at larger distances. This process generates some increase of the reconstructed size of the inclusion, visible in **Figure 4**. The result of the two effects is a "dilution" of the contrast that is no longer linear with the concentration having an asymptotic trend towards a maximum value that corresponds to the moment when all photons incident on the surface of the inclusion are absorbed. The detectability threshold could be reached by different combinations of volume and absorption. The contribution of a specific highly light-absorbing compound could significantly reduce the minimum volume visualized by the optical imaging system, possibly improving early detection of breast tumors. More investigations are needed to determine the minimum tumor size that can be detected for the largest amounts of dye (e.g. 1 μM SWNT) that can be delivered and accumulate at that site. In addition, more information is needed on relevant clinical imaging agent concentrations, i.e. how much of each imaging agent can realistically be delivered to the tumor site? De la Zerda et al. estimated concentrations of approximately 33.5 nM at the tumor site in their photoacoustic experiments [16]. Although SWNTs used in their study were about 5 times shorter than ours and in vivo delivery and accumulation depend on various factors, this gives some indication that the concentration ranges we were able to detect with the clinical optical breast scanner (0.8 – 20 nM) may be clinically relevant.

Results of our study are encouraging for optical transmission breast imaging as a modality, since these data support opportunities for application of molecular breast imaging using highly light-absorbing imaging agents. With the use of relevant target-specific imaging agents, optical imaging could be a valid candidate for the earlier detection of breast cancer, e.g. in young women with dense breasts who are at increased breast cancer risk and for whom mammographic screening

has very limited sensitivity [25, 26]. Other potential applications of this technique may be the selection of appropriate treatment, investigation of drug delivery, and early evaluation of response to treatment in breast cancer patients [27]. An important advantage of optical imaging is that it does not use any radioactive components or ionizing radiation and can thus be used more frequently, without restrictions for the timeline of the protocol. Because our strategy uses changes in light transmission (as opposed to fluorescence imaging), we do not encounter problems due to excitation light leaking through filters and causing high noise levels, an important problem in fluorescence optical imaging [28]. In addition, penetration depth with this technique (up to 15 cm) is more favorable than in other optical imaging techniques, such as optical coherence tomography (OCT) or Raman spectroscopy (up to 5 mm) [12, 29].

Linking nanotubes to relevant peptides has already been demonstrated and these target-specific molecular imaging agents have been imaged successfully in vivo [16]. In addition, preliminary toxicology studies showed no apparent toxicity which is encouraging for clinical translation [30]. We can imagine that each of the light-absorbing agents (from small molecules to larger nanoparticles) can be functionalized with selective targeting ligands, creating a spectrum of highly specific light-absorbing molecular imaging agents. Moreover, these agents could potentially be used as "theranostics", combining the process of diagnosis and therapy [31].

In future studies we plan to explore the effect of the position and size of the phantoms in the scanner, other potential light-absorbing molecular imaging agents (such as IRDye 800CW, gold and silver nanoparticles, etc.), and the influence of targeting ligands linked to these imaging agents (e.g. peptides targeting $\alpha v \beta 3$ integrin, epidermal growth factor receptor, etc.), aiming for their eventual evaluation in a clinical setting.

In conclusion, we have shown that nanomolar concentrations of SWNT and micromolar concentrations of BHQ-3 in physical phantoms can reproducibly be detected by a clinical optical breast imager based on transmission optical imaging. This shows the potential of using highly light-absorbing molecular imaging agents, with appropriate targeting ligands, as optical imaging agents for breast disease using a commercially available clinical optical breast scanner.

Supplementary Information

Supplementary figures

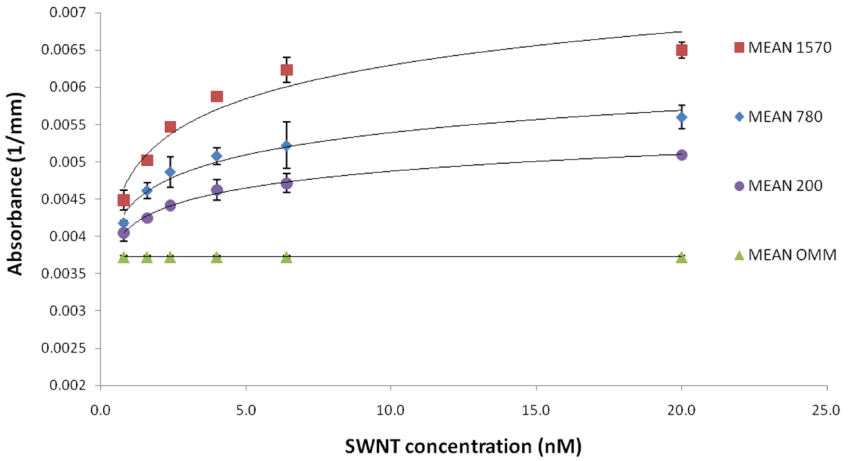

Figure 1. Average absorption measurements at 732 nm of phantoms of three sizes (200, 780, and 1570 mm^3) containing six concentrations of SWNTs (0.8, 1.6, 2.4, 4, 6.4, 20 nM). Error bars represent the standard deviation of duplicate measurements.

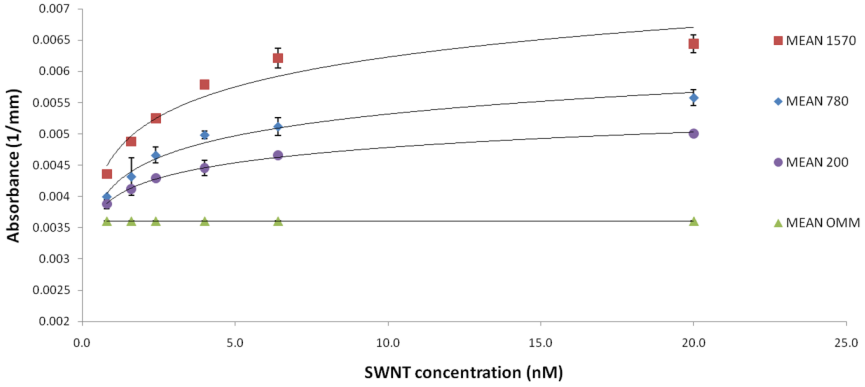

Figure 2. Average absorption measurements at 781 nm of phantoms of three sizes (200, 780, and 1570 mm^3) containing six concentrations of SWNTs (0.8, 1.6, 2.4, 4, 6.4, 20 nM). Error bars represent the standard deviation of duplicate measurements.

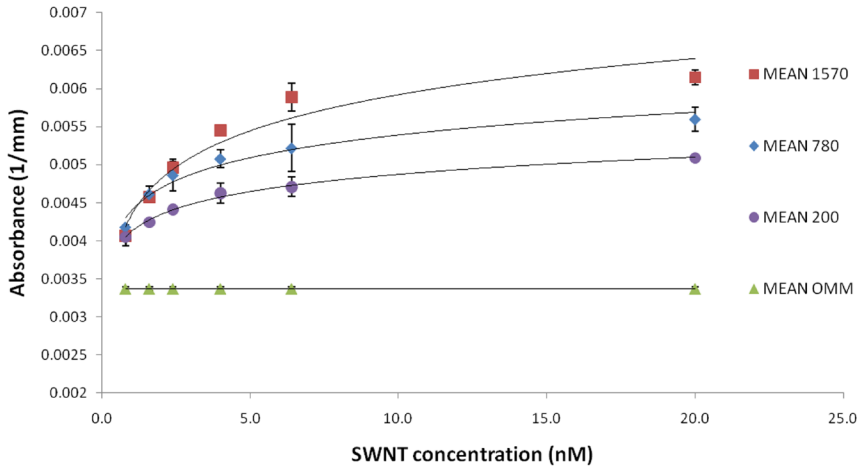

Figure 3. Average absorption measurements at 827 nm of phantoms of three sizes (200, 780, and 1570 mm^3) containing six concentrations of SWNTs (0.8, 1.6, 2.4, 4, 6.4, 20 nM). Error bars represent the standard deviation of duplicate measurements.

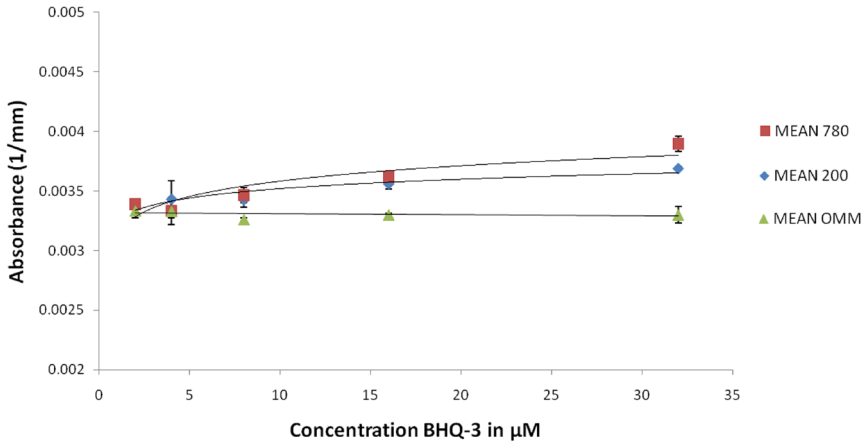

Figure 4. Average absorption measurements at 732 nm of phantoms of two sizes (200 and 780 mm^3) containing five concentrations of BHQ-3 (2.0, 4.0, 8.0, 16, 32 µM). Error bars represent the standard deviation of duplicate measurements.

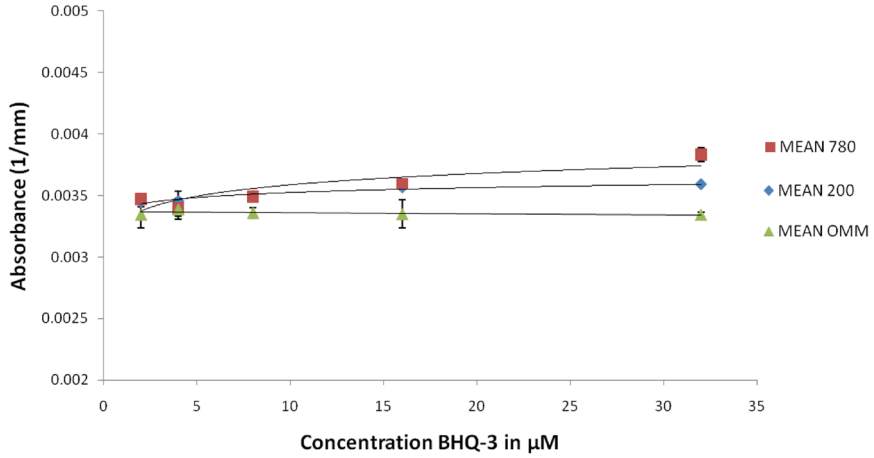

Figure 5. Average absorption measurements at 781 nm of phantoms of two sizes (200 and 780 mm^3) containing five concentrations of BHQ-3 (2.0, 4.0, 8.0, 16, 32 µM). Error bars represent the standard deviation of duplicate measurements.

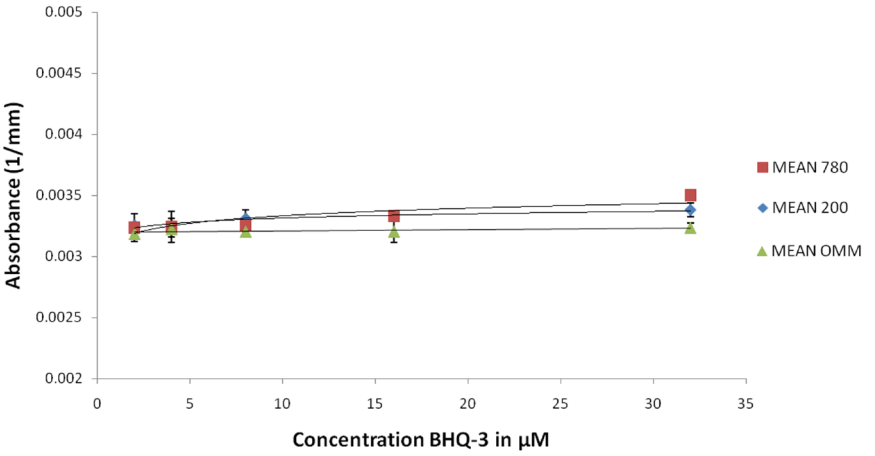

Figure 6. Average absorption measurements at 827 nm of phantoms of two sizes (200 and 780 mm^3) containing five concentrations of BHQ-3 (2.0, 4.0, 8.0, 16, 32 µM). Error bars represent the standard deviation of duplicate measurements.

Supplementary Tables

Supp. Table 1. Dependency of optical absorption signal (y) on SWNT/BHQ-3 concentration (x) for each phantom size and wavelength.

Wavelength	Equation for SWNT phantoms [R2]			Equation for BHQ-3 phantoms [R2]	
	200 mm^3	780 mm^3	1570 mm^3	200 mm^3	780 mm^3
684	y = 0.0003ln(x) + 0.0038 [0.98]	y = 0.0004ln(x) + 0.004 [0.93]	y = 0.0006ln(x) + 0.0045 [0.92]	y = 0.0002ln(x) + 0.0026 [0.94]	y = 0.0003ln(x) + 0.0025 [0.97]
732	y = 0.0003ln(x) + 0.0041 [0.99]	y = 0.0004ln(x) + 0.0044 [0.97]	y = 0.0006ln(x) + 0.0048 [0.93]	y = 0.0001ln(x) + 0.0033 [0.90]	y = 0.0002ln(x) + 0.0032 [0.82]
781	y = 0.0004ln(x) + 0.004 [1.00]	y = 0.0005ln(x) + 0.0042 [0.98]	y = 0.0007ln(x) + 0.0046 [0.93]	y = 0.00006ln(x) + 0.0034 [0.95]	y = 0.0001ln(x) + 0.0033 [0.74]
827	y = 0.0003ln(x) + 0.0041 [0.99]	y = 0.0004ln(x) + 0.0044 [0.97]	y = 0.0007ln(x) + 0.0043 [0.94]	y = 0.00005ln(x) + 0.0032 [0.87]	y = 0.00009ln(x) + 0.0031 [0.77]

Acknowledgements

This work was supported, in part, by funding from ART Advanced Research Technologies Inc., National Cancer Institute (NCI) In Vivo Cellular Molecular Imaging Center (ICMIC) grant P50 CA114747 (SSG), NCI Center of Cancer Nanotechnology Excellence (CCNE) CA119367 U54, and the Canary Foundation. We also thank Adam de la Zerda for helpful discussions.

References

1. Gibson AP, Hebden JC, Arridge SR. Recent advances in diffuse optical imaging. Phys Med Biol 2005; 50:R1-43.
2. Ntziachristos V, Chance B. Probing physiology and molecular function using optical imaging: applications to breast cancer. Breast Cancer Res 2001; 3:41-46.
3. Tromberg BJ, Shah N, Lanning R, et al. Non-invasive in vivo characterization of breast tumors using photon migration spectroscopy. Neoplasia 2000; 2:26-40.
4. Peters NH, Borel RI, Zuithoff NP, Mali WP, Moons KG, Peeters PH. Meta-analysis of MR imaging in the diagnosis of breast lesions. Radiology 2008; 246:116-124.
5. Raza S, Chikarmane SA, Neilsen SS, Zorn LM, Birdwell RL. BI-RADS 3, 4, and 5 Lesions: Value of US in Management--Follow-up and Outcome. In, 2008; 773-781.
6. Pisano ED, Gatsonis C, Hendrick E, et al. Diagnostic performance of digital versus film mammography for breast-cancer screening. N Engl J Med 2005; 353:1773-1783.
7. Yeh E, Slanetz P, Kopans DB, et al. Prospective comparison of mammography, sonography, and MRI in patients undergoing neoadjuvant chemotherapy for palpable breast cancer. AJR Am J Roentgenol 2005; 184:868-877.
8. Leff DR, Warren OJ, Enfield LC, et al. Diffuse optical imaging of the healthy and diseased breast: A systematic review. Breast Cancer Res Treat 2008; 108:9-22.
9. Godavarty A, Thompson AB, Roy R, et al. Diagnostic imaging of breast cancer using fluorescence-enhanced optical tomography: phantom studies. J Biomed Opt 2004; 9:488-496.
10. Corlu A, Choe R, Durduran T, et al. Three-dimensional in vivo fluorescence diffuse optical tomography of breast cancer in humans. Opt Express 2007; 15:6696-6716.
11. van de Ven S, Wiethoff A, Nielsen T, et al. A novel fluorescent imaging agent for Diffuse Optical Tomography of the breast: first clinical experience in patients. Mol Imaging Biol 2009; Epub ahead of print.
12. Zavaleta CL, Smith BR, Walton I, et al. Multiplexed imaging of surface enhanced Raman scattering nanotags in living mice using noninvasive Raman spectroscopy. Proc Natl Acad Sci U S A 2009; 106:13511-13516.
13. Ntziachristos V, Yodh AG, Schnall M, Chance B. Concurrent MRI and diffuse optical tomography of breast after indocyanine green enhancement. Proc Natl Acad Sci U S A 2000; 97:2767-2772.
14. Intes X, Ripoll J, Chen Y, Nioka S, Yodh AG, Chance B. In vivo continuous-wave optical breast imaging enhanced with Indocyanine Green. Med Phys 2003; 30:1039-1047.

15. Cuccia DJ, Bevilacqua F, Durkin AJ, et al. In vivo quantification of optical contrast agent dynamics in rat tumors by use of diffuse optical spectroscopy with magnetic resonance imaging coregistration. Appl Opt 2003; 42:2940-2950.

16. De la Zerda A, Zavaleta C, Keren S, et al. Carbon nanotubes as photoacoustic molecular imaging agents in living mice. Nat Nanotechnol 2008; 3:557-562.

17. Intes X. Time-domain optical mammography SoftScan: initial results. Acad Radiol 2005; 12:934-947.

18. Ntziachristos V, Chance B. Accuracy limits in the determination of absolute optical properties using time-resolved NIR spectroscopy. Med Phys 2001; 28:1115-1124.

19. Vernon ML, Freachette J, Painchaud Y, Caron S, Beaudry P. Fabrication and characterization of a solid polyurethane phantom for optical imaging through scattering media. Appl Opt 1999; 38:4247-4251.

20. Mincu N, Brunette J, Guilman O, et al. Diffuse optical tomography and spectroscopy performance assessment: phantoms and methodology. In:Design and Performance Validation of Phantoms Used in Conjunction with Optical Measurements of Tissue. 1 ed. San Jose, CA, USA: SPIE, 2008; 68700O-68710.

21. Contini D, Martelli F, Zaccanti G. Photon migration through a turbid slab described by a model based on diffusion approximation. I. Theory. Appl Opt 1997; 36:4587-4599.

22. Arridge SR, Schweiger M. Image reconstruction in optical tomography. Philos. Trans R Soc Lond B Biol Sci 1997; 352:717-726.

23. Black Hole Quencher® Dyes. Biosearch Technologies Inc. Novato, CA. http://www.biosearchtech.com/support/applications/dyes-from-biosearch-technologies/black-hole-quencher%C2%AE-dyes. Accessed February 19, 2010.

24. Kam NW, O'Connell M, Wisdom JA, Dai H. Carbon nanotubes as multifunctional biological transporters and near-infrared agents for selective cancer cell destruction. Proc Natl Acad Sci U S A 2005; 102:11600-11605.

25. Carney PA, Miglioretti DL, Yankaskas BC, et al. Individual and combined effects of age, breast density, and hormone replacement therapy use on the accuracy of screening mammography. Ann Intern Med 2003; 138:168-175.

26. Boyd NF, Guo H, Martin LJ, et al. Mammographic density and the risk and detection of breast cancer. N Engl J Med 2007; 356:227-236.

27. Mincu N, Djeziri S, Ichalalene Z, Leblond F, Khayat M. Sensitivity and repeatability of diffuse optical tomography: towards breast cancer neoadjuvant treatment monitoring. In:Optical Tomography and Spectroscopy of Tissue VII. 1 ed. San Jose, CA, USA: SPIE, 2007; 64341D-64349.

28. Godavarty A, Eppstein MJ, Zhang C, Sevick-Muraca EM. Detection of single and multiple targets in tissue phantoms with fluorescence-enhanced optical imaging: feasibility study. Radiology 2005; 235:148-154.

29. Weissleder R, Ntziachristos V. Shedding light onto live molecular targets. Nature Medicine 2003; 9:123.

30. Schipper ML, Nakayama-Ratchford N, Davis CR, et al. A pilot toxicology study of single-walled carbon nanotubes in a small sample of mice. Nat Nanotechnol 2008; 3:216-221.

31. Debbage P, Jaschke W. Molecular imaging with nanoparticles: giant roles for dwarf actors. Histochem Cell Biol 2008; 130:845-875.

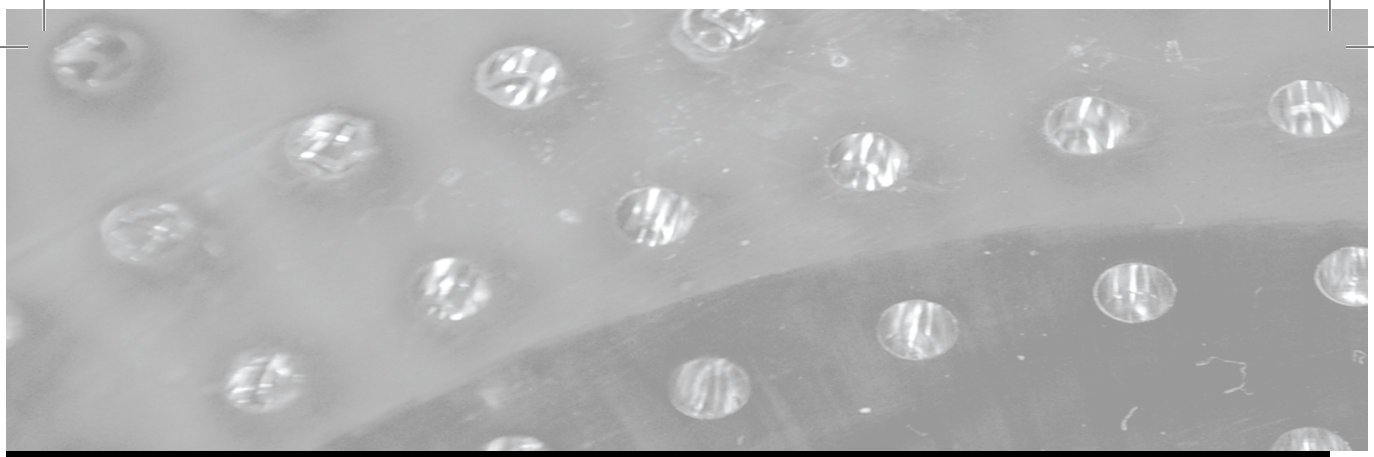

Authors

S.M.W.Y. van de Ven, S.G. Elias, C.T. Chan, Z. Miao, Z. Cheng, A. De, S.S. Gambhir.

Submitted.

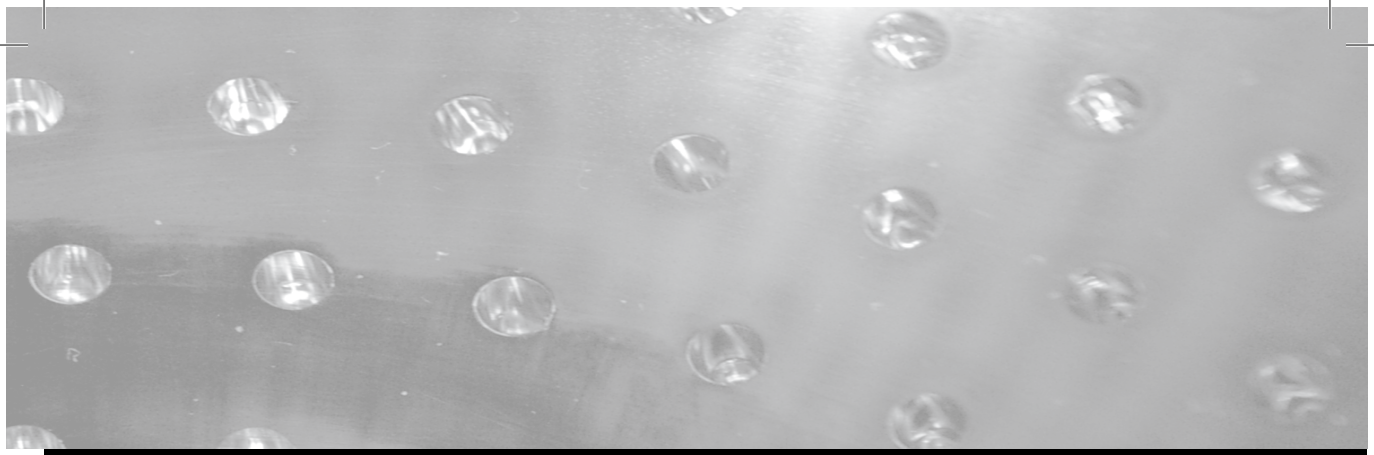

Optical imaging with HER2-targeted affibody molecules can monitor Hsp90 treatment response in a xenograft mouse model

Abstract

Purpose

To determine if optical imaging can be used for *in vivo* therapy response monitoring as an alternative to nuclear techniques. For this we evaluated the HER2 response to 17-DMAG treatment, a Hsp90 inhibitor.

Experimental design

After *in vitro* 17-DMAG treatment response evaluation of MCF7 parental cells and two HER2 transfected clones (Clone A medium, B high HER2 expression), we established human breast cancer xenografts in nude mice (only parental and clone B) for *in vivo* evaluation. Mice received 120 mg/kg of 17-DMAG in 4 doses at 12 hour intervals i.p. (n=10), or PBS as carrier control (n=5). Optical images were obtained both pre-treatment (day -1) and post-treatment (day 3, 6, and 9), always 5 hours post-injection of 500 pmol of anti-HER2 Affibody-AlexaFluor680 via tail vein (with pre-injection background subtraction). Day 9 *in vivo* optical imaging signal was correlated with *ex vivo* HER2 levels by western blot after sacrifice.

Results

HER2 expression decreased with 17-DMAG dose *in vitro*. *In vivo* optical imaging signal was reduced by 21% in Clone B (p=0.016) and by 13% in MCF7 parental tumors (p=0.063) at 3 days after 17-DMAG treatment; optical imaging signal recovered in both tumor types at day 6-9. In the carrier group no signal reduction was observed. Pearson correlation of *in vivo* optical imaging signal with *ex vivo* HER2 levels ranged from 0.74 to 0.89.

Conclusion

Optical imaging with an affibody can be used to non-invasively monitor changes in HER2 expression *in vivo* as a response to treatment with an Hsp90 inhibitor.

Introduction

Treatment monitoring is of key importance in patient management and drug development. As yet, response to treatment is predominantly determined by changes in the anatomy, e.g. tumor size changes on computed tomography (CT) in the Response Evaluation Criteria in Solid Tumors (RECIST) [1]. These anatomical changes occur relatively late in the treatment process and do not necessarily provide specific information on tissue function and viability. Magnetic resonance imaging (MRI) can provide additional functional information on blood flow and water diffusion, but no specific molecular information on early treatment response [2]. Nuclear imaging techniques such as positron emission tomography (PET) and single photon emission computed tomography (SPECT) with the use of selective radiotracers could partly offer a solution [3], but its radioactive components hinder repetitive imaging and tracers are relatively difficult to generate and expensive. Optical imaging could be a valuable tool for treatment monitoring at the molecular level. Optical molecular imaging is not yet available as a routine clinical modality, however optical breast imaging devices using diffuse near-infrared light are currently under evaluation in clinical studies [4-11]. The breast is an accessible target organ for diffuse optical imaging since light can penetrate deep enough (up to 15 cm) into the tissue without having to pass through other highly absorbing or scattering tissues (such as bone or lung) [12]. Optical imaging is widely used in the preclinical setting and new molecular imaging agents, specifically targeting cancer-associated molecules, are rapidly being developed [13]. The major advantages of optical imaging are that it uses no ionizing radiation and that the optical imaging probes are much cheaper and easier to generate than PET tracers. However, optical signal quantification is challenging and more complex than in PET imaging. We established a preclinical model to study the feasibility of optical imaging as a molecular imaging tool for treatment monitoring. If signal quantification is accurate enough to measure known treatment effects, optical imaging has great potential in selecting and tailoring clinical treatment protocols based on imaging results of the individual patient, as well as a key role in high throughput screening and testing of new drugs in preclinical models.

In our xenograft model we used human epidermal growth factor receptor-2 (HER2) positive human breast cancer cell lines. HER2 overexpression (up to 40-100 fold) is seen in approximately 25-30% of breast cancers and is associated with aggressive biological behavior [14]. There are various imaging agents available that target HER2 [15]. In our imaging experiments we chose to use an affibody for its small size (7KDa) and favorable pharmacokinetic characteristics [16-18]. Recently,

this affibody was used to image metastatic breast cancer in humans [19]. To influence the HER2 levels expressed by the tumor cells we used a heat shock protein 90 (Hsp90) inhibitor. Hsp90 is a molecular chaperone responsible for the correct folding, intracellular disposition, and function of a range of proteins, including oncoproteins (such as HER2) that are highly expressed or mutated in cancer cells [20]. Hsp90 inhibition can induce a transient degradation of HER2 as has been reported previously [21, 22].

We were able to show that optical imaging with a HER2-targeted affibody molecule can be used for non-invasive assessment of HER2 expression *in vivo* and for monitoring the Hsp90 treatment effect on HER2 expression in mice bearing human breast cancer xenografts.

Methods

Overview

The affibody was labeled with a fluorophore and cell lines with different levels of HER2 expression were established. *In vitro* flow cytometry and western blotting experiments were performed to determine HER2 expression and the effect of the Hsp90 inhibitor on HER2 levels. Tumor xenografts were then established in mice and *in vivo* optical imaging experiments were executed before, and 3, 6, and 9 days after mice were treated with the Hsp90 inhibitor or a carrier control. At 9 days post-treatment tumors were excised and western blotting was performed to correlate *in vivo* optical imaging signal with HER2 expression levels.

Affibody labeling

The anti-HER2 imaging agent, Affibody molecule $Z_{HER2:342}$ (7 KDa; Affibody AB, Stockholm, Sweden) was conjugated with Alexa Fluor 680 C2 Maleimide (Invitrogen, Carlsbad, CA). First, 0.5 mg of the affibody was reduced with 10 mM of tris(2-carboxyethyl)phosphine (TCEP; Thermo Fisher Scientific, Rockford, IL) at room temperature for 1 hour. Reduced Affibody was purified by High Performance Liquid Chromatography (HPLC) and resuspended in degassed Phosphate Buffered Saline (PBS) (Invitrogen, Carlsbad, CA). Then, 1 mg of the Alexa Fluor was dissolved in 100 µl of Dimethyl Sulfoxide (DMSO) (Sigma-Aldrich Inc.) and 50 µl of this solution was added to the reduced affibody sample. The mixture was vortexed at room temperature for 4 hours; progress of the reaction was monitored by HPLC at 280 nm and 550 nm. Finally, the end product was purified by HPLC and lyophilized overnight.

Cell culture

Human breast cancer (MCF7) cells (American Tissue Type Collection, Manassas, VA) innately expressing low levels of HER2 were transfected with a pcDNA 3.1-puromycin based plasmid containing full length human Her2/*neu* cDNA by using superfect and selected with 1 µg/ml puromycin. After 2 weeks, thirty single colonies were picked, populated separately and screened for HER2 expression by ELISA, using 15 µg of total protein lysates and following the manufacturer recommended protocol. Two clones were selected with a medium (Clone A) and a high (Clone B) expression level of HER2, respectively. Both the MCF parental cells and the two clones were cultured in RPMI 1640 medium supplemented with 10% fetal bovine serum (FBS) and penicillin (100 U/ml)- streptomycin (100 µg/ml) (Invitrogen, Carlsbad, CA). The clones were cultured under selection pressure by adding 1ug/ml puromycin (Invitrogen, Carlsbad, CA) to the medium. Cells were maintained in a humidified atmosphere of 5% CO_2 at 37°C. A confluent monolayer was detached with trypsin and dissociated into a single-cell suspension for further cell culturing.

Flow cytometry

MCF7 parental, Clone A, and Clone B cells in 75 cm^2 flasks were rinsed twice with PBS and trypsinized with 1.5 ml of 0.05% trypsin-EDTA at 37°C. The reaction was terminated when the cells were sufficiently detached by adding 5 ml of medium and the cells were pelleted at 300 g for 5 minutes and washed in PBS. Cells were re-suspended in ice-cold FACS buffer (PBS, 2% FBS, 0.05% Azide) and aliquoted at $2{\cdot}10^6$ cells per tube in 500 µl. Primary antibody against HER2 (c-erb-B-2 Ab-2, Thermo Fisher Scientific, Fremont, CA) was added in 1 ug/µl concentration (1 µl/1*10^6 cells) and the samples were incubated at 4°C for one hour. During incubation the samples were gently tapped to keep the cells in suspension. Following incubation, samples were washed three times with 1 ml FACS buffer and pelleted at 300 g for 5 minutes. Secondary antibody (Alexa Fluor 488 goat antimouse IgG_{2a} (γ2a), Invitrogen, Carlsbad, CA) was added in 1:100 dilution and samples were incubated for 1 hour at 4°C. As a control extra samples of MCF7 parental cells were only stained with the secondary antibody. Cells were washed three times with 1 ml FACS buffer and pelleted at 300 g for 5 minutes. Immediately before flow cytometry, samples were re-suspended in 200 µl FACS buffer containing 3 ug/ml propidium iodide (Invitrogen, Carlsbad, CA) and transferred to flow cytometry tubes. Samples were analyzed on a FACS Calibur system (Becton Dickinson, San Jose, CA) and the data analyzed using FlowJo Software (TreeStar, Inc, Ashland, OR). For each sample, 10 000 events were recorded and the population corresponding to viable single cells

was gated and analyzed as a histogram plot. Experiments were performed in triplicates.

Western Blot

Cell lysis and drug treatment

Approximately 4*10^6 cells of each cell line were plated overnight in 6 dishes of 10 cm diameter in 10 ml medium. The following day medium was aspirated and the cells were washed once with PBS. In 5 dishes of each cell line the Hsp90 inhibitor 17-Dimethylaminoethylamino-17-demethoxygeldanamycin hydrochloride (17-DMAG, LC Laboratories, Woburn, MA) dissolved in PBS was added in 5 doses in media, i.e. concentrations of 0.15, 0.30, 0.45, 0.60, and 0.90 µM respectively, and in the sixth dish medium only was added (dose 0 µM). The drug was allowed to incubate for 24 hours. After 24 hours, cells were lysed using 300 µl of NP-40 lysis buffer (Cell Signaling Technology Inc., Danvers, MA) with 1 tablet of protease inhibitor cocktail per 10.5 ml added (Roche Diagnostic Corporation, Indianapolis, IN). Cells with lysis buffer were incubated for 10 minutes at 4°C on ice. The cells/lysates were pipetted out of the dishes, transferred into microcentrifuge tubes and centrifuged at 10 000 g at 4°C for 30 minutes. The supernatant was collected and the protein concentration was quantified by Protein Dc assay (Bio-Rad Laboratories, Hercules, CA). Three independent experiments were performed for every treatment condition.

Tissue lysis

Xenograft tumor tissue from the animal experiments was lysed in 400 µl of NP-40 lysis buffer (Cell Signaling Technology Inc., Danvers, MA) with 1 tablet of protease inhibitor cocktail per 10.5 ml added (Roche Diagnostic Corporation, Indianapolis, IN) for 20 minutes at 4°C on ice. After incubation in lysis buffer the tissue was homogenized and lysates were transferred into microcentrifuge tubes and centrifuged at 10 000 g at 4°C for 30 minutes. The supernatant was collected and the protein concentration was quantified by Protein Dc assay (Bio-Rad Laboratories, Hercules, CA).

SDS PAGE and Blotting

Equal amount of protein from cell or tumor lysates (~30 µg) was loaded into a 10 or 15 well Bis-Tris 4-12% gradient polyacrylamide SDS gel (Invitrogen, Carlsbad, CA) together with 15 µl of protein ladders (SeeBlue Plus 2 and Novex Sharp Prestained Protein Standard, Invitrogen, Carlsbad, CA). The gel was electrophoresed at 85 V for 30 minutes and then at 110 V for ~2 hours in MOPS running buffer (Invitrogen,

Carlsbad, CA). After electrophoresis the gel was soaked in transfer buffer (3.63 g tris base, 14.4 g glycine, 0.37 g SDS, 200 ml methanol, H_2O to 1 l) and equilibrated for 15 minutes. Proteins were wet transferred to a nitrocellulose membrane. Sponges, filters, and membranes were soaked in transfer buffer prior to assembly of the transfer module and air bubbles were removed during assembly. The module was filled with transfer buffer and proteins transferred at 30 V for 1 hour. After transferring, the nitrocellulose membrane was blocked for 1 hour in 15 ml of TBST buffer (2.42 g Tris base, 8 g NaCl, 1 l H2O, 0.01% Tween 20, adjusted to pH 7.6) with 5% non-fat dry milk powder.

Primary antibodies against HER2 (c-erbB-2 Ab-17, Thermo Fisher Scientific, Fremont, CA) and α-Tubulin (clone B-5-1-2, Sigma-Aldrich Inc.) were added in 15 ml fresh blocking solution at 1:400 and 1:7500 dilutions and incubated with the membrane, overnight at 4°C. The membrane was washed 3 x 5 minutes with 15 ml TBST buffer and the secondary antibody (goat antimouse IgG (H+L)-horseradish peroxidase conjugate, Cell Signaling Technology Inc., Danvers, MA) was added in 15 ml fresh blocking solution at 1:3000 dilution and incubated with the membrane for one hour at room temperature. The membrane was washed 3 x 5 minutes with 15 ml TBST buffer. 4 ml of enhanced chemiluminescent substrate (Pierce ECL Western Blotting Substrate, Thermo Fisher Scientific, Rockford, IL) was added to the membrane. The membrane was wrapped in saran wrap and excess substrate and air bubbles were removed by gently rubbing the membrane with a paper towel. The membrane was exposed to blue autoradiography film (ISC BioExpress, Kaysville, UT) for 5 s, 10 s, 30 s, 1 minute, 2 minutes, and 5 minutes and developed using a Kodak X-OMAT 2000A Processor (Carestream Health Inc., Rochester, NY).

Protein density bands were analyzed using ImageJ software (Version 1.41, National Institutes of Health, Bethesda, MD). Regions of interest (ROIs) of equal size were drawn around the band and the adjacent inferior background and the integrated density value of each band was subtracted from its background. To evaluate the protein expression in the different samples, ratios of HER2 and α-Tubulin density were compared.

Tumor xenografts

All animal experiments were performed in accordance with the federal and local institutional rules for animal experimentation. Approximately 8 x 10^6 MCF7 Clone B cells and 5 x 10^6 MCF7 parental cells in 40 µl PBS were separately suspended with 50 µl Matrigel (BD Biosciences, San Jose, CA) and implanted subcutaneously on the shoulder region of a female athymic nude mouse (nu/nu, 6-10 weeks old, Charles River Laboratories, Inc., Wilmington, MA). For each mouse, Clone B cells

were inoculated on the right or the left side, and MCF7 parental cells on the other side; a ß-estradiol 17-valerate pellet (0.5 mg, 60 day release, Innovative Research of America) was implanted subcutaneously on the neck region to support tumor growth. Tumors were allowed to grow to a size of 5-10 mm diameter (2-4 weeks) before the mice (20 in total) were subjected to imaging studies. Tumor sizes were monitored at the imaging days by caliper measurements of the largest longitudinal (length) and transverse (width) diameter; tumor volume was then calculated by the formula: $tumor\ volume = 1/2(length \times width^2)$

Fluorescence Optical Imaging

Mice were anesthetized with 2% isofluorane in oxygen 2 l/minute and placed on a heating pad. Mice were maintained under anesthesia during fluorescence imaging using a time-domain *in vivo* small animal fluorescence imager (eXplore Optix, ART Advanced Research Technlogies, Montreal, Canada)[23]. A 670 nm pulsed diode laser was used for excitation. The average power of the laser was kept at approximately 1 mW at a repetition frequency of 80 MHz. The full width at half maximum (FWHM) of the laser pulse was approximately 100 ps. A 693 nm long-pass filter was used to let the emitted fluorescent signal pass through. The eXplore Optix detector is a fast photomultiplier tube coupled to a time-correlated single-photon counting system for time-resolved measurements. The overall time resolution of the detection module was approximately 250 ps.

Before injection of the fluorescently labeled affibody, pre-injection images were acquired in order to remove the auto-fluorescence or background signal later. Mice were injected intravenously (via the tail vein) with 500 pmol of Affibody-AlexaFluor680 dissolved in PBS in a total volume of 150 µl. Post-injection images were acquired after 5 hours as based on pilot data (best signal-to-background ratios). Mice were positioned on their left and right sides successively, each time adjusting the table height to allow for optimal fluorescence imaging of each tumor. The field of view was adjusted for each scan so that the entire tumor including some surrounding tissue was imaged (~200 - 300 mm^2). The scan resolution was 1.0 x 1.0 mm (i.e. scan step size of 1.0 mm in both x and y directions). Acquisition time varied between 3 and 9 minutes for each scan.

Images were analyzed using the Optiview software, Version 2.02 (ART Advanced Research Technlogies, Montreal, Canada). First, the pre-injection image was used to remove the background auto fluorescence signal. Then, a region of interest (ROI) was drawn around the tumor. Average normalized counts were calculated for each ROI. To assess whether the effect of treatment results would change if the ROIs were drawn in a different manner, we also calculated the average normal-

ized counts for a larger ROI (containing the entire tumor and some normal tissue surrounding the tumor) and for a smaller ROI (in the center of the tumor) for all images at all time points (**see supplementary Figure 2**). ROI size ranged from 5 to 121 mm^2. In pilot studies the coefficient of variation (COV) for the average normalized counts was determined. In six imaging sessions, Clone B xenografts were imaged thrice at approximately 5 hours after a single affibody injection. For each scan the mice were repositioned, the imaging system was readjusted, and average normalized counts were independently assessed.

Imaging procedures were started when tumors were ~5-10 mm in size. First, pre-treatment images were taken (Day -1). Then, mice were divided into two groups. One group (n=10) received treatment with 17-DMAG, 120 mg/kg dissolved in PBS in 4 doses intraperitoneal at 12 hour intervals, as described in Schwock et al. [24]. The other group (n=5) received only the carrier, PBS, intraperitoneal in an equal volume (Day 0). After treatment, fluorescence optical imaging was performed at Days 3, 6, and 9. This time interval ensured complete clearance of previous affibody injections as determined in a pilot study and as confirmed on the pre-injection images performed on each imaging day. A subgroup of 5 mice were only imaged once and did not undergo any treatment; these were used to collect more data for the correlation of the *in vivo* imaging signal with the HER2 expression as measured *ex vivo*. After the study procedures, the mice were euthanized by cervical dislocation and the tumors were isolated, frozen on dry ice, and stored at -80°C for tissue lysis and western blotting. At day 9, we experienced difficulties performing the tail vein injection in one of the mice in the carrier group, leading to administration of only a small amount of the imaging agent. Also, two Clone B tumors in the 17-DMAG treated group had shrunken to volumes too small to measure by caliper (< 10 mm^3) at day 9. Therefore, the respective images and tissue samples were left out of further analyses.

Statistical analysis

Data are presented as absolute numbers and means ± standard errors. For *in vitro* analyses, independent samples T-tests were used to test the differences within the cell lines for each drug dose compared to the non-treated cells. For *in vivo* analyses, independent samples T-tests were used to test the difference in optical imaging signal between the carrier and the 17-DMAG treated groups. Paired samples T-tests were used to test the differences within groups between imaging days (pre- and post-treatment). Correlation was determined with Pearson's correlation coefficient after the data was log transformed to obtain a normal distribution. All tests were two-sided and a p-value ≤ 0.05 was considered significant. The soft-

ware package SPSS 15.0 (SPSS Inc., Chicago, IL, USA) was used for the statistical computations.

Results

In vitro HER2 expression levels are down-regulated by 17-DMAG

Flow cytometry results showed that the three cell lines, MCF7 parental, Clone A, and Clone B, have low, intermediate, and high expression levels of HER2, respectively, and consist of pure populations (**Figure 1**). Western blot results confirmed these differences. Furthermore, HER2 expression decreased dependent on the 17-DMAG dose (**Figure 2**). HER2 down-regulation at 0.45 μM 17-DMAG compared to non-treated cells was 74 ± 5% for MCF7 parental cells ($p = 0.0003$), 66 ± 14% for Clone A cells ($p = 0.010$), and 72 ± 17% for Clone B cells ($p = 0.019$).

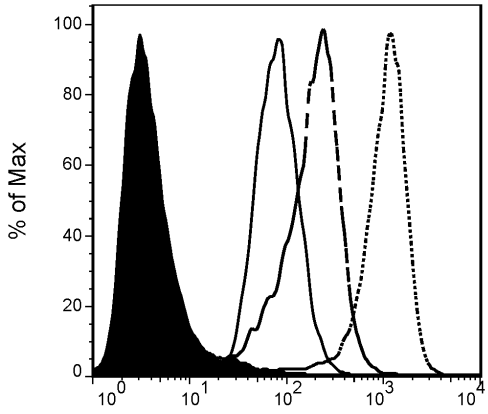

Figure 1. Flow cytometry results showed low (MCF7 parental), intermediate (Clone A), and high (Clone B) expression levels of HER2, respectively, in comparison with the control MCF7 parental cells that were only stained with the secondary (nonspecific) antibody. The single peaks for each sample indicate pure cell populations.

Optical imaging signal transiently decreases in living mice in response to 17-DMAG treatment

Before treatment was initiated, optical imaging confirmed that the overall mean optical imaging signal (average counts) was significantly higher for Clone B tumors than for MCF7 parental tumors (5042.0 vs. 2618.5 counts/mm^2; $p = 0.001$). Furthermore, imaging each tumor thrice, 5 hours after a single injection of affibody and after repositioning the mice, re-adjusting the imaging device and independently assessing the average counts for each exam, yielded an average COV of 5.9% (N=6).

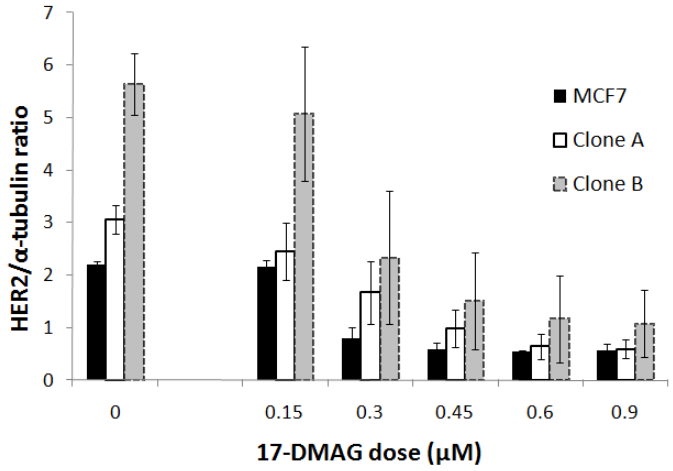

Figure 2. Western blots confirmed low (MCF7 parental) intermediate (Clone A) and high (Clone B) HER2 expression. On the left (no 17-DMAG, dose 0), samples of 3 experiments were loaded into 1 gel to show the standard error of the mean. HER2 expression decreased dependent on the 17-DMAG dose added to the cells. Data was normalized to the mean HER2 expression for each cell line at dose 0 in the same gel. All experiments were repeated 3 times. Results are statistically significant from 0.45 μM for Clone B and Clone A, and from 0.30 μM for MCF7 parental cells.

Optical imaging signal for Clone B tumors dropped significantly in the 17-DMAG treated group to 79 ± 4% at day 3 compared to pre-treatment ($p = 0.016$), then increased again to 106 ± 14% at day 6 and 135 ± 22% at day 9. In the carrier group, the optical imaging signal did not drop after carrier treatment but slightly increased to 112 ± 9% at day 3 compared to pre-treatment ($p = 0.527$), 123 ± 10% at day 6, and 142 ± 17% at day 9 (**Figure 3B**). The same trend was seen for the MCF7 parental tumors. MCF7 parental signal decreased compared to pre-treatment in the 17-DMAG treated group to 87 ± 6% at day 3 ($p = 0.063$), then increased again to 128 ± 7% at day 6, and 134 ± 9% at day 9 (**Figure 3A**). In the carrier group the optical imaging signal increased to 126 ± 15% at day 3 compared to pre-treatment ($p = 0.174$), 153 ± 24% at day 6, and 172 ± 30% at day 9. **Figure 4** summarizes the statistically significant 17-DMAG treatment effect (day 3 *post* vs. day -1 *pre*) between the 17-DMAG treated group and the carrier group for both MCF7 parental ($p = 0.018$) and Clone B ($p = 0.046$) tumors. Comparisons between the treatment and carrier groups for both tumor types at later time-points were not statistically significant. **Figures 5A** (MCF7 parental) and **5B** (Clone B) exemplify the *in vivo* optical images pre- and post-treatment, showing a decrease in optical imaging signal for the 17-DMAG treated mice and an increase in optical imaging signal for the carrier mice on day 3 compared to day -1.

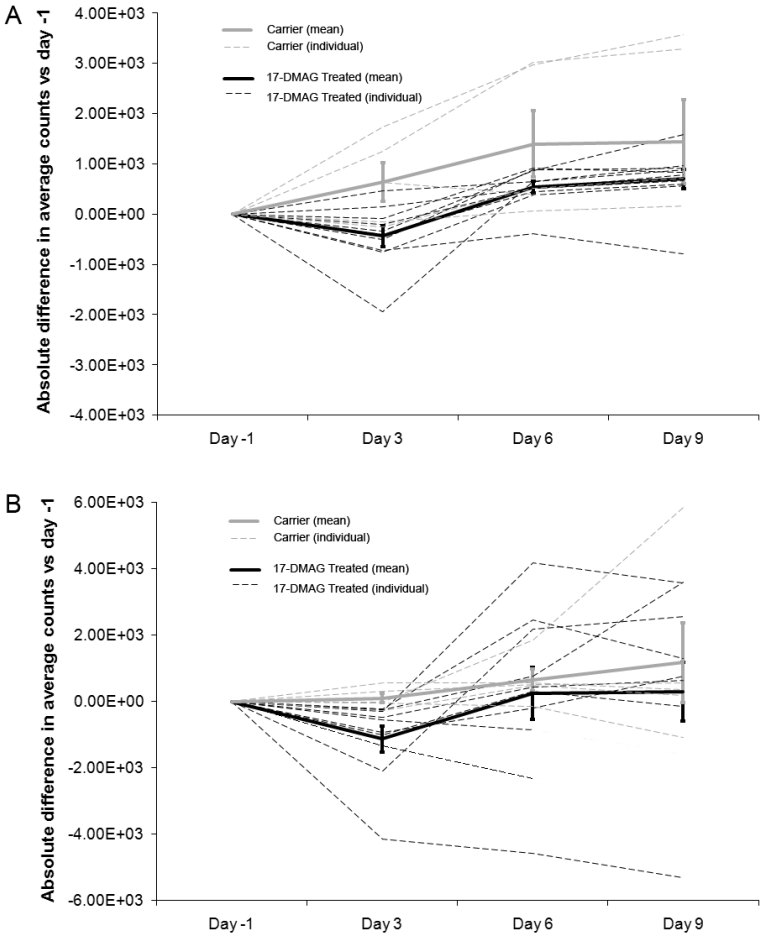

Figure 3. Absolute difference in average counts for MCF parental (A) and Clone B tumors (B): Treatment vs. Carrier compared to Day -1 (pre-treatment). Dashed lines represent the individual mice, solid lines the mean and error bars the standard error of the mean. Both MCF7 parental tumors (A) and Clone B tumors (B) showed a significant decrease in average counts at Day 3 for the 17-DMAG treated compared to the carrier group ($p = 0.018$ and $p = 0.046$, respectively). At day 3, optical imaging signal was reduced by 13% in 17-DMAG treated MCF7 parental tumors ($p = 0.063$) and by 21% in Clone B tumors ($p = 0.016$); signal recovered at day 6-9.

In contrast to the significant effects as assessed by *in vivo* molecular imaging, no significant changes in tumor volume were measured after 17-DMAG treatment up to 9 days post treatment, neither for Clone B, nor for MCF7 parental tumors (see supplementary information).

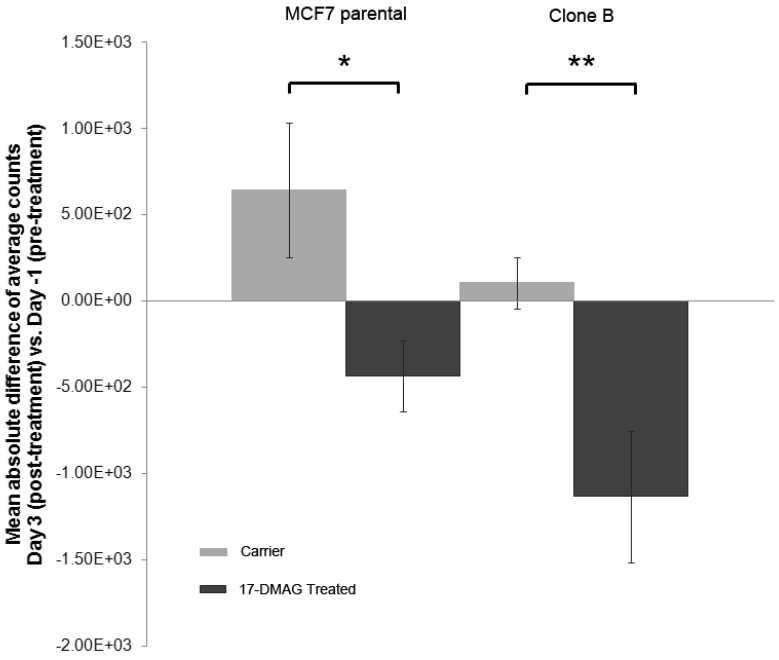

Figure 4. Mean absolute difference in average counts of Day 3 (post-treatment) vs. Day -1 (pre-treatment). Optical imaging signal decreased significantly for the 17-DMAG treated mice compared to the carrier mice for both MCF7 parental (* p = 0.018) and Clone B (** p = 0.046) tumors. Error bars represent the standard error of the mean.

Ex vivo HER2 expression levels correlate with *in vivo* optical imaging signal

In total 20 mice with two tumors each (MCF7 parental and Clone B) were sacrificed and the tumor tissue was surgically removed and processed for western blotting. A total of 36 tumors were available for determining the correlation of *ex vivo* HER2 levels with *in vivo* optical imaging signal (see methods). The overall Pearson correlation was 0.77; for subgroups it ranged from 0.74 to 0.89 (**Table 1**).

Table 1. Pearson's correlation coefficient of *ex vivo* HER2 levels and *in vivo* optical imaging signal

Group	Pearson (n)
Total	0.77 (36)
Carrier	0.84 (8)
Treated	0.74 (18)
Non-treated	0.89 (10)

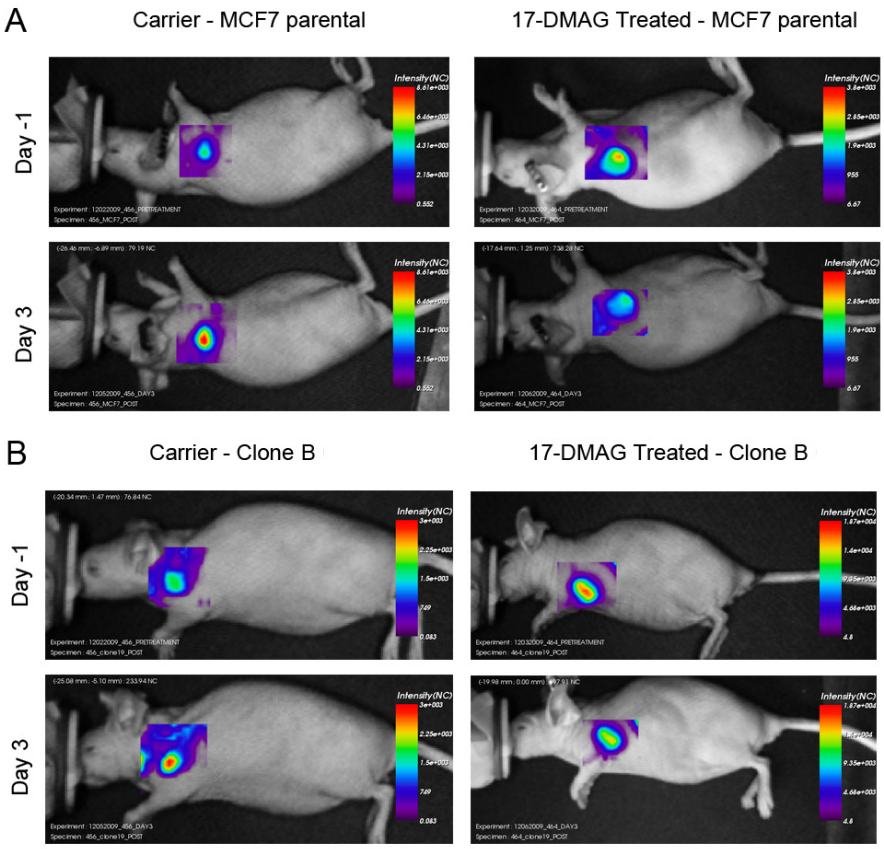

Figure 5. Examples of *in vivo* optical imaging results of mice bearing MCF7 parental (A) and Clone B tumor xenografts (B). Images were obtained before (day -1) and after (day 3) treatment with 17-DMAG or carrier control.

Discussion

We have shown that optical imaging with an affibody can be used to non-invasively monitor changes in HER2 expression *in vivo* as a response to treatment with an Hsp90 inhibitor, whereas effects of the therapy on tumor volume were limited during the study period and statistically non-significant. Results of this study are very promising for the use of optical imaging as a molecular imaging tool for treatment monitoring in a clinical setting. This is the first work we know of to show the feasibility of optical imaging in the visualization of the response to Hsp90 therapy at a molecular level in living subjects. Affibody molecules have been used successfully in optical imaging studies before [25], but the feasibility of treatment moni-

toring with the affibody in optical imaging studies has not been addressed. Other research groups have demonstrated the potential of target-specific radiotracers in PET imaging to measure the treatment effects on molecular targets [26-28]. Smith-Jones et al. monitored HER2 changes after treatment with a Hsp90 inhibitor (17-AAG) using PET imaging with ^{68}Ga-labelled trastuzumab F(*ab'*)$_2$ fragments [26]. They found a reduction in tumor uptake of 70% in BT474 breast tumor xenografts. The reduced uptake lasted until 5 days after treatment. HER2 levels were not determined *ex vivo*, only imaging studies were performed. Oude Munnink et al. used PET imaging with full length ^{89}Zr-labelled trastuzumab to measure HER2 downregulation after treatment with a Hsp90 inhibitor (NVP-AUY922) in SKOV-3 ovarian tumor xenografts [27]. They reported a reduction in tumor uptake of 41%. Immunohistochemistry confirmed the decrease in HER2 expression *ex vivo* in a qualitative way only. Kramer-Marek et al. measured changes in HER2 expression after 17-DMAG treatment using the same affibody as we used in our study, but instead of using optical imaging they labeled the affibody with ^{18}F for PET imaging and only performed a pre- and post-treatment scan [28]. They reported a reduction of 33% in a MCF7 cell line transfected with HER2 (Clone 18) and of 71% in BT474 breast tumor xenografts. HER2 downregulation was confirmed *ex vivo* by western blot and ELISA.

Both Oude Munnink et al. and Kamer-Marek et al. compared a single post-treatment measurement with pretreatment. HER2 expression was not monitored over a longer period of time. The strength of our study is that we followed each mouse over 10 days, which enabled us to see the HER2 levels decrease after treatment and recover after the treatment was stopped (which is in line with data from Smith-Jones et al.; [26]). This indicates that we can monitor the molecular changes non-invasively over time with our optical imaging strategy, whereas we did not observe significant changes in tumor volume by caliper measurement during the study. Our *in vivo* results of 21% signal reduction are consistent with the previous reports, considering that different cell lines were used for the tumor xenografts and that the imaging technique used was also different. In addition, correlating *in vivo* optical imaging signal with *ex vivo* HER2 levels by western blotting supported our results.

An important advantage of optical imaging in comparison with PET imaging is that it does not use radioactive components or ionizing radiation and can thus be used more frequently. An additional advantage is that optical imaging agents are easier to generate and cheaper than PET probes. In contrast to nuclear imaging approaches where over time the imaging signal disappears as a result of natural decay in addition to clearance from the subject, in optical imaging the clearance

of the imaging signal is predominantly dependent on clearance of the imaging probe from the body. For this reason, small molecules with quick clearance, such as affibody molecules, may be preferable over large molecules in optical imaging. In addition, pre-injection optical signal can be measured and subtracted from subsequent imaging exams in optical imaging to adjust for residual signal.

Limitations of optical imaging include its limited spatial resolution and the complexity of its image reconstruction/quantitation. These aspects make it difficult to draw ROIs precisely around the tumor border. Chances are that different observers would draw ROIs differently. To evaluate if this would influence the results of our study, two different sizes of ROIs were also drawn besides the medium ROI we used for the primary results (an ROI drawn as accurately as possible around the apparent tumor border): a very small ROI in the center of the tumor, and a very large ROI around the entire tumor including some surrounding normal tissue. Average counts of all of these ROIs were calculated at all imaging time points. We found comparable differences in optical imaging signal post- and pre-treatment for all ROI sizes (see supplementary information). This implies that the interpretation of the signal changes was not importantly influenced by the manner in which the ROI was drawn. Another limitation of the relatively low spatial resolution is that partial volume effects can lead to inaccurate optical imaging signals in very small lesions compared to the system's resolution.

Quantification of optical imaging signal is more complicated as compared to PET imaging in which percentage injected dose per gram of tissue can be calculated. However, we believe to have shown that relative signal quantification with the right optical imaging set up is achievable and that it is thus feasible to semi-quantitatively measure molecular changes over time using optical imaging.

In ongoing studies we are evaluating other molecular imaging agents, such as engineered antibodies and peptides, in the same xenograft model to make better comparisons between the different imaging agents. We aim to translate (one or more of) these molecular imaging agents to clinical studies. Future preclinical studies will include administering 17-DMAG more than once to repeatedly monitor the transient effect on HER2 expression over time, and investigating whether repeated probe injection within hours yields reproducible imaging results after pre-injection background subtraction to adjust for residual probe levels. If possible, we will be able to show the reproducibility of the entire optical imaging procedure, and not only from probe injection onwards which we showed to be highly reproducible (average COV 5.9%). This will give a better understanding of the magnitude of effects that can be measured with this optical imaging assay.

In conclusion, optical imaging with an affibody can be used for non-invasive *in vivo* imaging of HER2 expression and for monitoring the changes in HER2 expression as a response to treatment. This makes optical imaging a promising molecular imaging tool for treatment monitoring in preclinical models and potentially in patients.

Acknowledgements

We would like to thank the Dutch Cancer Society (travel grant (SMWYvdV); fellowship (SGE)), NCI ICMIC P50CA114747 (SSG), and NCI RO1 CA082214 (SSG) for financial support.

Supplementary Information

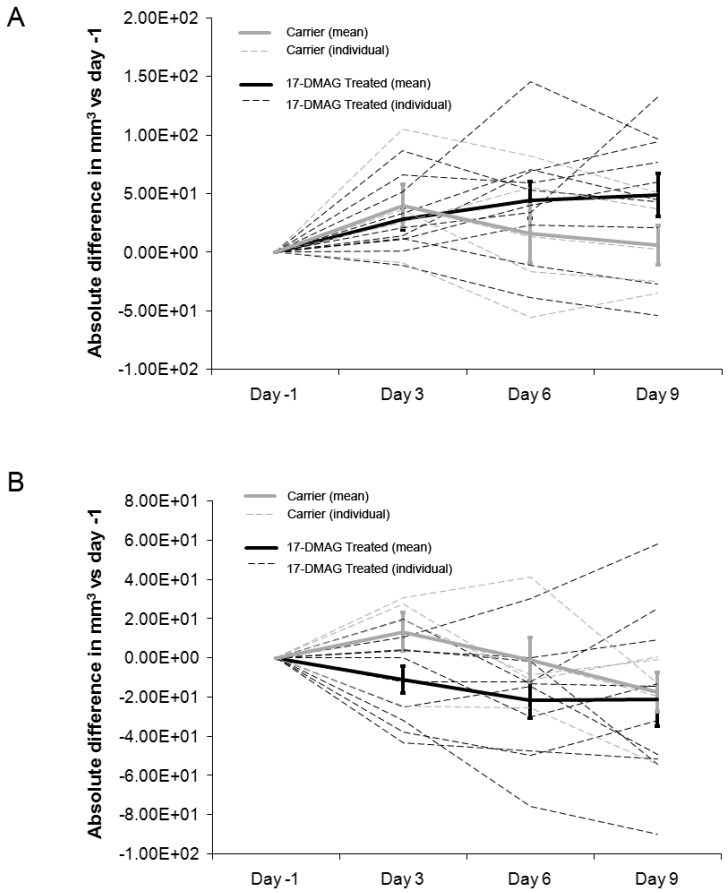

Figure 1. Absolute difference in volume (mm^3) for MCF7 parental (A) and Clone B tumors (B): Treatment vs. Carrier compared to Day -1 (pre-treatment). Dashed lines represent the individual mice, solid lines the mean and error bars the standard error of the mean (differences were not significant).

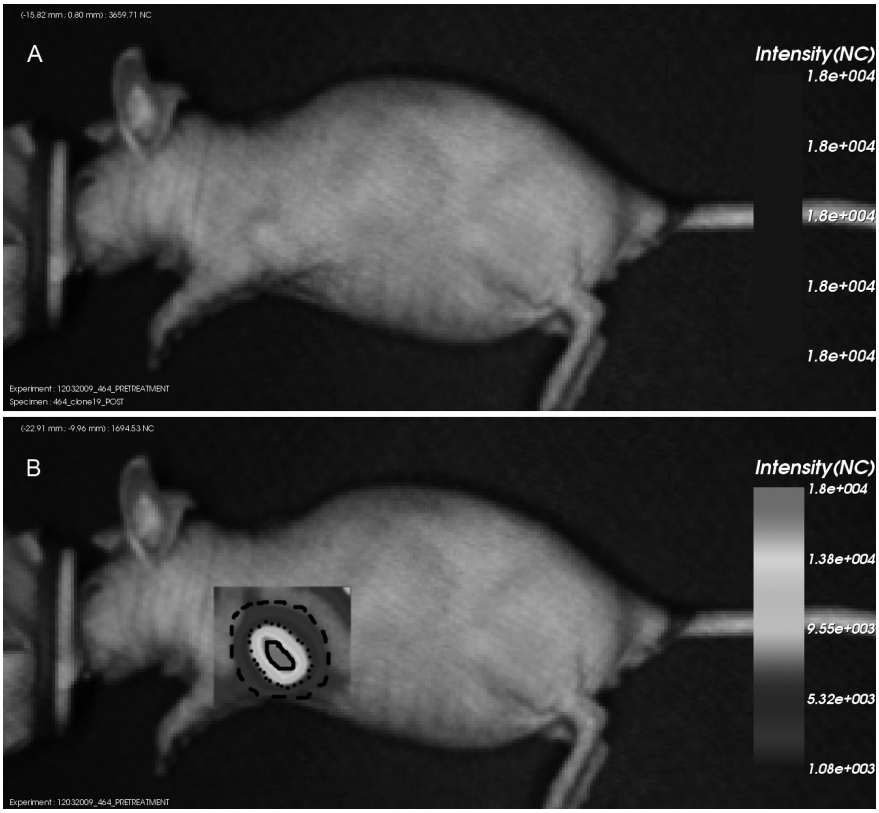

Figure 2. Mouse bearing Clone B xenograft on the left shoulder; in A the tumor is depicted without the optical imaging signal, in B the different sizes of ROIs drawn for image analysis are demonstrated.

Table 1. Treatment effect at Day 3: Comparison of the influence of different ROI sizes

ROI size	Clone B 17-DMAG (95% C.I.)	Clone B Carrier (95% C.I.)	MCF7 parental 17-DMAG (95% C.I.)	MCF7 parental Carrier (95% C.I.)
Tumor border	-20.64% (-28.67% to -12.62%)	11.95% (-6.58% to 30.49%)	-13.46% (-26.13% to -0.80%)	26.23% (-3.74% to 56.19%)
Smaller	-15.71% (-25.46% to -5.96%)	24.11% (-31.74% to 79.97%)	-9.67% (-24.67% to 5.33%)	25.18% (-5.65% to 56.02%)
Larger	-19.70% (-28.66% to -10.74%)	-5.31% (-38.01% to 27.39%)	-7.95% (-22.29% to 6.39%)	21.89% (-11.12% to 54.91%)

References

1. Eisenhauer EA, Therasse P, Bogaerts J, et al. New response evaluation criteria in solid tumours: revised RECIST guideline (version 1.1). Eur J Cancer 2009; 45:228-247.
2. Woodhams R, Kakita S, Hata H, et al. Identification of residual breast carcinoma following neoadjuvant chemotherapy: diffusion-weighted imaging--comparison with contrast-enhanced MR imaging and pathologic findings. Radiology 2010; 254:357-366.
3. Wahl RL, Jacene H, Kasamon Y, Lodge MA. From RECIST to PERCIST: Evolving Considerations for PET response criteria in solid tumors. J Nucl Med 2009; 50 Suppl 1:122S-150S.
4. van de Ven S, Wiethoff A, Nielsen T, et al. A novel fluorescent imaging agent for diffuse optical tomography of the breast: first clinical experience in patients. Mol Imaging Biol 2010; 12:343-348.
5. van de Ven SM, Elias SG, Wiethoff AJ, et al. Diffuse optical tomography of the breast: preliminary findings of a new prototype and comparison with magnetic resonance imaging. Eur Radiol 2009; 19:1108-1113.
6. Zhu Q, Cronin EB, Currier AA, et al. Benign versus malignant breast masses: optical differentiation with US-guided optical imaging reconstruction. Radiology 2005; 237:57-66.
7. Cerussi A, Hsiang D, Shah N, et al. Predicting response to breast cancer neoadjuvant chemotherapy using diffuse optical spectroscopy. Proc Natl Acad Sci U S A 2007; 104:4014-4019.
8. Rinneberg H, Grosenick D, Moesta KT, et al. Scanning time-domain optical mammography: detection and characterization of breast tumors *in vivo*. Technol Cancer Res Treat 2005; 4:483-496.
9. Floery D, Helbich TH, Riedl CC, et al. Characterization of benign and malignant breast lesions with computed tomography laser mammography (CTLM): initial experience. Invest Radiol 2005; 40:328-335.
10. Jiang S, Pogue BW, Carpenter CM, et al. Evaluation of breast tumor response to neoadjuvant chemotherapy with tomographic diffuse optical spectroscopy: case studies of tumor region-of-interest changes. Radiology 2009; 252:551-560.
11. Intes X. Time-domain optical mammography SoftScan: initial results. Acad Radiol 2005; 12:934-947.
12. Weissleder R, Ntziachristos V. Shedding light onto live molecular targets. Nature Medicine 2003; 9:123.
13. Pierce MC, Javier DJ, Richards-Kortum R. Optical contrast agents and imaging systems for detection and diagnosis of cancer. Int J Cancer 2008; 123:1979-1990.

14. Moasser MM. The oncogene HER2: its signaling and transforming functions and its role in human cancer pathogenesis. Oncogene 2007; 26:6469-6487.

15. Capala J, Bouchelouche K. Molecular imaging of HER2-positive breast cancer: a step toward an individualized 'image and treat' strategy. Curr Opin Oncol 2010; Epub Sept 14.

16. Orlova A, Wallberg H, Stone-Elander S, Tolmachev V. On the selection of a tracer for PET imaging of HER2-expressing tumors: direct comparison of a 124I-labeled affibody molecule and trastuzumab in a murine xenograft model. J Nucl Med 2009; 50:417-425.

17. Cheng Z, De Jesus OP, Namavari M, et al. Small-animal PET imaging of human epidermal growth factor receptor type 2 expression with site-specific 18F-labeled protein scaffold molecules. J Nucl Med 2008; 49:804-813.

18. Ren G, Zhang R, Liu Z, et al. A 2-helix small protein labeled with 68Ga for PET imaging of HER2 expression. J Nucl Med 2009; 50:1492-1499.

19. Baum RP, Prasad V, Muller D, et al. Molecular imaging of HER2-expressing malignant tumors in breast cancer patients using synthetic 111In- or 68Ga-labeled affibody molecules. J Nucl Med; 51:892-897.

20. Whitesell L, Lindquist SL. HSP90 and the chaperoning of cancer. Nat Rev Cancer 2005; 5:761-772.

21. Zsebik B, Citri A, Isola J, Yarden Y, Szollosi J, Vereb G. Hsp90 inhibitor 17-AAG reduces ErbB2 levels and inhibits proliferation of the trastuzumab resistant breast tumor cell line JIMT-1. Immunol Lett 2006; 104:146-155.

22. Solit DB, Zheng FF, Drobnjak M, et al. 17-Allylamino-17-demethoxygeldanamycin induces the degradation of androgen receptor and HER-2/neu and inhibits the growth of prostate cancer xenografts. Clin Cancer Res 2002; 8:986-993.

23. Keren S, Gheysens O, Levin CS, Gambhir SS. A comparison between a time domain and continuous wave small animal optical imaging system. IEEE Trans Med Imaging 2008; 27:58-63.

24. Schwock J, Dhani N, Cao MP, et al. Targeting focal adhesion kinase with dominant-negative FRNK or Hsp90 inhibitor 17-DMAG suppresses tumor growth and metastasis of SiHa cervical xenografts. Cancer Res 2009; 69:4750-4759.

25. Lee SB, Hassan M, Fisher R, et al. Affibody molecules for *in vivo* characterization of HER2-positive tumors by near-infrared imaging. Clin Cancer Res 2008; 14:3840-3849.

26. Smith-Jones PM, Solit D, Afroze F, Rosen N, Larson SM. Early tumor response to Hsp90 therapy using HER2 PET: comparison with 18F-FDG PET. J Nucl Med 2006; 47:793-796.

27. Oude Munnink TH, Korte MA, Nagengast WB, et al. (89)Zr-trastuzumab PET visualises HER2 downregulation by the HSP90 inhibitor NVP-AUY922 in a human tumour xenograft. Eur J Cancer 2010; 46:678-684.

28. Kramer-Marek G, Kiesewetter DO, Martiniova L, Jagoda E, Lee SB, Capala J. [18F]FBEM-Z(HER2:342)-Affibody molecule-a new molecular tracer for *in vivo* monitoring of HER2 expression by positron emission tomography. Eur J Nucl Med Mol Imaging 2008; 35:1008-1018.

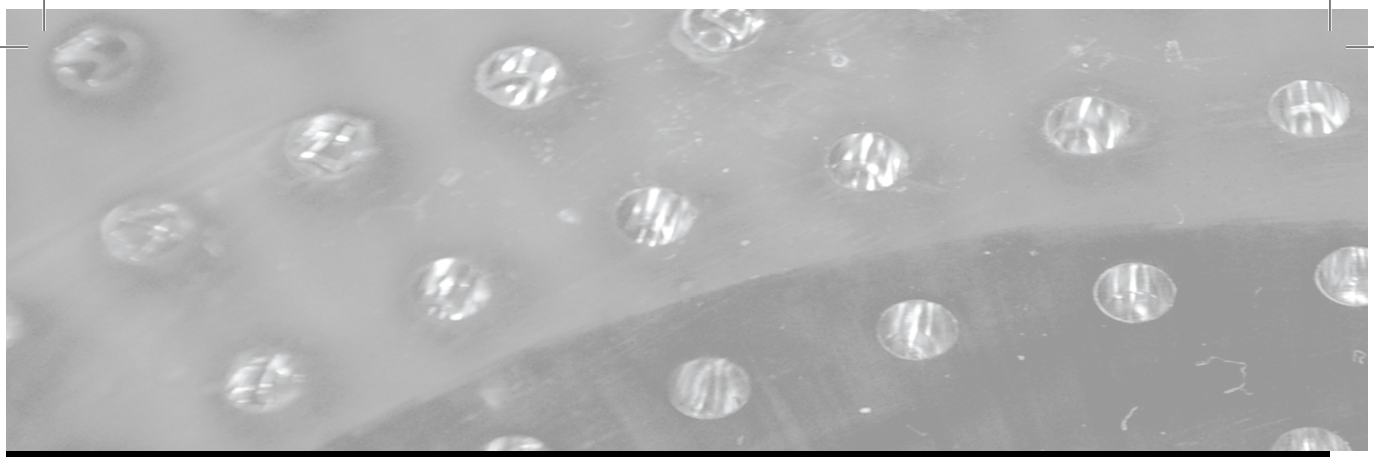

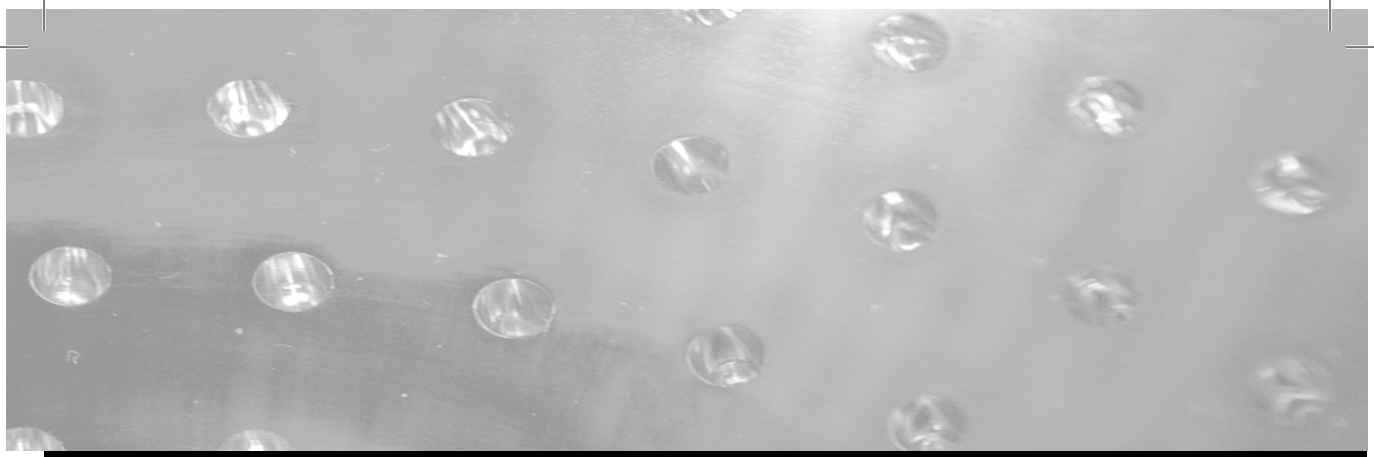

General discussion

Optical imaging is a very promising imaging technique. Major power lies in its ability to non-invasively provide biophysical and molecular information on disease processes in living tissue. The optical imaging technique has several strengths. Its sensitivity for probe detection is very high. Optical imaging systems can detect imaging agents in picomolar to nanomolar concentration ranges, whereas for instance magnetic resonance imaging (MRI) needs larger molecular masses before probe detection is possible (at least micromolar concentrations). In contrast to X-ray, computed tomography (CT) and positron emission tomography (PET), optical imaging uses no ionizing radiation. Repeated imaging is therefore possible without radiation risks. Moreover, optical imaging is relatively cheap, and imaging agents are easy to generate and have long shelf-live, particularly compared to PET tracers. These strengths make optical imaging an outstanding technique for preclinical application, for instance for high-throughput screening and testing of new drugs, and potentially also for clinical application, provided that certain challenges can be overcome.

Main challenges in optical imaging are depth penetration, signal quantification, and the development, validation and approval of relevant imaging agents for human use. Light penetration in tissue is limited, but with the use of near-infrared light and the development of more sensitive detection equipment, penetration in human tissue is now possible up to 15 centimeters deep. This makes optical imaging a possible candidate for imaging of the breast. To reach successful clinical translation, several steps need to be taken; some of them are addressed in this thesis. First, available optical imaging systems need to be improved (or new systems developed). As described previously, the prototype we tested in this thesis has several limitations (**Chapter 3-5**). It was unable to visualize some of the breast lesions located close to the chest wall. Because these lesions were physically too far above the upper optical fibers in the cup, they were not able to influence the light pathways in our prototype. To improve the visualization of these lesions, advances in cup geometry are needed. Furthermore, the spatial resolution of optical tomography is poor, resulting in a lower signal-to-noise ratio and limited detectability for small lesions. Because longer light pathways decrease spatial resolution, lesion detection is more difficult and size measurement less precise in the center of the cup compared to the edge. This may limit the visualization of centrally located lesions in large breasts. To solve this problem, optical data could be acquired using slab geometry with slight breast compression. This type of geometry alteration may also improve the detection of lesions located close to the chest wall. Additionally, recent developments in optical cameras and detectors

could also improve lesion detection. Another way to deal with the lower spatial resolution is a multimodality approach. Optical imaging could be fused with other anatomical imaging techniques, such as ultrasound (photoacoustic imaging) or MRI, similar to what happened in nuclear imaging techniques as PET/CT. Besides spatial resolution, signal quantification is also challenging in optical imaging. In contrast to PET imaging in which the percentage injection dose per gram of tissue can be calculated relatively easily and reproducibly, optical imaging has to deal with the scattering and absorption properties of light in tissue which requires complex reconstruction algorithms. Absolute signal quantification is therefore not feasible with optical imaging. However, we have shown in our preclinical treatment monitoring study that relative signal quantification is achievable in a reproducible way (**Chapter 7**). This is especially important in measuring molecular changes (i.e. protein expression levels) over time.

The other key challenge in clinical translation of optical imaging is the development of relevant imaging agents. Crucial for this step is the full understanding of the molecular biology of breast cancer to identify potential targets. Biologic processes to study for target identification include for example tumor metabolism, angiogenesis, proliferation, apoptosis, and hypoxia. Once appropriate targets are identified it is important to validate these targets, and questions like 'is it possible to reach this target with an imaging agent?', 'in what amount is the target available?', and 'which target or combination of targets would give the most significant clinical information?' should be answered. In the design of an imaging agent, the agent should be non-toxic, able to reach the target site, be specific to the target, and stay at the target site in large enough amounts to be detected by the imaging system over the background signal. It is not easy to predict from preclinical tests whether an imaging agent will have this potential in human use. However, estimates can be made from preclinical studies; we found for instance in our phantom studies that nanomolar concentrations of nanotubes and micromolar concentrations of a small molecule dye could be detected by the respective clinical optical breast scanner (**Chapter 6**). After the designing and the required preclinical testing, the newly developed imaging agent can finally be evaluated in clinical studies. Recently, the human epidermal growth factor receptor-2 (HER2)-targeting affibody we used in our treatment monitoring studies (**Chapter 7**) was used in a PET imaging study in metastatic breast cancer patients with promising results [1].

When clinical translation of appropriate optical imaging agents is successful, optical breast imaging could possibly improve early detection of breast cancer. For example in women with dense breasts who are at increased risk for breast cancer. X-ray mammographic screening has very limited sensitivity in these women due to the tumor-camouflaging projection of the dense glandular tissue [2, 3], while near-infrared light is far less hindered by dense breast tissue. Optical breast imaging could also have a role in the selection of appropriate adjuvant treatment, the evaluation of response to treatment, and the fine-tuning of treatment strategy in the individual breast cancer patient. Moreover, optical imaging agents could potentially be used as 'theranostics', combining the process of diagnosis and (local) therapy [4].

In this thesis we have described the early steps in the evaluation of a new prototype for diffuse optical tomography of the breast; showed the potential of a commercially available optical breast scanner in combination with molecular imaging agents; and highlighted the potential of treatment monitoring using target-specific optical imaging agents in a preclinical setting. Further technical developments and the availability of relevant molecular imaging agents for human use in the near future could eventually allow for this technique to be used in routine clinical practice.

References

1. Baum RP, Prasad V, Muller D, et al. Molecular imaging of HER2-expressing malignant tumors in breast cancer patients using synthetic 111In- or 68Ga-labeled affibody molecules. J Nucl Med 2010; 51:892-897.
2. Carney PA, Miglioretti DL, Yankaskas BC, et al. Individual and combined effects of age, breast density, and hormone replacement therapy use on the accuracy of screening mammography. Ann Intern Med 2003; 138:168-175.
3. Boyd NF, Guo H, Martin LJ, et al. Mammographic density and the risk and detection of breast cancer. N Engl J Med 2007; 356:227-236.
4. Debbage P, Jaschke W. Molecular imaging with nanoparticles: giant roles for dwarf actors. Histochem Cell Biol 2008; 130:845-875.

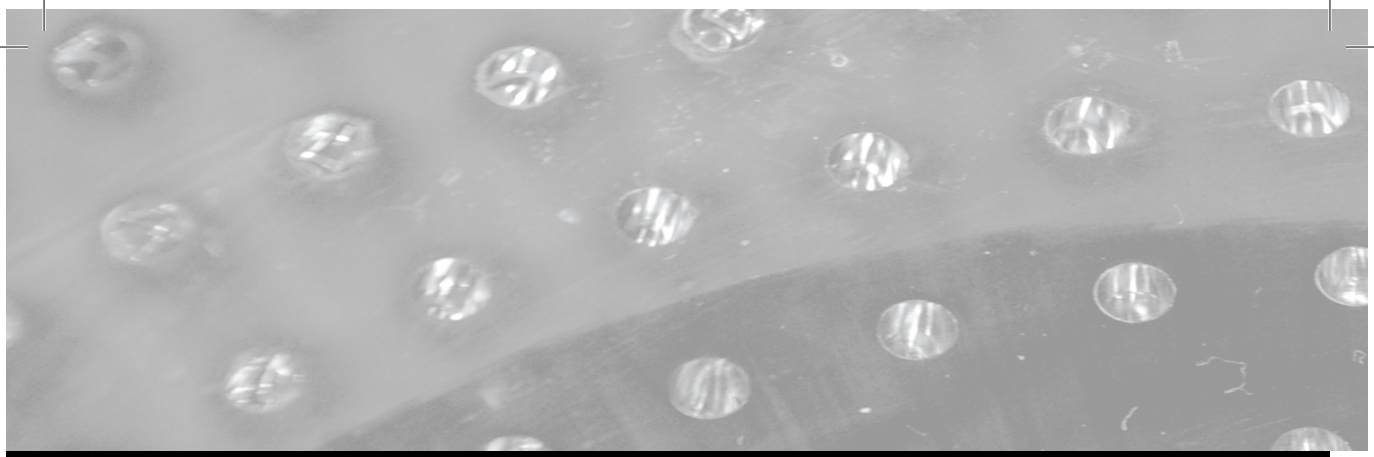

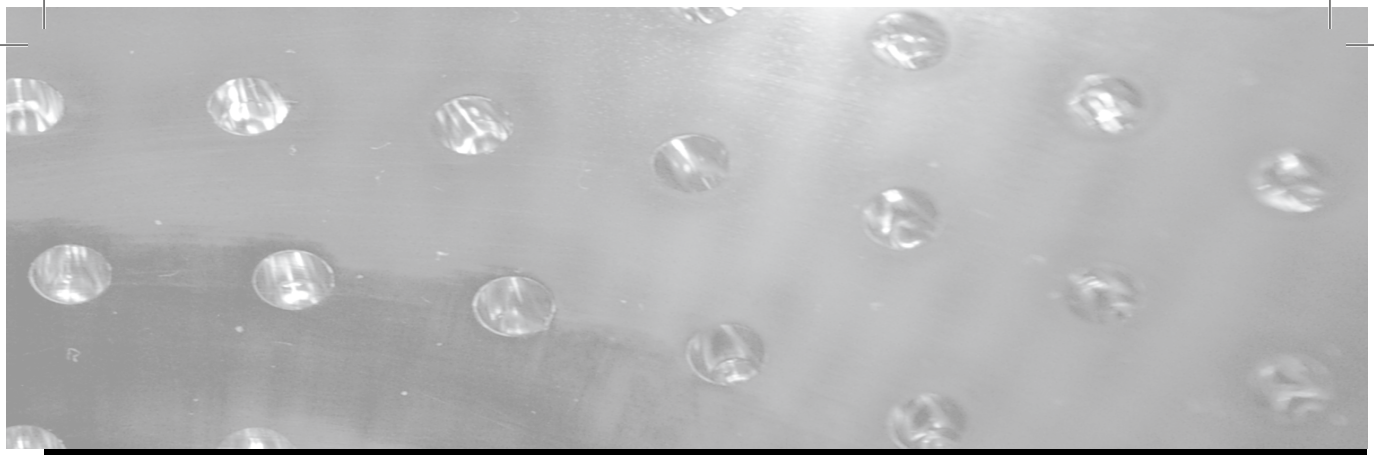

Summary

Samenvatting

Optical breast imaging uses near-infrared light to assess the optical properties of breast tissue. It can be performed relying on intrinsic breast tissue contrast alone or with the use of exogenous imaging agents that accumulate at the tumor site. Different tissue components have unique scattering and absorption characteristics for each wavelength. Using multiple wavelengths allows for the calculation of relative concentrations of oxy- and deoxyhemoglobin, lipid, and water in the tissue (spectroscopic imaging), which may enable discrimination between malignant and benign tissue. With the use of exogenous imaging agents, such discrimination may be improved even further, especially with imaging agents specifically targeted to cancer-associated molecular changes (molecular imaging).

Currently used breast imaging modalities (X-ray mammography, ultrasound, and magnetic resonance imaging) have limitations in clinical utility, including early detection, diagnosis, and treatment monitoring of breast cancer. Optical breast imaging is being pursued as an adjunct to the current modalities for its potential to provide biophysical and molecular information on tissue. Moreover, important strengths of optical imaging are that the technique uses no ionizing radiation, is relatively cheap, has a very high sensitivity for probe detection, and its imaging agents are easy to generate.

In **chapter 2** a literature overview is given of the various clinical optical breast imaging studies and the preclinical optical imaging studies in the evaluation and development of novel target-specific imaging agents for breast cancer. The early evaluation of a new diffuse optical tomography prototype dedicated for breast imaging is described in **chapter 3 to 5**. In **chapter 3** we showed that based on intrinsic breast tissue contrast alone, our new prototype has the potential to discriminate malignant from benign breast tissue by assessing the optical properties of breast tissue in a reproducible quantitative and qualitative way. In **chapter 4** we demonstrated the ability of the technique to visualize cysts and elucidate their high water and low total hemoglobin content by spectroscopic analysis. **Chapter 5** highlights the use of the fluorescent imaging agent Omocyanine in combination with our new prototype. We showed its ability to safely detect malignant breast tumors in patients using a low dose of the imaging agent. Main limitations of the prototype included geometry issues hindering the visualization of lesions close to the patient's chest wall, and the poor spatial resolution limiting the detection of very small breast lesions. **Chapter 6 and 7** report our preclinical optical imaging studies. **Chapter 6** describes the evaluation of a commercially available optical breast scanner in phantom studies. We showed its potential to detect newly developed molecular imaging agents based on modulating light transmission.

Nanomolar concentrations of nanotubes and micromolar concentrations of a small molecule dye could be detected by the clinical optical breast scanner. In **chapter 7** we assessed treatment monitoring with optical imaging in a mouse model. We showed that non-invasive *in vivo* monitoring of changes in protein expression as a response to treatment is feasible using optical imaging.

Although optical breast imaging is still in its infancy, the technique is certainly promising in breast cancer detection and treatment management. Further technical developments and the availability of relevant molecular imaging agents for human use in the near future could eventually allow for this technique to be used in routine clinical practice.

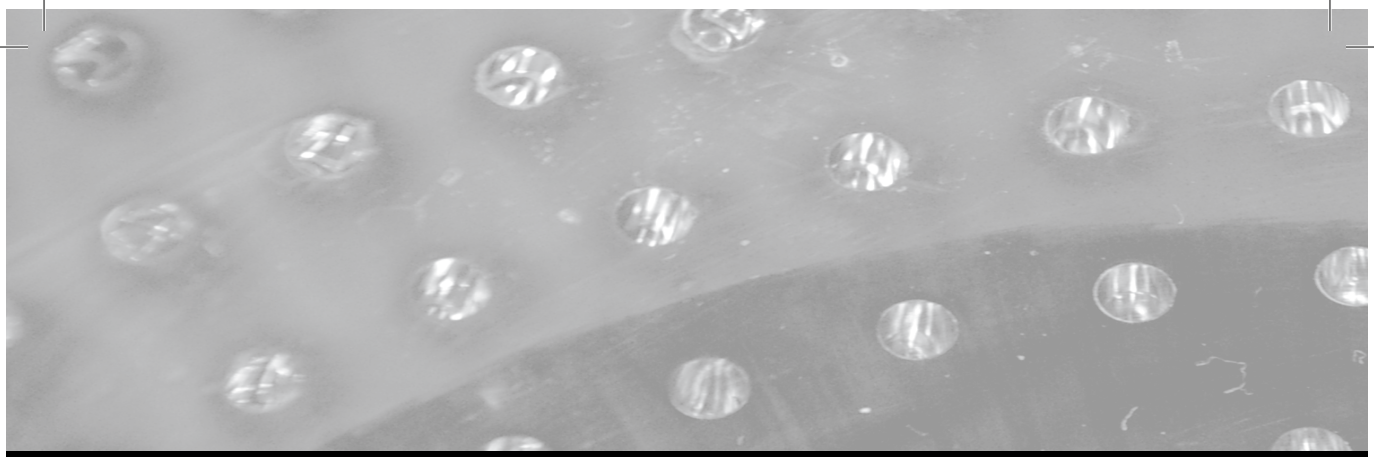

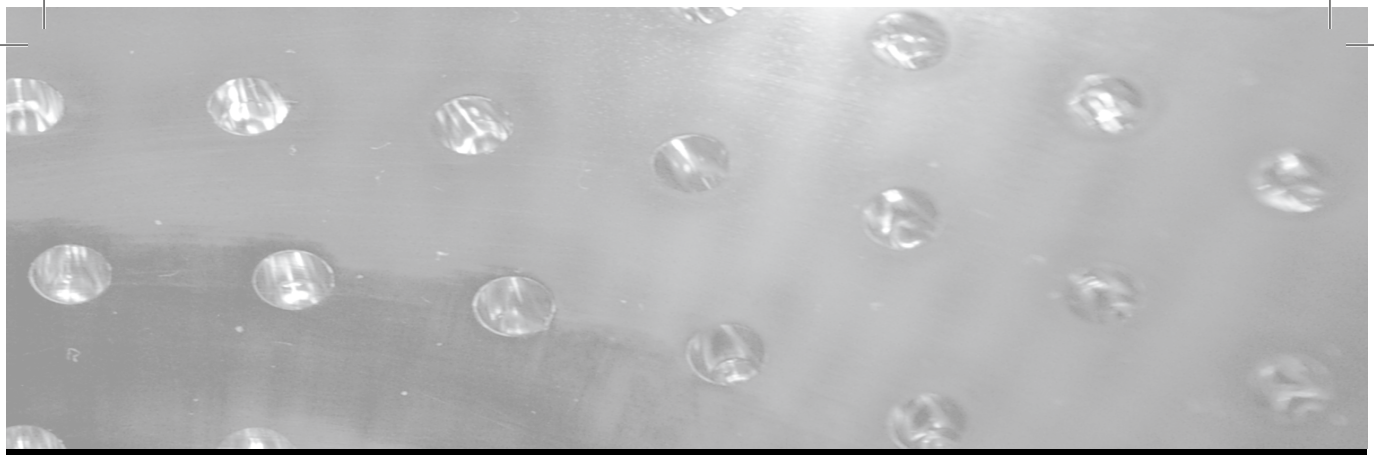

Summary

Samenvatting

Optische beeldvorming van de borst maakt gebruik van nabij infrarood licht om de optische eigenschappen van borstweefsel te bepalen. De techniek kan *of* gebruik maken van de intrinsieke optische contrasteigenschappen van borstweefsel alleen, *of* daarbij ook een exogeen contrastmiddel gebruiken dat zich in/rond het tumorweefsel ophoopt. De verschillende weefselcomponenten in de borst hebben voor elke golflengte hun eigen unieke verstrooiings- en absorptie-eigenschappen. Door metingen uit te voeren bij meerdere specifieke golflengten kunnen de relatieve concentraties van de componenten oxyhemoglobine, deoxyhemoglobine, vet en water in de borst bepaald worden (spectroscopie); hierdoor wordt het mogelijk om kwaadaardige en goedaardige weefsels in potentie van elkaar te onderscheiden. Wanneer exogene contrastmiddelen toegediend worden, kan dit onderscheidend vermogen wellicht nog verder verbeterd worden, in het bijzonder bij het gebruik van contrastmiddelen die specifiek aangrijpen op moleculaire veranderingen die met kanker geassocieerd zijn (moleculaire beeldvorming). De beeldvormingstechnieken van de borst die momenteel klinisch toegepast worden (röntgenmammografie, echografie en magnetic resonance imaging [MRI] van de borst), zijn niet altijd in staat om borstkanker in een vroeg stadium te detecteren, diagnostiseren en het verloop van de behandeling te monitoren. Optische beeldvorming van de borst wordt beoogd als aanvulling op de huidige beeldvormingstechnieken, omdat er door middel van deze techniek relevante biofysische en moleculaire informatie over het weefsel verkregen zou kunnen worden. Belangrijke voordelen van optische beeldvorming zijn bovendien dat deze techniek geen gebruik maakt van ioniserende straling, relatief goedkoop is, een zeer grote gevoeligheid heeft voor de detectie van contrastmiddelen en dat de optische contrastmiddelen gemakkelijk te ontwikkelen en produceren zijn.
In **hoofdstuk 2** wordt een literatuuroverzicht gegeven van de verschillende klinische optische beeldvormingsstudies en de preklinische studies in de evaluatie en ontwikkeling van nieuwe target-specifieke optische contrastmiddelen voor borstkanker. De eerste evaluatie van een nieuw 'diffuse optical tomography' prototype toegespitst op beeldvorming van de borst wordt beschreven in **hoofdstuk 3 tot en met 5**. In **hoofdstuk 3** hebben we aangetoond dat, gebaseerd op intrinsiek borstweefselcontrast alleen, ons nieuwe prototype in potentie kwaadaardig van goedaardig borstweefsel kan onderscheiden door de optische eigenschappen van borstweefsel te bepalen op een reproduceerbare kwantitatieve en kwalitatieve manier. In **hoofdstuk 4** hebben we gedemonstreerd dat we met deze techniek cysten kunnen visualiseren en hun hoog water- en laag hemoglobinegehalte kunnen aantonen door middel van spectroscopische analyse. **Hoofdstuk 5**

belicht het gebruik van het fluorescerende contrastmiddel Omocyanine in combinatie met ons nieuwe prototype. We hebben aangetoond dat het mogelijk is om kwaadaardige borsttumoren veilig op te sporen met een lage dosis van het contrastmiddel. De belangrijkste beperkingen van het prototype bleken de geometrische vormgeving die de visualisatie van afwijkingen vlakbij de borstwand belette, alsook het lage ruimtelijk oplossend vermogen dat het opsporen van zeer kleine borstafwijkingen beperkte. **Hoofdstuk 6 en 7** rapporteren over onze preklinische optische beeldvormingsstudies. **Hoofdstuk 6** beschrijft de evaluatie van een commercieel beschikbare optische borstscanner in fantoomstudies. We lieten het vermogen zien om nieuw ontwikkelde moleculaire contrastmiddelen te detecteren door middel van modulatie van de lichttransmissie. Nanomolaire concentraties van nanobuisjes en micromolaire concentraties van een laagmoleculaire kleurstof konden worden gedetecteerd door de klinische optische borstscanner. In **hoofdstuk 7** hebben we het monitoren van behandeling middels optische beeldvorming onderzocht in een muismodel. We hebben aangetoond dat het op niet-invasieve wijze *in vivo* monitoren van veranderingen in eiwit expressieniveau als respons op behandeling uitvoerbaar is middels optische beeldvorming.
Hoewel optische beeldvorming van de borst nog in de kinderschoenen staat, is de techniek zeker veelbelovend in de opsporing en de behandelingsstrategie van borstkanker. Verdere technische ontwikkelingen en het beschikbaar komen van relevante moleculaire contrastmiddelen voor humaan gebruik in de nabije toekomst kunnen het mogelijk maken dat deze techniek uiteindelijk toepasbaar wordt in de dagelijkse klinische praktijk.

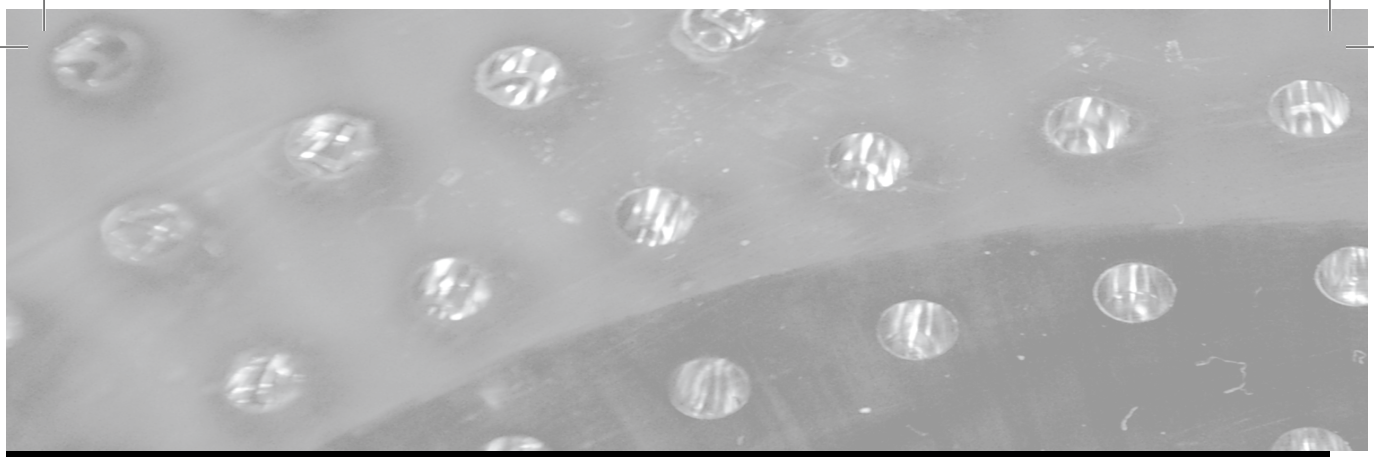

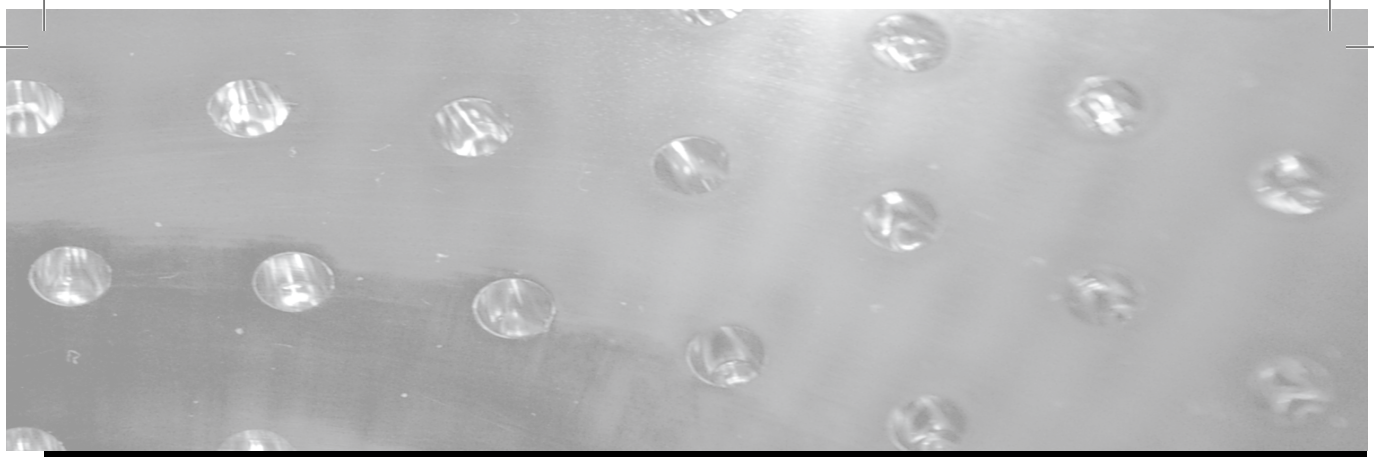

Acknowledgements

Curriculum vitae

List of publications

This thesis would not have been possible without the help of many people. I would like to express my sincere thanks to *everyone* who has supported me during these years of research, and re- and re-search. Without being complete, I would like to mention some of them here.

Prof. Willem Mali, mijn promotor, bijzonder veel dank voor uw vertrouwen en de geboden mogelijkheden om studies uit te voeren in binnen- en buitenland. Ik heb veel respect voor de manier waarop u onderzoek doet en mensen bij elkaar brengt. Ik bewonder uw visie en enthousiasme voor de wetenschap.

Prof. Peter Luijten, mijn tweede promotor, zeer veel dank voor alle hulp en ideeën rondom de uitvoering van dit onderzoek. Je vakinhoudelijke ervaring en je rol in de samenwerking met de industrie waren van groot belang. Je optimisme en interesse zorgen voor een prettig onderzoeksklimaat.

Dr. Sjoerd Elias, mijn copromotor, heel hartelijk dank voor je onuitputtelijke inzet, alle waardevolle aanwijzingen bij het opzetten van studies en het schrijven van artikelen, het epidemiologisch inzicht, maar ook niet te vergeten je persoonlijke interesse en gevoel voor humor (*shake it like a Polaroid picture*).

Dr. Andrea Wiethoff, my second copromotor, your great communication and management skills together with your research experience saved me from getting lost in an industrial research jungle. Besides that, it has always been pleasant and fun to work with you and I am happy with your friendship.

Prof. Debra Ikeda, you immediately took me on a trip (both literally and figuratively) and taught me valuable lessons about work and life during my time at Stanford University. I am very thankful for the opportunity to work with you, especially for all your support and advice, and I hope to be working together again in the future.

Prof. Sam Gambhir, I can't thank you enough for having me work in your lab, lacking every possible lab experience, and exposing me to the fundamentals of molecular imaging. You are always inspiring to work with and I am greatly appreciative of the opportunities you have given me. Looking forward to coming back some time...

Prof. P.H.M. Peeters, prof. E. van der Wall, prof. E.G.E. de Vries, prof. P.J. van Diest, en prof. R. van Hilligersberg, de beoordelingscommissie, hartelijk dank voor het beoordelen van mijn manuscript.

Natuurlijk wil ik alle patiënten en vrijwilligers heel hartelijk danken voor hun onmisbare deelname aan het onderzoek.

The dedication of the various departments of Philips made this research possible and therefore my sincere thanks to Philips Application Technology for the technical support, Philips Research Hamburg for the constant improvements in reconstruction algorithms, and Philips Research Eindhoven for the spectroscopic analyses and further system developments. Sjaak Deckers, Dirk van Pijkeren, Marjolein van der Voort, Michiel van Beek, Leon Bakker, Martin van der Mark, Rami Nachabe, Anais Leproux, Rik Harbers, Tim Nielsen, Bernhard Brendel, Claas Bontus, Ronny and Andy Ziegler, Robert Jochemsen, J.P. Meeuwse, Zoran Stankovic, Fons Schippers, Gertjan Keesman, Wim Bor en Patrick Bonne, it has been a pleasure working with you.

Without the expertise of Bayer Schering Pharma, the clinical trial would not have been performed. I would like to thank everyone involved in this project, with special thanks to Marianne Mahler, Lueder Fels, Gerhard Holl, and Beate Grossmann.

De samenwerking met de verschillende afdelingen van het UMC Utrecht, het Albert Schweitzer ziekenhuis Dordrecht en het Diakonessenhuis Utrecht was van groot belang voor de uitvoering van de studies. Anneke Hamersma, Mathilde Hissink, Quirijn van den Bouwhuijsen, Nicky Peters, Stijn van Esser, Ria Roozendaal en Marianne Deelen, veel dank voor de praktische hulp bij mijn studies, in het bijzonder de inclusie van patiënten, het inplannen en het scannen zelf. Remmert Storm en Thijs van Dalen, dank voor het mogelijk maken van de samenwerking met Dordrecht en het Diakonessenhuis Utrecht. De "mammapoli", Sieta en Marieke, prof. Borel Rinkes, dank voor de hulp bij de inclusie van patiënten. Het technisch cluster ben ik zeer erkentelijk voor de hulp bij de vele vaatjes *matching fluid* en de overige technische ondersteuning. Ook de laboranten en de arts-assistenten in het UMC Utrecht, dank voor de fijne samenwerking. Arancha Fernandez en Gerard Stapper, dank voor het beoordelen van de MRI scans. Medewerkers van het stafsecretariaat radiologie, ook jullie waren onmisbaar in het onderzoeksproces.

Mijn collega's, alle Q-gang onderzoekers, arts-assistenten radiologie en radiologen in Utrecht en in Amersfoort, bedankt voor het meeleven en de gezelligheid tijdens het werk (en ook daarbuiten natuurlijk). Audrey en Sandra, fijn dat jullie nu ook in Amersfoort zijn. Reinoud, Niek, JW, PJ, BJ, Q-overburen, sorry voor het verstoren van jullie rust door uitingen van enthousiasme of frustratie.

Annemarie en Carla, helaas zijn we nu opgesplitst, maar het moet niet te gek worden natuurlijk... ons *breast team* heeft al veel mooie ervaringen gedeeld, maar het wordt weer eens tijd voor de volgende trip! Ongelooflijk hoe jij alles combineert Carla, hoe houd je toch zoveel energie over? Ik kijk ook al uit naar jouw promotie! Lieve Ann, we hebben de afgelopen jaren ontzettend veel gelachen samen, maar Berlijn zal me altijd bijblijven... super mooi en bijzonder dat we op dezelfde dag promoveren!

De "Fotografie": Karin, Eugene, Jan en Roy, jullie maakten mijn werk een stuk makkelijker maar ook vooral een stuk leuker! Fijn om af en toe even mijn hart te kunnen luchten over wasgoed, klitteband en zware tonnetjes vloeistof. Bedankt voor al jullie hulp met folders, kaartjes, stickers, etc., en Roy natuurlijk voor de lay-out.

Dr. Maurice van den Bosch, in *no time* regelde je dat ik naar Stanford kon komen. Voor het mogelijk maken van die geweldige ervaring kan ik je niet genoeg bedanken. Ik waardeer je betrokkenheid en aanstekelijke positieve energie.

It was an unforgettable experience to join The Molecular Imaging Program at Stanford (MIPS). I would like to thank everyone who helped me during my stay in California, either with my experiments or just to feel at home.

Dear Gambhir lab members, all of you were so important to me, you all taught me different techniques or skills. I would like to thank Tim Doyle, Laura Pisani, Adam de la Zerda, and Frezghi Habte for their help with the optical imaging systems and data quantification. Carmel Chan *(BA Asian teacher)*, thanks for taking my Western Blot experience to a whole 'nother level. Paul, Shahriar, Robert, Gayatri, Ataya, Abhijit, Ben, Zhen, and Fred, thanks for your help and advice in various projects. The admins, Elizabeth, Bonita, Donna, Joe, and others, thank you for your help.

ART Advanced Research Technology Inc., especially Niculae Mincu, Guobin Ma, Mario Khayat, and Sébastien Gignac, I am very thankful for your support and help with our phantom studies. The techs and research nurse at the Stanford Cancer Center, Marsha, Sabine, and Leslie, thank you for your help with the ART imaging system. Also, the radiologists involved in other projects, Bruce Daniel, Andy Quon, Priya Sareen, and Jafi Lipson, it has been a pleasure working with you.

Michelle, Cristina, Aloma, Carsten, Scott, Sharon, Andrei, Nick, Natesh, Anca, John, Ian, David, Deepak, Bryan, Adam, Robert & Sunil, and also all my other friends (and pseudo-family) in California, without you so many things (coffee, happy hour, pool parties, cooking, WMIC, karaoke, biking, skiing, thanksgiving, being on a boat, dancing, softball, tennis, goat farms, road trips, etc. etc.) would NOT have been the same...

Thanks for the cover Shell... *anything is possible!*

Lieve Audrey, jij hebt me al door veel situaties heengesleept en zonder jou had ik een stuk minder gelachen. Ik ben ontzettend blij dat je mijn paranimf bent.

Lieve vrienden en familie, ik ben de laatste jaren vaak afwezig geweest, maar toch betekenen jullie enorm veel voor mij. Het is zo belangrijk om te weten dat er mensen zijn die altijd achter me staan. Ik hoop de komende tijd weer meer mee te kunnen doen aan alle gezelligheid. Lieve oma, ik vind het extra speciaal dat je er vandaag bij kunt zijn.

Lieve papa en mama, ik ben elke dag blij met jullie als ouders. Niets is jullie te veel en -*waar ik ook ben*- jullie zijn er altijd voor mij. Jullie liefde en betrokkenheid hebben mij gemaakt tot wie ik nu ben. Lieve Annick, ik ben heel enthousiast dat je naast mijn belangrijkste, reislustigste en grappigste zus, ook mijn paranimf bent. We hebben altijd al veel samen ondernomen en ik kijk vol verwachting uit naar ons volgende avontuur!

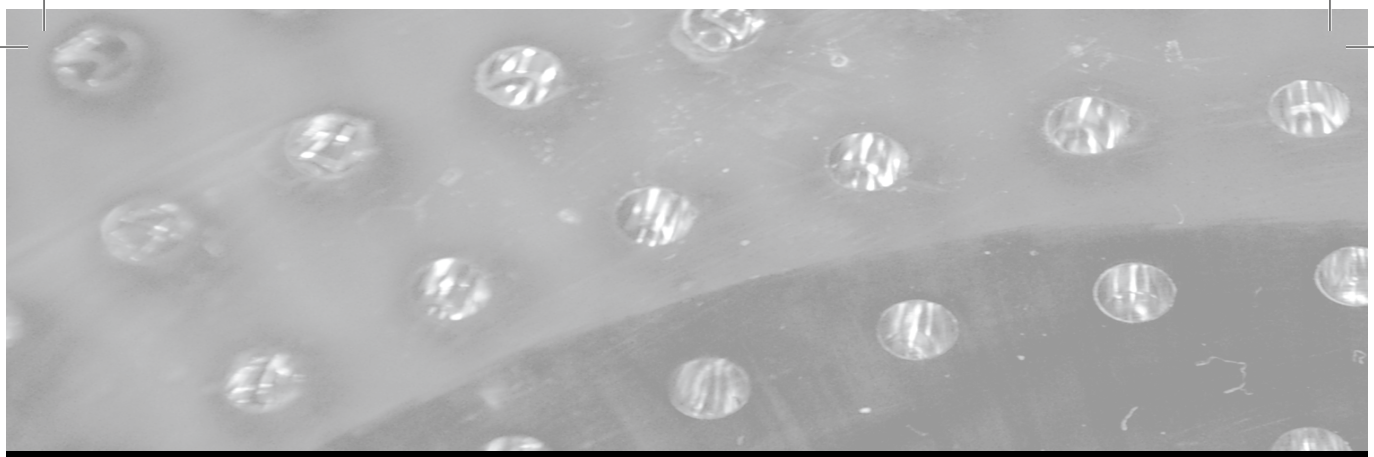

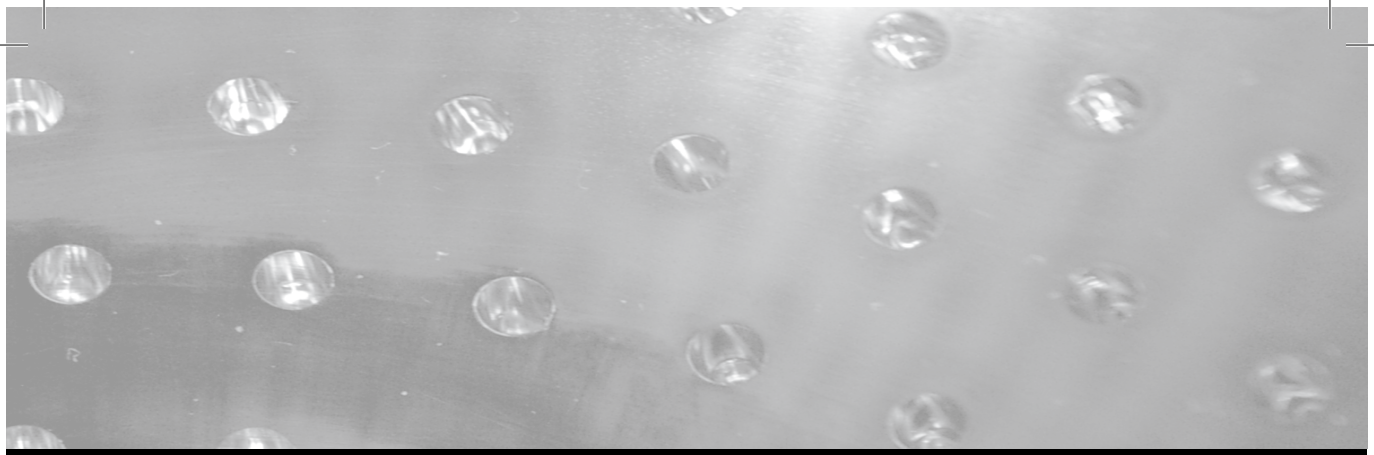

Acknowledgement
Curriculum vitae
List of publications

Stephanie van de Ven was born on April 18th, 1980 in Eindhoven, The Netherlands. In 1998 she completed secondary school (*cum laude*) at the Strabrecht College in Geldrop, The Netherlands. In preparation of medical school she started pharmacy studies at the University of Utrecht, The Netherlands and went to Vancouver, Canada for a six-month work/study program. In 1999 she started medical training at Maastricht University, The Netherlands. During this training she performed scientific research at the Radiology department of University Medical Center Maastricht in collaboration with the research group of Biomedical Image Analysis of the Eindhoven University of Technology (dr. M.E. Kooi) and followed an elective rotation at the Radiology department of the University Medical Center Utrecht, The Netherlands (prof. dr. J.P.J. van Schaik). An elective rotation of obstetrics and gynaecology was followed at the Academic Hospital Paramaribo, Republic of Suriname, and the rotation of ear, nose, and throat medicine was performed at the Stellenbosch University and Tygerberg Hospital in Cape Town, South Africa. In 2005 she obtained her medical degree (*cum laude*) and started her PhD studies at the department of Radiology, University Medical Center Utrecht (prof. dr. W.P.Th.M. Mali). From 2007 to 2009 she performed a two-year research fellowship at the Radiology department of Stanford University Medical Center and the Molecular Imaging Program at Stanford, Stanford, CA, USA (prof. dr. D.M. Ikeda, prof. dr. S.S. Gambhir). Results of this research are presented in this thesis. In 2010 she obtained an MSc degree in Clinical Epidemiology at the University of Utrecht (dr. S.G. Elias). In March 2010 she started her residency in Radiology at the Meander Medical Center Amersfoort, The Netherlands (dr. H.J. Baarslag).

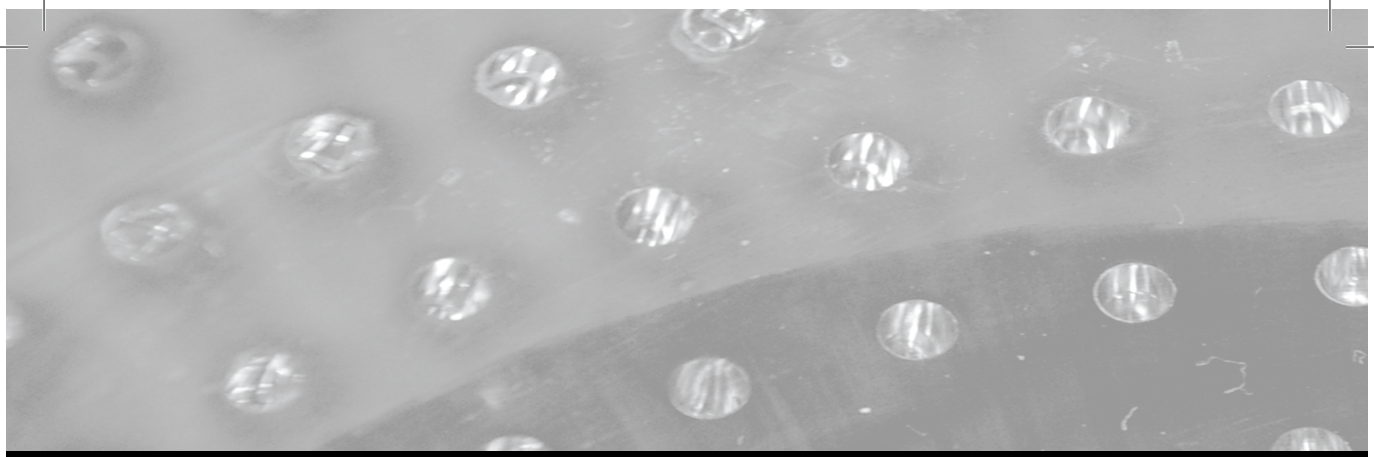

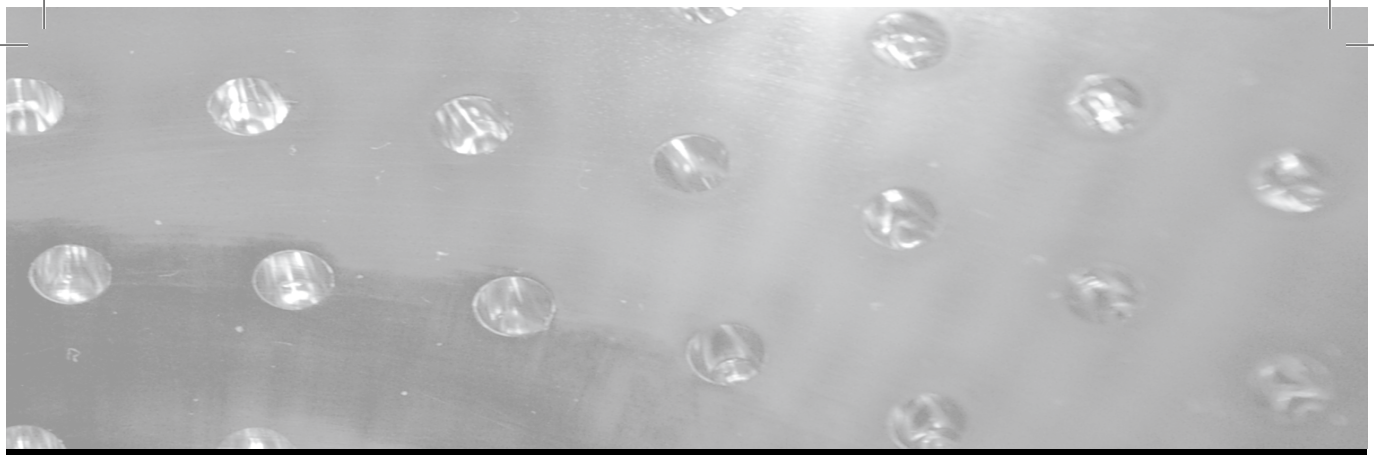

Acknowledgement

Curriculum vitae

List of publications

Journal articles

S.M.W.Y. van de Ven, S.G. Elias, P. Luijten, W.P.Th.M. Mali. Optische beeldvorming van de borst. [Optical Imaging of the Breast] Nederlands Tijdschrift voor Oncologie 2007; 4:299-307.

S.M.W.Y. van de Ven, S.G. Elias, M.A.A.J. van den Bosch, P. Luijten, W.P.Th.M. Mali. Optical Imaging of the Breast. Cancer Imaging 2008;8:206-215.

S.M.W.Y. van de Ven, S.G. Elias, A.J. Wiethoff, M. Van der Voort, T. Nielsen, B. Brendel, L.. Bakker, M.B. Van der Mark, W.P.Th.M. Mali, P. Luijten. Diffuse Optical Tomography of the breast: initial validation in benign cysts. Molecular Imaging and Biology 2009;11:64-70. Epub 2008 Nov 22.

S.M.W.Y. van de Ven, S.G. Elias, A.J. Wiethoff, M. Van der Voort, T. Nielsen, B. Brendel, C. Bontus, R. Nachabe, R. Harbers, M. Van Beek, L.. Bakker, M.B. Van der Mark, W.P.Th.M. Mali, P. Luijten. Diffuse optical tomography of the breast: preliminary findings of a new prototype and comparison with magnetic resonance imaging. European Radiology 2009;19:1108-1113. Epub 2009 Jan 10.

C. Meeuwis, **S.M.W.Y. van de Ven**, G. Stapper, A.M. Fernandez Gallardo, M.A.A.J. van den Bosch, W.P.Th.M. Mali, W.B. Veldhuis. Computer-aided detection (CAD) for breast MRI: evaluation of efficacy at 3.0 T. European Radiology 2010;20:522-8. Epub 2009 Sep 2.

S.M.W.Y. van de Ven, A.J. Wiethoff, T. Nielsen, B. Brendel, C. Bontus, M. Van der Voort, R. Nachabi, M.B. Van der Mark, M. Van Beek, L. Bakker, L. Fels, S.G. Elias, P. Luijten, W.P.Th.M. Mali. A novel fluorescent imaging agent for Diffuse Optical Tomography of the breast: first clinical experience in patients. Molecular Imaging and Biology 2010;12:343-8. Epub 2009 Oct 2.

S.M.W.Y. van de Ven, M.C. Lin, B.L. Daniel, P. Sareen, S. Pal, F.M. Dirbas, D.M. Ikeda. Freehand MRI-guided preoperative needle localization of breast lesions after MRI-guided vacuum-assisted core needle biopsy (VACNB) without marker placement. Journal of Magnetic Resonance Imaging 2010;32:101-9.

S.M.W.Y. van de Ven, N. Mincu, J. Brunette, G. Ma, M. Khayat, D.M. Ikeda, S.S. Gambhir. Molecular Imaging using Light-Absorbing Imaging Agents and a Clinical Optical Breast Imaging system – a Phantom Study. Molecular Imaging and Biology. Epub 2010 Jun 8.

S.M.W.Y. van de Ven, W.P.Th.M. Mali, S.G. Elias, A.J. Wiethoff, M. Van der Voort, M.B. van der Mark, P. Luijten. Optical imaging of the breast: clinical research using an experimental Diffuse Optical Tomography system. Medica Mundi 2010; 54/1. (Invited paper)

S.M.W.Y. van de Ven, S.G. Elias, C.T. Chan, Z. Miao, Z. Cheng, A. De, S.S. Gambhir. Optical Imaging with HER2-targeted Affibody Molecules can monitor Hsp90 treatment response in a xenograft mouse model. *Submitted.*

Conference proceedings (abstracts)

S.M.W.Y. van de Ven, A.J. Wiethoff, M. Van der Voort, T. Nielsen, B. Brendel, L.. Bakker, M. Van der Mark, S.G. Elias, W.P.Th.M. Mali, P. Luijten. Spectroscopic Diffuse Optical Imaging of the breast: first clinical experiences in the characterization of cysts. Oral presentation Joint Molecular Imaging Conference 2007, Travel Stipend Awarded.

S.M.W.Y. van de Ven, A.J. Wiethoff, M. Van der Voort, T. Nielsen, B. Brendel, L.. Bakker, M. Van der Mark, S.G. Elias, W.P.Th.M. Mali, P. Luijten. Spectroscopic Diffuse Optical Imaging of the breast: first clinical experiences in the characterization of cysts. Poster presentation International Society for Magnetic Resonance in Medicine (ISMRM) 2008, Educational Stipend Awarded.

S.M.W.Y. van de Ven, M.A.A.J. van den Bosch, A. Kwong, J. Rosenberg, A. Kamaya, G. Lo, D.M. Ikeda. Reproducibility of scoring systems used for breast density and breast parenchymal pattern assessment on X-ray mammography. Poster presentation American Society of Clinical Oncology (ASCO) 2008. J Clin Oncol 26: 2008 (May 20 suppl; abstr 1547)

S.M.W.Y. van de Ven, A.J. Wiethoff, T. Nielsen, B. Brendel, M. Van der Voort, R. Nachabi, M.B. Van der Mark, M. Van Beek, L. Bakker, L. Fels, S.G. Elias, P. Luijten, W.P.Th.M. Mali. A novel fluorescent imaging agent for Diffuse Optical Tomography of the breast: first clinical experience in patients. Poster presentation World Molecular Imaging Conference 2008.

S.M.W.Y. van de Ven, N. Mincu, J. Brunette, G. Ma, M. Khayat, D.M. Ikeda, S.S. Gambhir. Molecular Imaging using Nanotubes and a Clinical Optical Breast Imaging System. Poster presentation World Molecular Imaging Conference 2009.

S.M.W.Y. van de Ven, S.G. Elias, C.T. Chan, Z. Miao, Z. Cheng, A. De, S.S. Gambhir. Optical Imaging with HER2-targeted Affibody Molecules can monitor Hsp90 treatment response in a xenograft mouse model. Poster presentation World Molecular Imaging Conference 2010.